T.R.
GEBZE TECHNICAL UNIVERSITY
GRADUATE SCHOOL OF NATURAL AND APPLIED SCIENCES

EFFECTS OF PORT AND BURNER ANGLES ON THE ENERGY EFFICIENCY OF GLASS FURNACES

PENBE MERVE DURUBAL
A THESIS SUBMITTED FOR THE DEGREE OF
MASTER OF SCIENCE
DEPARTMENT OF MECHANICAL ENGINEERING

GEBZE
2019

T.R.

GEBZE TECHNICAL UNIVERSITY

GRADUATE SCHOOL OF NATURAL AND APPLIED SCIENCES

EFFECTS OF PORT AND BURNER ANGLES ON THE ENERGY EFFICIENCY OF GLASS FURNACES

PENBE MERVE DURUBAL

A THESIS SUBMITTED FOR THE DEGREE OF MASTER OF SCIENCE

DEPARTMENT OF MECHANICAL ENGINEERING

THESIS SUPERVISOR

PROF. DR. ALP ER ŞEVKİ KONUKMAN

GEBZE

2019

T.C.
GEBZE TEKNİK ÜNİVERSİTESİ
FEN BİLİMLERİ ENSTİTÜSÜ

CAM FIRINLARINDA PORT VE BEK AÇILARININ ENERJİ VERİMLİLİĞİ ÜZERİNDEKİ ETKİSİ

PENBE MERVE DURUBAL
YÜKSEK LİSANS TEZİ
MAKİNA MÜHENDİSLİĞİ ANABİLİM DALI

DANIŞMANI
PROF. DR. ALP ER ŞEVKİ KONUKMAN

GEBZE
2019

GEBZE TEKNİK ÜNİVERSİTESİ	YÜKSEK LİSANS JÜRİ ONAY FORMU

GTÜ FBE Enstitüsü Yönetim Kurulu'nun 03/04/2019 tarih ve 2019/17 sayılı kararıyla oluşturulan jüri tarafından 11/04/2019 tarihinde tez savunma sınavı yapılan Penbe Merve Durubal'ın tez çalışması Makine Mühendisliği Anabilim Dalında YÜKSEK LİSANS tezi olarak kabul edilmiştir.

JÜRİ

ÜYE
(TEZ DANIŞMANI) : PROF. DR. ALP ER ŞEVKİ KONUKMAN

ÜYE : PROF. DR. HÜSNÜ ATAKÜL

ÜYE : DOÇ. DR. AHMET SİNAN ÖKTEM

ONAY

Gebze Teknik Üniversitesi Fen Bilimleri Enstitüsü Yönetim Kurulu'nun ...../...../..... tarih ve ...../..... sayılı kararı.

SUMMARY

Glass manufacturing is an energy-intensive industry. Energy efficiency of a conventional end-fired container glass furnace is between 55% and 60% under recent industrial conditions. Combustion space design parameters of a glass furnace affect the mixing of fuel and air, hence flame formation and energy efficiency in the furnace. In this thesis, the interactive effects of the three combustion space design parameters which are burner angle, port crown angle, and port base angle of a container glass furnace are investigated statistically based on factorial design in order to increase energy efficiency of the furnace by decreasing the required number of computational runs at the design stage for an example of specific glass furnace. Firstly, a total of 27 experimental cases are set to run computationally and the results of energy efficiency data are fitted to the empirical third-order polynomial model for maximum energy efficiency. Degrees of angles for burner, port crown, and port base are 9, 25.3, and 10, respectively, are found to be optimal for the maximum furnace efficiency. Secondly, 27 experiments are classified into three groups, each having nine cases, according to their port base angle. Results of energy efficiency data are fitted to the empirical second-order polynomial model for maximum energy efficiency for each group while burner and port crown angles vary. It is found that higher burner, port crown, and port base angles result in higher temperature regions in flame since the air and fuel meet at an earlier point along the furnace. Hence, the energy efficiency of the furnace increases. Additionally, it is found that the glass surface temperatures increase with decreasing burner and port base angle whereas increasing port crown angle.

Key Words: Glass Furnaces, Energy Efficiency, Full Factorial Design, Statistical Analysis, Temperature Profiles.

ÖZET

Cam üretimi enerji yoğun bir endüstridir. Tipik bir arkadan ateşlemeli cam ambalaj fırınının enerji verimliliği, günümüz endüstriyel koşullarında %55 ile %60 arasındadır. Bir cam fırınının yanma atmosferi tasarım parametreleri; yakıt ve havanın karışmasını, dolayısıyla alev oluşumunu ve fırının enerji verimliliğini etkiler. Bu tez kapsamında fırın enerji verimliliğini artırmak amacıyla bek açısı, port kemer açısı ve port taban açısı olmak üzere üç adet yanma atmosferi tasarım parametresinin etkileşimli ilişkisi, seçilen spesifik bir cam fırınında tam faktöriyel deney tasarımına dayanarak istatistiksel incelenmiştir. Amaç, yeni bir cam ambalaj fırını tasarımı aşamasında gereken simülasyon çalışması sayısını azaltmaktır. İlk olarak; toplamda 27 adet deneysel durum hesaplamalı olarak çalışılmış ve fırın enerji verimliliği sonuçları, maksimum enerji verimliliğini elde etmek amacıyla üçüncü dereceden deneysel bir polinom modeline yerleştirilmiştir. Maksimum enerji verimliliği için bulunan açılar bek, port kemeri ve port tabanı için sırasıyla 9, 25.3 ve 10 derece bulunmuştur. İkinci olarak; 27 adet deney, port taban açısına göre her biri dokuz adet deney içeren üç gruba ayrılmıştır. Bu üç grubun kendi içinde port baz açısı sabitken, bek açısı ve port kemer açısı değişmektedir. Fırın enerji verimliliği sonuçları, her grup için maksimum enerji verimliliğini elde etmek amacıyla ikinci dereceden deneysel bir polinom modeline yerleştirilmiştir. Çalışma sonucunda çizilen sıcaklık profilleri ile bek açısı, port kemer açısı ve port baz açısı artıkça, hava ve yakıtın fırın uzunluğu boyunca daha erken bir noktada karşılaşması sebebiyle alevde daha yüksek sıcaklık bölgeleri oluştuğu gözlenmiştir. Bunun sonucu olarak fırın enerji verimi sayısal olarak artmaktadır. Buna ek olarak, cam yüzey sıcaklıklarının; azalan bek ve port taban açısıyla artığı; azalan port kemer açısıyla ise azaldığı bulunmuştur.

Anahtar Kelimeler: Cam Fırınları, Enerji Verimliliği, Tam Faktöriyel Deney Tasarımı, İstatistiksel Analiz, Sıcaklık Profilleri.

ACKNOWLEDGEMENTS

First and foremost, I would like to express my sincerest gratitude to my advisor Prof. Dr. Alp Er Şevki Konukman. It has been an honor and pleasure for me to be his student. His invaluable support, encouragement, and suggestions made it possible for me to finish my master studies. Also, I would like to thank to Prof. Dr. Hüsnü Atakül and Assoc. Prof. Dr. Ahmet Sinan Öktem for taking part in my thesis committee.

I would like to express my sincerest gratitude to Mrs. Zeynep Eltutar and Mrs. Lale Önsel for giving me the chance to work with them at Şişecam at the beginning of my career. They have contributed immensely to my engineering background and provided an admirable example as a successful woman in the work life.

I am exceptionally grateful to Türkiye Şişe ve Cam Fabrikaları A.Ş., Şişecam Science and Technology Center; especially Atilla Ünsal and Dr. Adnan Karadağ for their guidance and support throughout my studies. I would like to show my gratitude in particular to my colleague Burçin Gül. I am also grateful for her understanding of sharing computer resources throughout this study. I would like to express my sincere thanks to my colleagues Dr. Başak Renklioğlu, Özkan Gül, Emre Kartal, Emre Dumankaya, Neşet Arzan, Barış Orhan, Efe Çağlayan, Murat Telli, Banu Çopuroğlu for having contributed greatly to my professional life at Şişecam.

Invaluable contributions of Dr. Aydın Ungan in the field of glass furnace modeling is remembered with great respect.

I would like to show my gratitude to my dearest friends: Dr. Hasan Şıldır for motivating me to pursue graduate studies. Once from Ankara, all over the world now: Hazal Bal Özcan, İlknur Özçakıroğlu, Pelin Karakılıç, Irmak Ece Şener, Dr. Pelin Yılmaz, Gizem Kocalar, Özge Öztürk, Tuğçe Güçlü, Başak Anayurt, Merve Aktaş, Dicle Taşkın. They have always been a family to me and supported me through good and bad times. I would like to express my special thanks to my flatmate Meltem Ayyıldız. She has become a family to me in İstanbul and it is hard to imagine completing this study without her friendship.

Lastly, I owe the most to my beloved family; my mother Ayfer Durubal, my aunt Asuman Eldaş, my uncle Serdar Durubal and my late uncle Erdoğan Eldaş and my late father Selçuk Durubal. They have raised me with endless love, trust, and support. I would not have made it this far without them.

TABLE of CONTENTS

LIST of ABBREVIATIONS and ACRONYMS

Abbreviations and Acronyms		**Explanations**
α_{Ross}	:	Gray absorption coefficient
Γ	:	Exchange coefficient
ΔH_{melt}	:	Enthalpy per unit mass of molten glass
ε	:	Dissipation rate of turbulence
η_c	:	Energy efficiency of computational run
η_s	:	Energy efficiency of the statistical model
κ	:	Absorption coefficient
λ	:	Phononic heat conductivity
μ	:	Viscosity
ν	:	Frequency
ρ	:	Mixture density
$\sigma_{\varepsilon,eff,}$	:	Effective Schmidt number in dissipation rate of turbulence equation
σ_f	:	Prandtl number in mixture fraction equation
σ_g	:	Prandtl number in species fluctuation equation
σ_h	:	Effective Prandtl number in stagnation enthalpy equation
$\sigma_{k,\,eff}$	:	Effective Schmidt number in the turbulent kinetic energy equation
σ_{ms}	:	Prandtl number in soot mass fraction equation
σ_{SB}	:	Stefan-Boltzmann constant
φ	:	Dependent variable
$\boldsymbol{\Omega}$	:	Direction
B	:	The Plank function
C_1, C_2	:	Constants in turbulence equation
$C_{g,1}, C_{g,2}$	:	Constants in the transport equation
E_b	:	Blackbody emissive power
f	:	Mixture fraction
g	:	Species fluctuation
G	:	Irradiance
G_k	:	Generation term for the kinetic energy of turbulence

h_o	:	Stagnation enthalpy
$\boldsymbol{I}$	:	Spectral radiation intensity
k	:	Turbulent kinetic energy
K_a	:	Absorption coefficient
L_b	:	Batch length
m_s	:	Soot mass fraction
R^2	:	The coefficient of determination in statistics
S	:	Source term
S	:	Standard error in statistics
$S_{s,0}$	:	Soot oxidation rate
$S_{s,f}$	:	Soot formation rate
T	:	Temperature
U	:	The overall heat transfer coefficient
$\boldsymbol{u}$	:	Velocity field
u, v, w	:	Velocity components
W	:	The width of the furnace
x, y, z	:	Space coordinates

ANOVA	:	Analysis of Variance
CFD	:	Computational Fluid Dynamics
CPU		Central processing unit
3D	:	Three-dimensional
FVM	:	Finite Volume Method
SCRS	:	Simple Chemically-Reacting Systems
SIMPLE	:	Semi-Implicit Method for Pressure-Linked Equations
SIMPLER	:	SIMPLE Revised
TDMA	:	Tri-Diagonal Matrix Algorithm

LIST of FIGURES

LIST of TABLES

1. INTRODUCTION

In this chapter, general information on energy consumption trend in energy-intensive sectors and glass manufacturing, in particular, are introduced. Then objectives and motivations of the study are presented. The chapter concluded with the thesis organization.

1.1. General

In the modern world, energy is one of the most vital inputs of economic development and social welfare. Energy requirement of the world has increased due to increase in population, industrialization, and advancement in technology. Total energy consumption has been more than doubled within the last 45 years. This tendency is represented in Figure 1.1 [1].

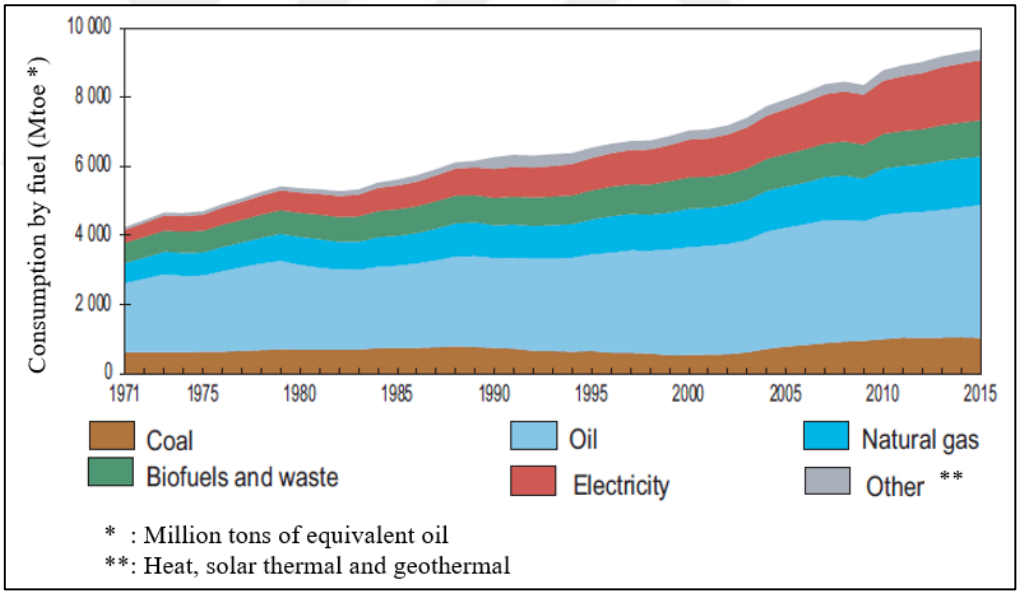

Figure 1.1: World total energy consumption from 1971 to 2015 by fuel.

According to the projections of U.S. Energy Information Administration (EIA), as illustrated in Figure 1.2, the industry will continue to remain as the world's largest energy consuming sector with its energy use increasing by 18% from 2015 to 2040 [2].

Between 2005 and 2016, final energy consumption in the European Union decreased by 7.1% whereas Turkey experienced the largest increase by 53% after

Iceland (63%) in final energy consumption. This trend is expected to continue in Turkey according to European Environment Agency by 35% increase in final energy consumption in 2020 while 11% decrease in European Union due to the economic shift toward less energy-intensive industries [3].

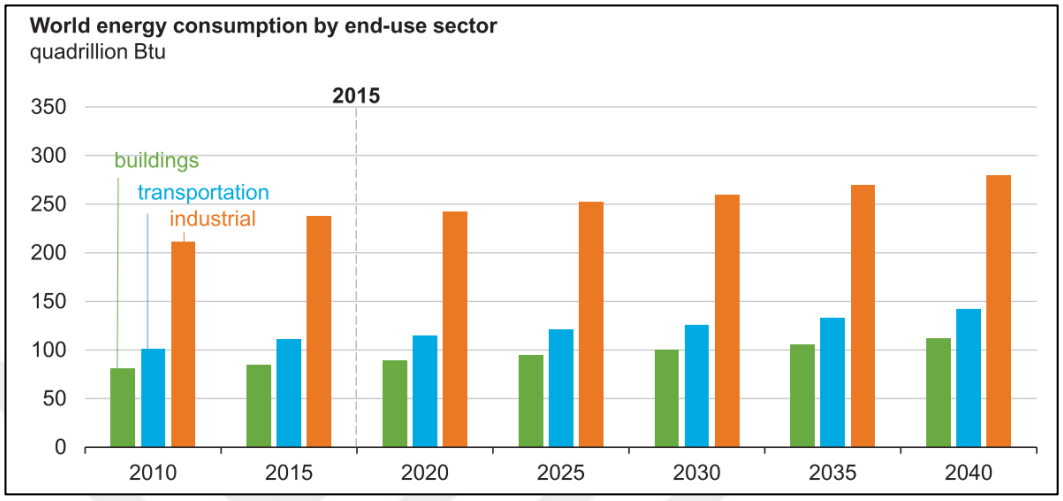

Figure 1.2: Future projections of world energy consumption by end-use sector.

One of the most energy consuming areas in terms of industrial sense is the production of glass. Glass manufacturing is an energy-intensive industry. Energy-intensive sectors are the ones that they account for approximately 50% of the total final industrial energy use such as iron and steel industry, chemical and petrochemical industry, paper and pulp industry, and non-metallic mineral industry (in which cement, ceramic and glass manufacturing is included), etc. [4]. In glass production, 0.5-0.8 EJ of energy per year is used worldwide [5]. Average energy usage per metric ton of glass varies between 5.75-9.0 GJ in practice [6] while primary production of steel requires 20-30 GJ/t and aluminum 90-100 GJ/t.

Considering growth in energy demand and limited energy resources in the world, reasonable use of energy comes into prominence and energy efficiency has become an essential matter. Energy efficiency is described by reducing the amount of energy per product by providing the same quality [7]. In the glass manufacturing process, there are two targeted areas to examine energy efficiency. First one is the operational efficiency that includes more efficient use of raw materials, fuel and air, advanced process control, and improved furnace tuning, etc. The second one is the design efficiency that consists of furnace design, equipment design, heat recovery systems, and new combustion technologies. In glass plants, approximately, glass furnaces may

account 65% of the total energy input of the glass manufacture with an average efficiency of 50-60%. The losses stand for structural losses and flue gas losses are 20-25% and 25-35%, respectively [8].

Operational efficiency can be controlled and manipulated during operation whereas parameters related to furnace design cannot be changed once the furnace put into use. Considering the average furnace lifetime (10-14 years), the design stage of a glass furnace becomes important for an efficient melting. Design stage includes the geometry of a furnace, combustion technology used in a furnace and equipment design/selection.

Heat transfer in the glass furnace affects the furnace efficiency and is related to furnace design along with equipment. The ideal approach to furnace design is to design a furnace/burner system to obtain the ideal heat flux profile for the melting process [9]. In order to do so, adequate flame formation is required. Flame formation depends on the mixing of the combustion material (fuel and air) and chemical reactions between them. The mixing process is mainly a technical phenomenon consisting of fluid flow. On the other hand, combustion of fuel and air is part of both a physical phenomenon in regard of preparation of fluid flow and a chemical phenomenon in regard of acceleration of chemical reactions due to high temperatures but slowing down the mixing process due to the high viscosity of hot gases [10]. In order to overcome physical problems mentioned above, the mixing of fuel and air must be studied. There are several physical parameters related to design that have an impact on mixing of fuel and air such as port geometry (port dimensions and port angles) and burner geometry (number and placement of burners, burner angle and burner nozzle diameter). In addition to that, there are additional parameters related to furnace geometry, such as furnace dimensions and the distance between burner tip-glass surface, etc. that affect heat transfer from combustion space to the glass melt.

1.2. Objectives and Motivations of the Thesis

There have been some studies on furnace design parameters at the industrial scale, which will be mentioned in detail in Section 2.4, since simulation models have been developed specifically for glass furnaces. However, a systematic investigation by factorial design is not available to date. Despite glass manufacturing regarded as a “mature” industry, there is a limited number of publications of industrial-scale glass

furnaces available due to the fact that it requires huge computational effort as well as confidential know-how of each company.

Although every furnace performance must be examined individually, the main idea behind the heat transfer optimization in the combustion space remains the same. Enhanced heat transfer gives rise to furnace efficiency. While it is influenced by a number of factors, the fundamental driving force for high furnace efficiency is the effective heat transfer within the furnace. There are ways to enhance furnace efficiency in terms of design and operational parameters. This study is centered on three particular combustion space design parameters (burner angle, port crown angle, and port base angle) that have no possibility to change, except for burner angle in some cases, when the furnace is engaged in production.

The objective of this study is to investigate the interactive effects of these three combustion space design parameters mentioned above for high energy efficiency in glass furnaces. To fulfill this aim, a conventional end-port furnace for container glass production having a capacity of 350 metric tons per day was used. In order to do so, 27 experiments that are determined by factorial design was performed computationally. An in-house developed 3D mathematical model describing the physical phenomena occurring in a glass melting furnace has been used in the thesis. Accordingly, the results of the study on statistical analysis of combustion efficiency, the amount of energy transferred into the glass bath and the temperature profiles of the study cases will be discussed. Motivations of this study are given below:

- Providing a practical approach for the design of a combustion space of a glass furnace to enhance energy efficiency by investigating three combustion space design parameters by full factorial design.
- Providing a case study on how to utilize a statistical approach to a glass furnace at the design stage by decreasing the required computational time to run a complex furnace code.
- Investigating numerical range thoroughly for three design parameters related to the combustion space of a glass furnace. By taking a step further, examining the extended upper and lower limits of the design range for these parameters.
- Contributing to literature by investigating a real industrial furnace in terms of a statistical approach for the first time.

- Understanding the numerical and statistical relationship between three designs parameters of combustion space in a furnace.
- Presenting a varied and inexpensive method of gathering information and guidelines to design a container furnace.
- Contributing to glass furnace design in terms of a practical approach by providing a heuristic technique.

1.3. Thesis Organization

The thesis is divided into six chapters and the corresponding summaries of each chapter are given in the following way:

In Chapter 2, background information and literature review on glass and glass manufacturing followed by a brief overview of the glass industry are presented. Industrial glass furnaces with elaborate emphasis given on melting, burners, and ports are introduced.

In Chapter 3, the application of mathematical modeling to glass furnaces is reviewed briefly. Then, the model description of the container glass furnace used in this study is explained in detail. Also, the governing equations employed in the thesis are given.

In Chapter 4, a parametric study is conducted in order to investigate three combustions space design parameters in a container glass furnace. The investigation cases are explained. Then, the geometry and gridding of the furnace are presented.

In Chapter 5, the results of the study are presented. A statistical approach is proposed using the energy efficiency of the furnace in both cubic and quadratic equation model to investigate the relationship between the aforementioned three combustion space parameters. This is followed by the combustion space evaluations in terms of temperature profiles comparing the study cases and evaluation of the results in terms of economic sense.

In Chapter 6, the thesis is concluded by summarizing the results of the study followed by future recommendations for improvements to this work.

2. BACKGROUND INFORMATION AND LITERATURE REVIEW

In this chapter, glass is introduced as a material in order to provide background information to the reader. The overview of the glass industry is summarized, and the description of glass furnaces with a section in the heat transfer mechanism is given. The chapter is concluded with a literature review on energy efficiency in glass melting furnaces.

2.1. Glass as a Material

Glass takes a vital role in the civilization of humanity and has been in use since ancient times. Today, glass as an innovative material utilized in daily life from tableware to high-tech products. Some of the most prevalent areas of glass products and components are packaging, housing and buildings, automobiles, appliances and electronics, medical technology and solar energy.

The glass is produced by fused or melted crystalline materials at elevated temperatures and has been cooled to a rigid condition without crystallization. The chemical composition of glass is largely inorganic, and the major constituent is silica (SiO_2). Besides silica, most commercial glasses have roughly similar compositions including sodium oxide (Na_2O), calcium oxide (CaO), magnesium oxide (MgO), aluminum oxide (Al_2O_3), and some minor ingredients vary based on type, color, and functionality of glass. Some important types of commercial glasses are presented in Table 2.1 [11].

From an engineering perspective, what makes glass differ from other inorganic materials is that it does not have a definite melting point temperature. When the glass is heated, it will deform and eventually form a viscous liquid [12]. From the past to present, many definitions have been proposed to define glass as either a liquid or a solid. These attempts come to a point that glass has features of both liquids and solids along with its unique properties. On an observation time scale, glass is an amorphous solid material and properties of glass rely heavily on thermal and pressure histories experienced by the glass as well as its composition and current condition [13].

Table 2.1: Commercial types of glass and its applications and characteristics.

Type of Glass	Application	Characteristics
Soda lime-silica glass ($Na_2O \cdot CaO \cdot SiO_2$)	Flat glass, container glass, tableware, lamp glass, lenses.	Mass production, low cost.
Sodium-borosilicate ($Na_2O \cdot B_2O_3 \cdot SiO_2$)	Ovenware, laboratory glass, headlights.	Thermal shock resistant.
E-glass ($CaO \cdot Al_2O_3 \cdot B_2O_3 \cdot SiO_2$)	Textile glass fiber, reinforcement fibers for plastics, fibers for circuit boards.	Mechanical strength, low electrical conductivity, fiberizing.
A-glass ($Na_2O \cdot CaO \cdot B_2O_3 \cdot SiO_2$)	Glass wool (insulation), glass fiber (reinforcement).	Low cost, fiberizing.
Display glass ($Al_2O_3 \cdot CaO \cdot B_2O_3 \cdot BaO \cdot SiO_2$)	Glass for a thin-film-transistor liquid-crystal display.	Low electrical conductivity, ultra-thin (down to 50 μm), high melting temperatures.
Lead glass ($PbO \cdot K_2O \cdot SiO_2$)	Art glass, tableware, decoration.	High purity, high refractive index value.
Vitreous silica (SiO_2)	Optical glass fiber, halogen lighting, laboratory, and chemical equipment.	Purity, high-temperature resistance, high thermal shock resistance.

Properties of glass are numerous such as it is a material that combines mechanical rigidity and elasticity. Thus, glass is an inherently strong material that is harder many types of steel [14] while being brittle at the same time. It can be engineered to be tremendously strong and damage resistant. Additionally, glass is a chemically inert material due to the continuous network of silicon-oxygen bonds that makes it suitable as a packaging item for beverages. Besides, it has a low electrical conductivity as a result of tightly bonded electrons which makes glass one of the finest insulator materials. Glass also exhibits optical transparency behavior. Therefore, it is used for optical and radio frequency transmission [15]. Finally, since being produced naturally abundant raw materials, glass is an environmentally friendly material that can be recycled continuously.

2.2. Glass Manufacturing

2.2.1. Overview of Glass Industry

Owing to the accelerating pace of glass innovation, a recent argument states that the era we are living in now is the “Glass Age” [15]. Although some of the smaller glass sectors serve for high-tech products, it is still a commodity industry whose over 80% of products are sold to other industries including mainly beverages, food, and buildings. Considering both product range and manufacturing techniques employed, the glass industry is highly diverse. Products vary from handmade delicate ones to mass volumes of float glass. Manufacturing techniques range from electrically heated furnaces to huge cross-fired regenerative furnaces in flat glass in accordance with production capacity range from a couple of metric tons to 1000 tons per day.

Glass manufacturing can be divided into five segments based on product type – flat glass, container glass, tableware, fiberglass, and specialty glass – that are listed in detail in Table 2.2. In this thesis, since a container glass furnace is studied, the focus will be the container glass industry.

Container glass production within the European Union has increased by 39.5% for the last twenty-five years [16]. In 2017, container glass production constituted nearly 50% of the total glass production in the world. Flat glass and tableware production follow this with 40% and 10%, respectively. Today, energy consumption in the container glass sector is between 5 GJ/t to 16 GJ/t based on product type [17].

Table 2.2: Glass industry segments and typical products.

Segment	Key Products
Flat glass	Sheet plate and float glass for residential and commercial construction, automotive applications, tabletops, and mirrors.
Container glass	The packaging of foods, beverages, household chemicals, pharmaceuticals, and cosmetics.
Tableware	Pressed and blown glass for tableware.
Fiberglass	Glass wool insulation for buildings, roofing, and panels. Textile and plastic reinforcement fibers for the construction, transportation, and marine industries.
Specialty glass	Cookware, lighting, televisions, liquid crystal displays, laboratory equipment, and optical communications.

Although each product segment has its own process characteristics, the process of glass melting is primarily similar. Glass manufacturing consists of different sub-processes, starting from raw materials preparation to the packaging of products and delivering to the customer. The flow diagram of a typical container glass production is given in Figure 2.1.

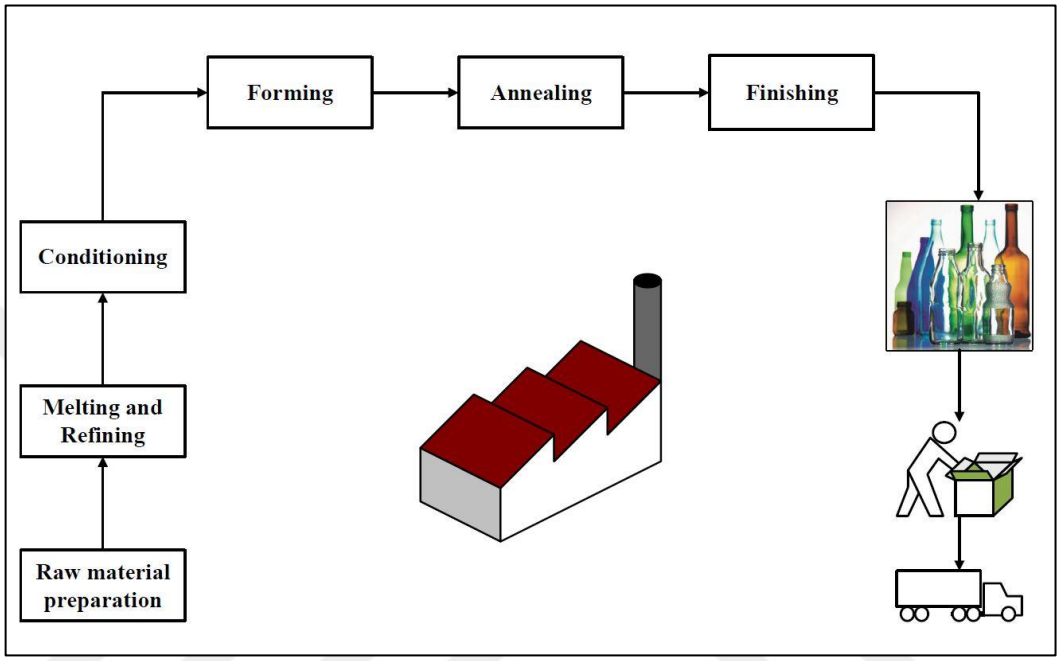

Figure 2.1: The flow diagram of a typical container glass production.

The sub-processes constitute glass making are given below respectively:

- Raw material preparation (mixing of raw materials as a *batch* based on desired glass composition).
- Melting (melting of the prepared batch to obtain glass).
- Conditioning (chemical and thermal homogenization of glass melt, removal of gas bubbles in glass melt).
- Forming (getting the form of glass products that is desired such as a container, tableware, sheets, fibers, etc.).
- Annealing (relieving existing internal stresses for thermal stabilization).
- Finishing (secondary processes involving coating, cutting, winding based on glass product).

Glass melting is the most energy used process in the glass industry. It is carried out using natural gas, a combination of natural gas and electricity (electric boost), or all electricity for specialty glasses. Natural gas accounts for 73% of the overall fuel use. The rest is electricity (24%) and some other fuels (3%) [18].

Energy consumption is affected by several variables such as production capacity; cullet in raw materials *(batch)*; type and color of glass; size, age and firing mode of the furnace. Elaborated information regarding these variables is given in Section 2.4.

2.2.2. Description of a Glass Furnace

Furnaces have been in use since the industrial revolution to produce metal and chemical products, cement and bricks, food and drink items as well as to dry natural products like timber and pulp. A furnace is a box-shaped enclosed structure to attain a higher processing temperature and used to facilitate a wide range of chemical reactions and/or physical processes [9]. A glass furnace serves as a chemical reactor where the raw materials are melted at high temperatures to turn into the glass through simultaneous and/or consecutive physical and chemical mechanisms.

There are a couple of ways to classify glass furnaces. In the following paragraphs, glass furnaces are roughly classified into two ways, which are based on their continuity and the firing position.

Firstly, glass furnaces are classified into two categories based on their continuity. There are discontinuous (pot furnaces) or semi-continuous (day tanks) furnaces used for hand-made or the specialty glass production. Their production capacity is small and can be defined with kilograms up to a couple of tones. On the other hand, there are continuous furnaces that are suitable for massive glass productions such as container glass, tableware, flat glass, and fiberglass.

Secondly, glass furnaces are divided into two groups with respect to the position and direction of the flames within the furnace. There are cross-fired and end-fired glass furnaces, respectively as shown in Figure 2.2 [19]. The first one is used to sustain heat transfer throughout the furnace that is larger in wide and longer in length with many sets of burners firing from two sides. Cross-fired furnaces are suitable for flat glass production in conventional industrial applications. The end-fired system is used for relatively small furnaces to produce container glass and tableware. In both cross-fired and end-fired furnaces, the inlets of fuel and combustion air are located separately.

There are different firing modes present in the glass industry. These modes have their own unique mixing characteristics which influence the flame shape and heat transfer [20].

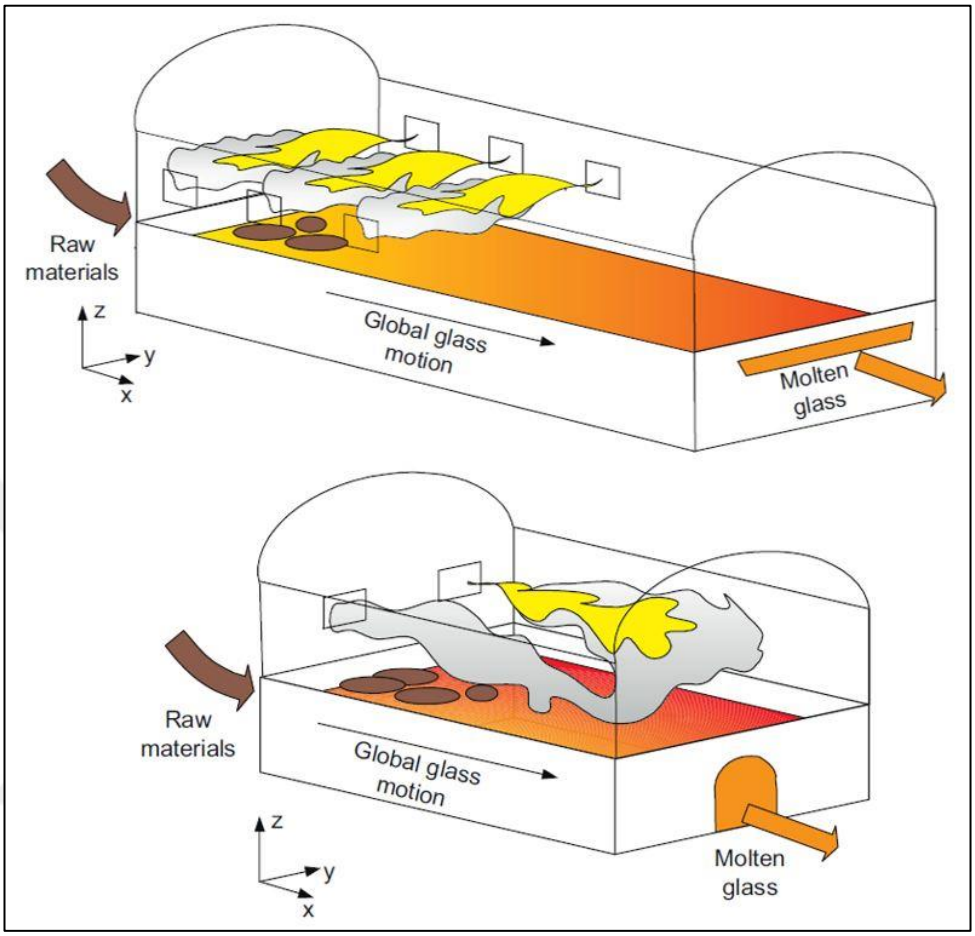

Figure 2.2: Two furnace types a) Cross-fired furnace b) End-fired furnace.

In general, a glass furnace is an enclosure with charging inlet *(doghouse)* and discharging outlet *(throat)*, a-crown-shape-top covering combustion space, four side walls and a bottom. Dimensions of a glass furnace vary depending on the capacity *(the pull rate*) and type of glass being produced. The building material is called refractory which has high-temperature resistance. Despite the presence of different kinds of furnaces, a typical glass furnace has the following sections: melter, delivery channels, and heat recovery system as shown in Figure 2.3. The focus of this study is the melter, in which the combustion process takes place, in an end-fired container glass furnace.

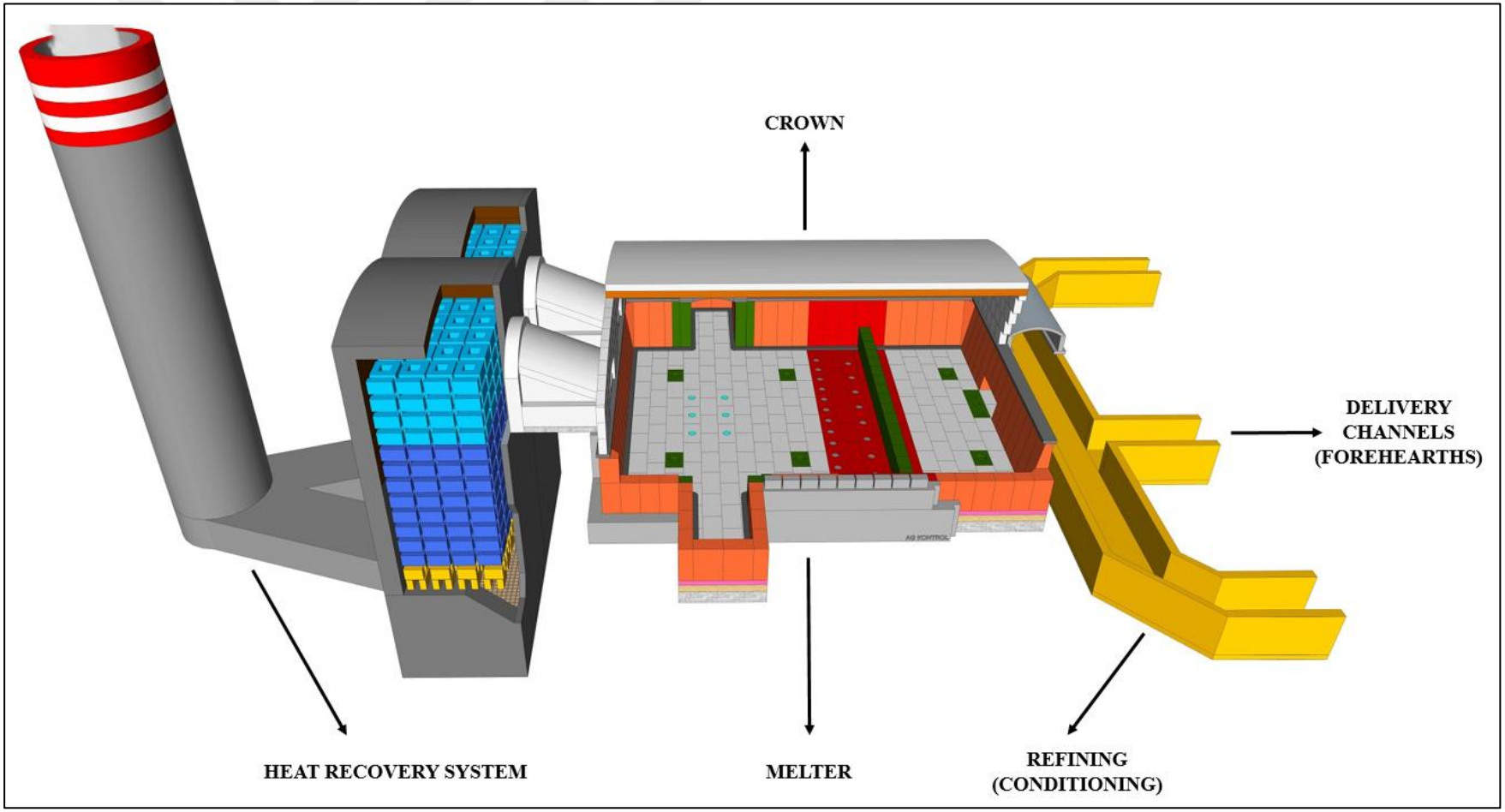

Figure 2.3: Schematic of a typical end-fired container glass furnace.

•Melter

A conventional glass furnace is an insulated reactor where the raw materials (silica sand, soda ash, limestone, dolomite, cullet, etc.) are continuously fed into the inlet which is called *doghouse.* The raw materials are converted into glass melt in the melting tank.

The chemical reactions of raw materials take place at a temperature range from 850^0C to 1200^0C within the batch. Melting energy is received from combustion space from the top (1600^0C) where the peak flame temperatures could be higher up to 1800^0C and the glass melt from the bottom (1200^0C to 1500^0C) [21].

Molten glass interacts with the flames of flue gases from fuel. The fuels used in glass furnaces are generally liquid or gaseous fuel since the fuels in solid phase may disturb the molten glass [22]. In some cases, such as the production of high iron content glass, electrical energy is used for auxiliary energy supply to maintain glass temperatures at certain degrees.

The final glass product must be chemically homogeneous and free of gas bubbles to obtain optically, mechanically and aesthetically high-quality glass. Another section called *refiner* or *conditioning section* is located after melter. The molten glass flows across the refiner which supply extra time to eliminate gas bubbles. The bubbles contain nitrogen and oxygen due to trapped air, and decomposition products of raw materials such as carbon dioxide, sulfur dioxide, and water vapor. Large bubbles rise to the glass surface due to viscosity difference but most of the bubbles are too small to be eliminated in this way. Therefore, dissolution of them is carried out by fining agents that are added to glass batch [23].

•Delivery Channels (Forehearths)

The glass delivery system in the furnace is called forehearths. The function of forehearths is to reduce the thermal gradients while providing the bulk glass temperature required for forming process [21]. For that reason, the colder glass melt flowing near the side walls is being heated while the relatively hotter glass melt at the center of the axis is being cooled down.

•Heat Recovery System

Regenerators are the heat recovery systems utilized in glass furnaces that basically serves as a heat exchanger. The principal objective of the regenerators is to use the thermal energy of waste gases to preheat the combustion air at elevated temperatures such as 1100 to 1400^0C. Hence, better heat transfer is achieved through high flame temperatures. Regenerator dimensions and arrangement of the packing determine the surface area available for heat transfer. The exit temperature of the exhaust gases ranges from 300 to 600^0C according to regenerator size.

Regenerative furnaces, as in this study, operates a cycle-based firing *(inversion).* One cycle proceeds approximately twenty to thirty minutes and takes place in one half of the furnace. Subsequently, the other cycle begins in the other half of the furnace. In one cycle, the heat in the regenerator is transferred from flue gases to refractory walls. Following this, in the other cycle, the combustion air is heated by the refractory bricks within the regenerator structure.

Indicative points in the furnace are monitored during the melting process by locating several thermocouples for temperature and sensors for gas concentration, emissions, pressure, etc. Moreover, an additional process involving glass forming is also mentioned below since a container glass furnace is employed in this study.

•Forming

Different sectors in glass industry apply forming processes after forehearths depending on the product type. Container glass manufacturing includes three steps that are pressing, stretching, and blowing. Molten glass coming out of melter is cut into gobs by machines with high speed. These gobs, standardized as having the same shape and size, fall into a first mold. They partially form the containers that are called *parisons* by pressed or blown against the mold. The final shape is obtained by the effect of gravity and pressure by transferring the parison to the second mold as seen in Figure 2.4 [24].

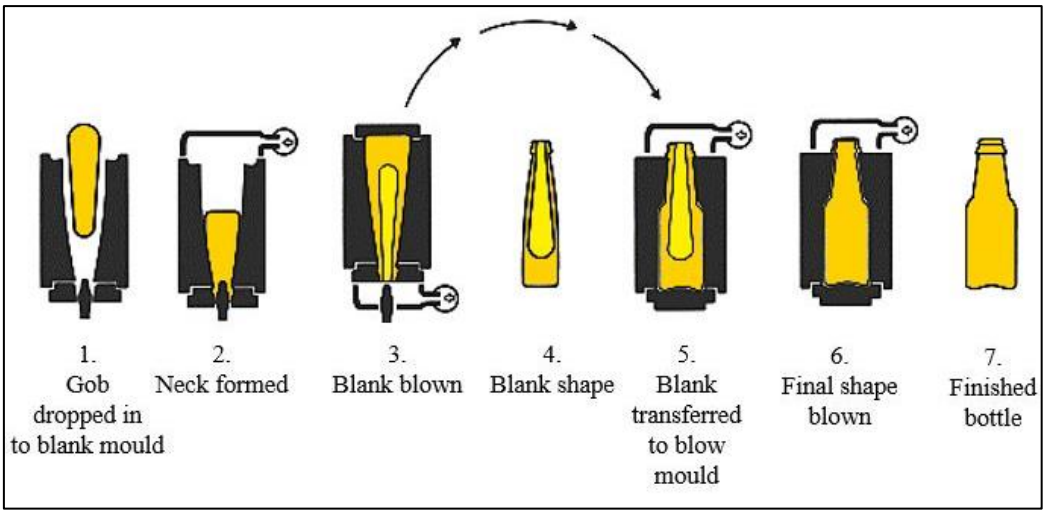

Figure 2.4: Schematic of the glass forming process.

2.2.3. Burners and Ports

A burner is equipment used for providing melting energy into the furnace. The chemical energy in the fuel is converted into heat energy by using burners through a series of chemical reactions in the combustion space. In glass furnaces, the main goal of a burner is to burn the fuel at maximum efficiency and to obtain the optimum heat flux profile to glass melt. It is the way to measure the performance of a burner which directly affects the production, hence, furnace efficiency. In practice, the desired flame in the glass furnace is a diffusion flame which is long, yellow, and quieter [9]. In addition to that, the reactions are incomplete to form soot particles which enhance radiative heat transfer in the combustion space.

Burners are selected and supplied based on furnace requirements. At the furnace design stage, the heat requirement specifies the number as well as the type of the burners. This stage investigates the parameters including the radius of the burner, the distance between the burner tip and glass surface, and burner angle which specifies the meeting point of air and fuel. In this study, a pipe-in-pipe burner, which is seen in Figure 2.5 [25], is used. It is made up of two coaxial hollow cylinders with different diameters. The purpose of this configuration enables gradual mixing of fuel and air. Hence, the region with maximum flame temperatures elongates along the furnace which means more effective heat transfer throughout the furnace.

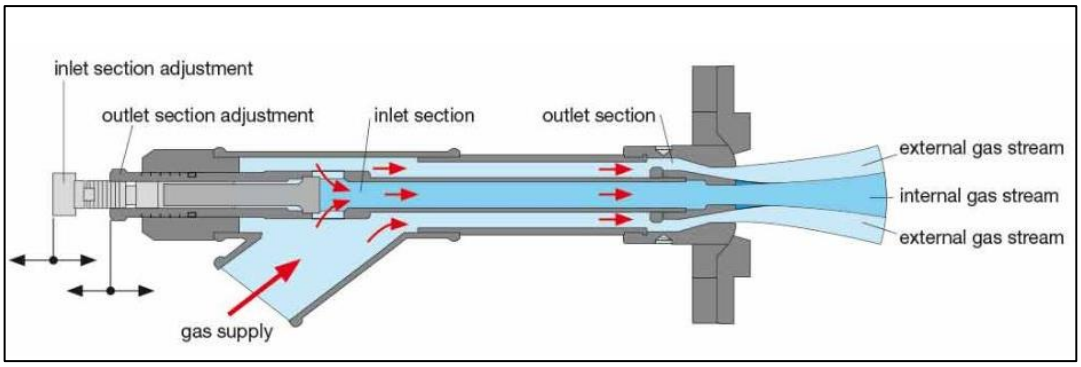

Figure 2.5: A typical pipe-in-pipe burner for glass furnace.

Fuel and air streams are introduced into the furnace in separate inlets. Air is introduced into the furnace through a hole called *port.* There are two ports present in an end-fired glass furnace. The first one is the inlet port which is an entrance for combustion air coming into the furnace. The second one is the outlet port which serves an exit for exhaust gases coming out of the furnace (Figure 2.6).

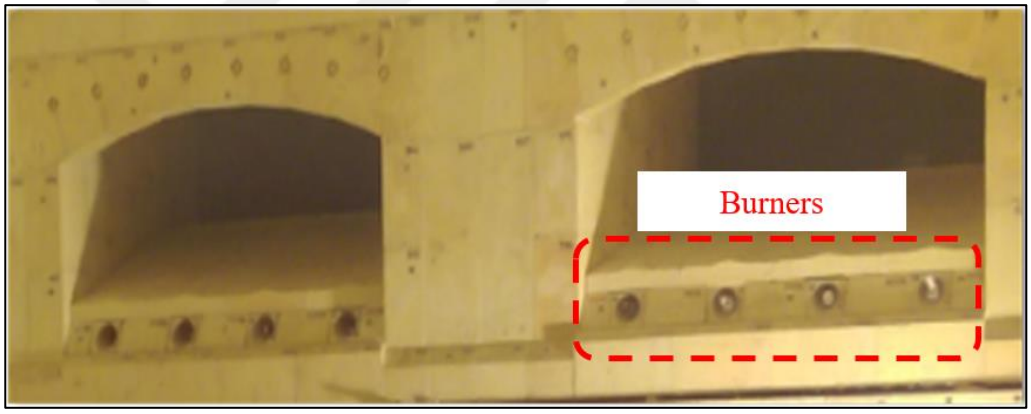

Figure 2.6: Inlet and outlet ports of a furnace.

The dimensions of the port also affect heat transfer inside the furnace. At the furnace design stage, parameters related to ports such as dimensions and angles are examined as well. Port is inclined towards the furnace with two angles which are at the top and the bottom, respectively. The top angle is called the *crown angle* while the bottom angle is called the *base angl*e. These angles provide optimum bending to help air to meet with fuel efficiently inside the furnace. In this study, these two angles in accordance with the burner angle are studied. The schematic of the angles relative to each other is given in Section 4.2.

2.3. Heat Transfer in Glass Furnaces

In today's world, natural gas is the dominant fuel that is supplied to furnaces in the glass industry. Natural gas consists of mainly methane (CH_4) and the rest of it is the mixture of alkanes. In most of the industrial furnaces, as well as the one used in this study, the simplified chemistry of Simple Chemically-Reacting Systems (SCRS) [26] is applied to define the combustion process taking place in an enclosure. Hence, only CO_2, H_2O, unburned and inert materials are included in the reactions. The model used in this thesis assumes that the reaction is irreversible, forward, a single-step mechanism (combustion of fuel and air) occurring fast. The following equations given below characterize the chemical reactions that take place in a furnace.

The combustion of fuel and air:

$$CH_4 + 2O_2 \rightarrow CO_2 + 2H_2O + Energy \tag{2.1}$$

The complete oxidation of carbon:

$$C + O_2 \rightarrow CO_2 + Energy \tag{2.2}$$

The complete oxidation of hydrogen:

$$2H_2 + O_2 \rightarrow 2H_2O + Energy \tag{2.3}$$

The incomplete oxidation of carbon:

$$2C + O_2 \rightarrow 2CO + Energy \tag{2.4}$$

The oxidation of carbon monoxide:

$$2CO + O_2 \rightarrow 2CO_2 + Energy \tag{2.5}$$

Heat transfer has an impact on both furnace efficiency and product quality. In this study, the efficiency is defined as the ratio of the amount of heat transferred from combustion space into the glass melt to the total energy given to the furnace. Although it is affected by several parameters, the major factor to increase energy efficiency is the effective heat transfer. As shown in Figure 2.7, heat is transferred in glass furnaces by radiation, convection, and conduction mechanisms. 90% of the heat is transferred

from flame to the glass melt is through radiation while a portion of heat is absorbed by furnace crown. In this way, the heated furnace crown contributes to heating of the glass by radiation as well.

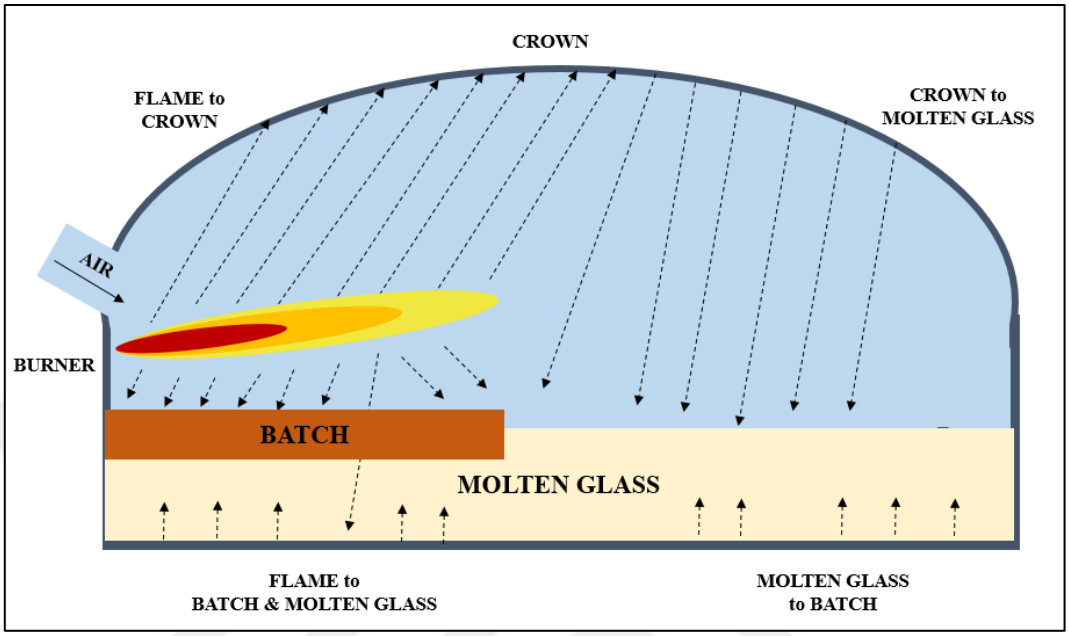

Figure 2.7: The representation of heat transfer mechanisms in glass furnaces.

Mixing of air and fuel controls the combustion process in the furnace. It affects flame stability, emissions, and the thermal release profile [9]. Rapid mixing is not favored in the furnace since it increases the temperature of the flame suddenly near the burner. On the contrary, slow mixing with a long flame is preferred due to gradual heat release along the furnace.

The molten glass is semi-permeable for heat transfer and optically thick. Based on the spectral properties of molten glass, propagation of radiation is present only in a short distance before absorption. The presence and concentration of the colorant metal ions in the raw material, especially ferrous ion (Fe^{+2}), significantly influences the heat transfer by radiation in the molten glass [12]. Radiation can be assumed as a diffusion process and explained by photon transmission in the glass melt. Therefore, Rosseland approach, given in Equation (2.6) and Equation (2.7), is valid and can be applied to define the heat transfer mechanism in the glass melt.

$$k_{eff} = k_c + k_r \tag{2.6}$$

$$k_r = \frac{16}{3}\frac{n^2\sigma_{SB}T^3}{\alpha_{Ross}} \quad (2.7)$$

where k_{eff} is the effective conductivity in the glass melt; k_c and k_r are the conductivity in conduction and radiation, respectively; n is the refractivity index of the glass melt; σ_{SB} is Stefan-Boltzmann constant; T is the temperature, and α_{Ross} is the gray absorption coefficient.

2.4. Literature Review on Energy Efficiency in Glass Melting Furnaces

In the past two decades, there has been a growing interest in both energy efficiency and the ways to reduce consumption of energy in glass melting furnaces. Glassmaking is an energy-intensive process as a result of a large amount of energy required to melt and refine glass. In the glass industry, significant progress has been made in reducing energy consumption over the years through advanced process control systems, the development and use of advanced refractory materials, and technologies such as oxy-fuel firing and electric boost which increase production capacity [27]. Improved technology has reduced the amount of fuel consumed per metric tons of glass melted by 25% since the early 1990s.

Despite a number of works exist in the literature on the reduction of energy consumption in glass manufacturing, most of them associated with research of glass companies' and not publicly available. Many works concentrate on benchmarking and statistical information in the glass industry around the world rather than design parameters of furnaces [4], [28]–[30]. Glass industry is known to be conservative and resistant to novel design changes since it includes complex physical and chemical processes. Therefore, in literature, there is much information is accessible in operational efficiency compared to the design stage of a glass furnace. In this section, some recent works on energy efficiency techniques proposed for glass furnaces are analyzed in terms of parameters in operation and design, respectively. Since the current thesis focuses only on a container glass furnace, studies dealing with container furnaces are presented here.

Studies targeted operational efficiency show that energy efficiency opportunities found in using recycled cullet, batch & cullet preheating, optimum air/fuel ratio and

flow rates, and model-based optimization. There are several studies investigating operational parameters to increase furnace efficiency. In a report of Glass Technology Services [31], the effect of using recycled cullet is discussed. It is estimated that production of one metric ton of glass from cullet requires 322 kWh less natural gas than the production of the same amount of glass from virgin raw materials. Another technique involving cullet is preheating of the batch and cullet. Beerkens [32] provided an explanation of using the batch & cullet preheating above 100^0C will eliminate the water content from the batch that yields no extra fuel needed in the furnace to evaporate the moisture in the batch. Thus, heat losses of flue gas decrease in parallel to decreasing water content in the flue gas. However, pay-back of the capital costs of batch & cullet preheating systems limits this application to furnaces. Another study of Beerkens [33] and Beerkens *et al.* [28] surveyed the energy consumption and furnace efficiencies for 123 furnaces including both container and float glass furnaces in different countries. They investigated in depth the effect of furnace size, the age of the furnace, cullet-to-batch ratio, specific load, and type of furnace and glass color. In this benchmarking study, they found that the most efficient container furnaces are the ones that are end-port-regenerative furnaces with a pull rate of 200-250 tons per day with an increase of 0.8-0.9% energy consumption each year while the glass color has a minimal effect on energy consumption.

In the same context, Lankhorst *et al.* [34] carried out a comprehensive study by applying their own energy balance model to a 220 tons per day container glass furnace that shows the potential energy savings with using varying percentages in these three parameters: excess air, batch moisture, and cold air leakage. Galitsky *et al.* [29] also analyzed energy improvement opportunities to reduce production costs in subtopics ranging from batch preparation and melting to auxiliary units and control systems in a glass manufacturing plant in the primary segments of the glass industry. For the melting process, they specified the minimizing of excess air down to the stoichiometric ratio which yields reduced energy loses. They also indicated to use a premix burner to hinder the infiltration of excess air and properly positioned burner. Nonetheless, they did not elaborate on the orientation of the burners that is the subject of this thesis. A recent study conducted by Dorn *et al.* [35] using an alternative measure to compare the energy consumption of five different glass furnaces. They developed a thermodynamic model to analyze scale dependencies on the specific energy consumption. However, since they proposed a novel technology under development,

microwave heating, the study is only an indication for energy consumption and needs to be worked through.

Reduction in energy consumption by operational alterations is achievable up to some point. To go beyond that, design parameters must be improved. Design parameters could be reviewed under two sections that are glass bath design and combustion space design, respectively. Since the context of this thesis is combustion space, the studies that investigated design parameters regarding only the combustion space are reviewed in this section. These parameters are the type of fuel/firing system, heat recovery systems, and furnace geometry, respectively that are emphasized in the following paragraphs.

The fuel will be used in the furnace determines the design of the combustion space. Type of glass and size of production specify the fuel type as well as energy market and the geographical location of the furnace. The fuel can be natural gas, electricity or combination of both. In addition to that, it can be an oxy-fuel firing system which analyzed in literature extensively. The fuel efficiency of oxy-fuel fired furnaces is significantly better than that of the conventional air-fired furnaces due to the elimination of the nitrogen in the combustion system. However, there are some restrictions on applications that are operational and maintenance costs of the oxygen firing and also redox state of the glass surface for colored glass production [36].

In literature, the design efficiency of glass furnaces is also linked to waste heat recovery systems. Since the exhaust gases have heat content that corresponds to 25-30% of the furnace energy input, advanced utilization of waste heat recovery in glass furnaces is a way to reduce the specific energy consumption and CO_2 emissions [32]. Recent studies explored the waste heat recovery with using batch and cullet pre-heating [37] and designing an effective regenerator for a specific furnace [38].

Furnace geometry is an important parameter to investigate the reduction of energy consumption in glass furnaces. Investigation of the burner positioning is a problem encountered in different industrial areas involving combustion [39]. In glass industry literature, one of the early studies [40] showed that changing the angle of injection changes the concentration of combustion gases and heat flux in the vicinity of the injector. The concept has been analyzed in detail for a container glass furnace by Eltutar *et al.*[41] and Uçar *et al.* [42] in terms of combustion space design that evaluates the parameters including the number of burners, symmetry/asymmetry of burners, burner angle, and port area. Considering this research, it is suggested that NO_X

and thermal efficiency are opposing values and the conditions should be optimized for each one. The other notable work carried out by Boerstoel [20] by his in-house developed code to compare just two cases both empirically and numerically which have a different burner and port angles. Studies targeting design efficiency, like the aforementioned studies [41] and [20], cover parametric analyses that concentrate on only limited cases since heavy computational time load of computational fluid dynamics (CFD) models and long tests.

The current study aims to further investigate three combustion space design parameters (burner angle, port crown angle, and port base angle) with 27 numbers of cases created by the method of full factorial design in their design range. By taking a step further, the extended upper and lower limits of the design range for these parameters are also examined.

3. MODEL DESCRIPTION OF THE STUDY

In the first section of this chapter, the application of mathematical modeling to glass furnaces is briefly summarized. In the following part, the description of the model used in this study for a container glass furnace is explained, and the solution procedure is presented. In the last part, the equations that govern the conservation equations of heat, mass, and momentum are given.

3.1. Mathematical Modelling in Glass Furnaces

Mathematical modeling is a vital tool in glass manufacturing for design, operation, and control of industrial processes due to the fact that investment cost, capital cost, and cost of trial production in glass industry are high. In addition to this, the lifetime of a furnace ranges between eight to fourteen years. Therefore, it is used for the design of new furnaces, optimization of existing ones, evaluation of product quality, and environmental considerations. In addition to that, it is utilized to investigate the effects of operational parameters independently and determine the possible ranges both for design and operation.

The basis of mathematical modeling in the glass industry is based on physical modeling since the second half of the twentieth century. Although significant contributions were done to development in glass industry through physical modeling, it was agreed that the identical physical modeling is hard to achieve since lots of complex physical and chemical processes were present in a furnace. Therefore, modeling and simulation in the glass industry is a powerful tool to comprehend the mechanisms occurring inside a furnace. For instance, as Cable [43] says;

"It is extremely difficult to find any type of feed to the furnace that could represent the melting of the batch, and radiant heat transfer could not be modeled in a system operating near room temperature."

Nowadays, nearly all modeling is carried out through mathematical modeling using advanced numerical techniques. Mathematical equations that explain the complex physical and chemical processes involving flow, heat, and mass transfer phenomena in glass manufacturing requires advanced numerical techniques and high computational time. Advancements in computing power, as well as numerical

techniques over the years, enable development of three-dimensional modeling in the glass industry. The prominent models in literature are beginning in one-dimension, then continued by Mase and Oda [44], Hrma [45], Xiqi and Viskanta [46], Ungan and Viskanta [47]–[51], Ungan [52], Schill [53], Carvalho [54], [55], Beerkens [32], [33], [56], [57], and Choudhary [21]. The historical perspective on the development of mathematical models in glass furnaces at industrial scale could be found in [21], [58], and [59].

3.2. Description of the Model

The study in this thesis is performed by using a special in-house developed code (The Glass Furnace Model) for glass melting furnaces. This code has been in use within Şişecam since the nineties. It was developed with Fortran programming language by Dr. Aydın Ungan [47]–[52], [60], [61] and purchased by Şişecam as an open code for development. With the contributions of researchers throughout the years in Modelling and Simulation Group in Şişecam Glass Science and Technology Center, the program has been improved to cover all the elements used in glass furnace design within the company. These improvements include parallelization twice in 2001 and 2014, respectively [62], [63].

The Glass Furnace Model consists of two parts for two solution domains. The first part is for the combustion space domain (COMBUS) and the second one is for glass bath domain (GLASS). The outputs of these programs are the inputs of the main program COMBINED as an initial value as seen in Figure 3.1 [Appendix B].

In GLASS and COMBUS, glass bath domain and combustion space domain are investigated separately. In COMBINED, both domains are investigated as a whole considering the effect of the batch. The energy requirement for the batch to melt is compared at each iteration with the total energy transferred from combustion space and molten glass into the batch. When the required and calculated energies are equal, the batch is assumed to melt.

Since this study examines the combustion atmosphere of the furnace, only combustion atmosphere calculations and descriptions are given in this section.

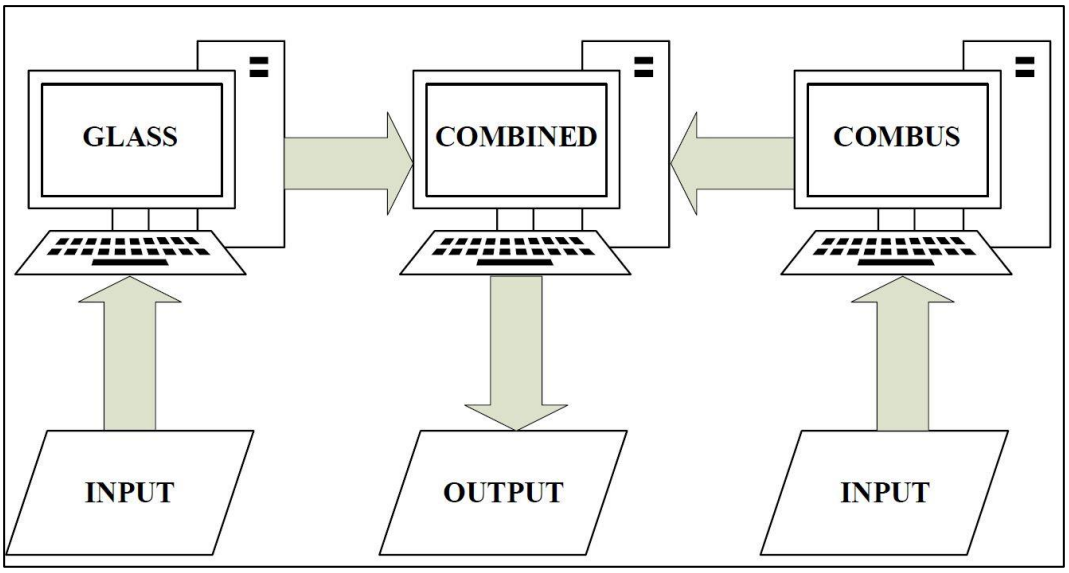

Figure 3.1: Description of the Glass Furnace Model used in the study.

The model, whose copyright fully belongs to Türkiye Şise ve Cam Fabrikaları A.Ş., and used in Domazet's thesis [63] as well, has been used with permission on the condition that the content remains confidential. The general scheme of the COMBUS algorithm, whose detailed information could not be published due to copyright issues, is seen in Figure 3.2 [63].

The solution method used in the glass furnace simulation is built upon SIMPLER solution method which is the revised version of SIMPLE (Semi-Implicit Method for Pressure-Linked Equations solution method) [64]. The turbulence model is Harlow and Nakayamas' [65] high Reynolds number k-ε two-equation model that is developed by Launder and Spalding [66] where k stands for specific turbulent kinetic energy and ε stands for turbulence dissipation rate. Radiation model is a finite volume method of Raithby and Chuie [67].

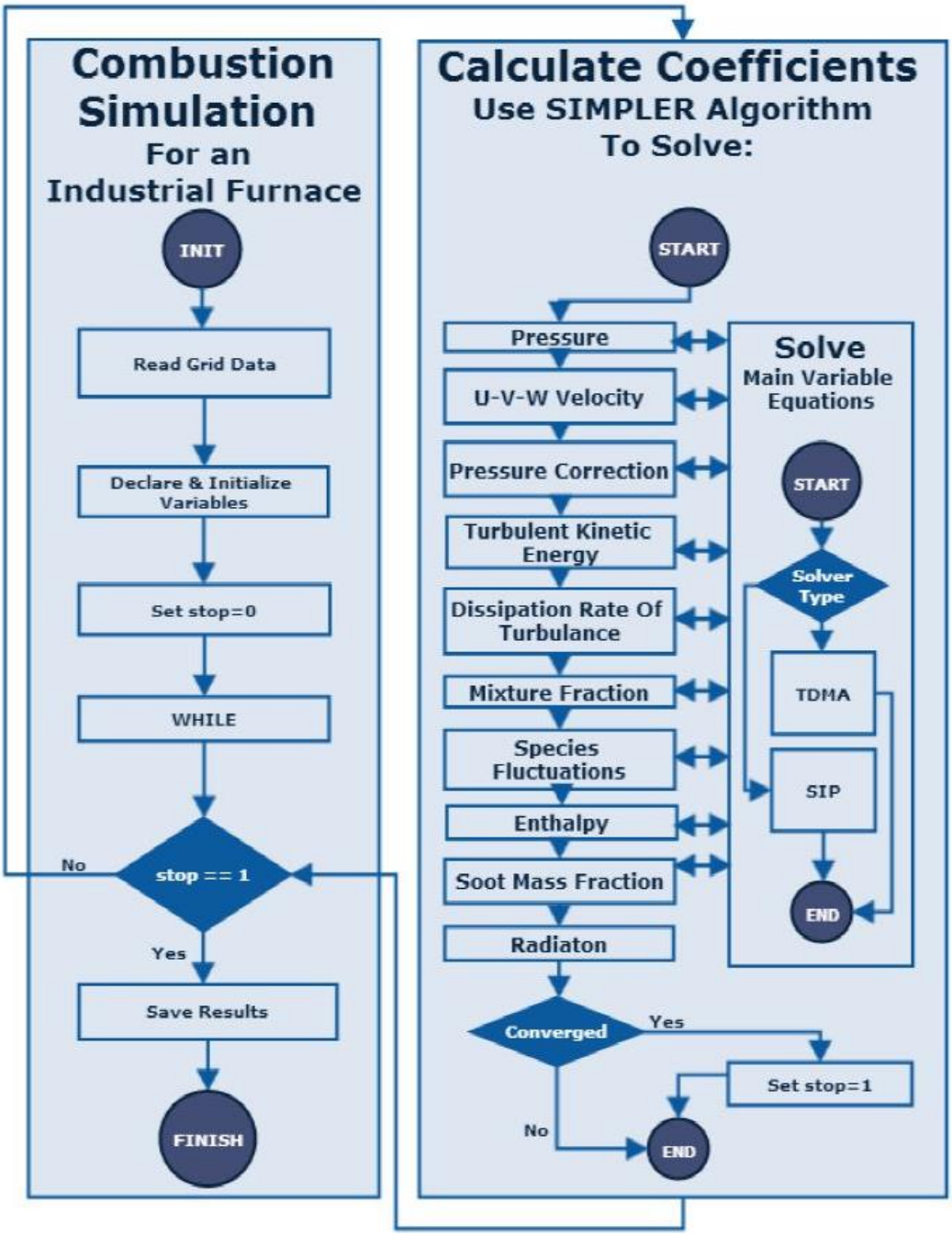

Figure 3.2: High-level structure of the Glass Furnace Simulation program.

Firstly, COMBUS program starts by reading a finite difference grid and the variables are initialized. Then, the execution steps that are listed below are computed iteratively in a loop by using the results from the previous iteration until convergence criteria are reached. In this study, the convergence criteria are $1x10^{-6}$ for mass balance and $1x10^{-2}$ for energy balance. Nine execution steps given below are performed in a single iteration. The SIMPLER algorithm that is applied to solve the linear systems of equations in each step excluding radiation is based on Tri-Diagonal Matrix Algorithm

(TDMA) [68] or SIP linear system solvers of Stone's [69]. In radiation calculations, the Finite Volume Method (FVM) is applied to discretize the differential equations. Detailed information on both SIMPLER and FVM algorithm could be found in [62]. COMBUS solves mass, energy, and momentum conservation equations that are presented in Section 3.3. Execution steps are given below.

- U-V-W Velocity
- Pressure Correction
- Turbulent Kinetic Energy Calculation
- Dissipation Rate of Turbulence
- Mixture Fraction
- Species Fraction
- Enthalpy
- Soot Mass Fraction
- Radiation

3.3. Governing Equations

In this section, characteristics of flow and heat transfer phenomena are emphasized. The transport and constitutive equations applied to the mathematical model used in this study are summarized.

The field of mathematical modeling of combustion chambers consists of complex physical models which require advanced numerical solution techniques. Relevant equations of the models are in partial differential forms and expressed in three-dimensional spatial coordinates. In this study, a multi-stream, turbulent, compressible flow with chemical reaction, significant thermal radiation in combustion space are present.

The partial differential equations that define the complex physical phenomena in a glass furnace need to be discretized to solve the problem. In order to do so, the domain is divided into grids that characterize the solution. These equations are solved by line-by-line procedure after derivation by integration of the governing differential equations over finite-control volume. Since this study examines the combustion atmosphere of the furnace, only the equations governing the combustion atmosphere are given in this section.

The solution is carried out for each unit volume in the furnace by SIMPLER algorithm that is explained in Section 3.3. Representation of a unit volume is presented in Figure 3.3

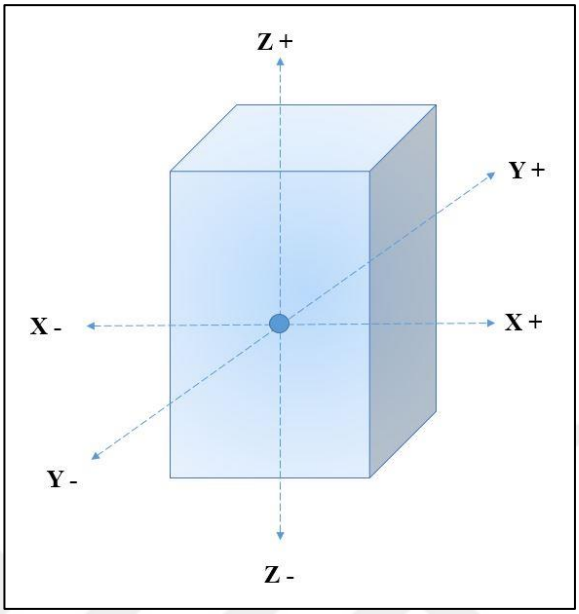

Figure 3.3: The representation of a unit volume for numerical solution.

Several assumptions in combustion space and glass melt listed below are made to simplify the complex structure of the model:

- Combustion gas is grey with having an emissivity, $\varepsilon_{g.}$
- The gaseous flow in combustion space is a turbulent flow.
- All the thermophysical properties of the gaseous flow in combustion space are expressed as a function of temperature.
- The molten glass is incompressible, viscous and Newtonian fluid and laminar flow.
- The density of the glass melt is assumed constant since only small variation is present over the temperature range in the furnace, from 1000 K to 2000 K [70]. Variation in density is considered only in the buoyancy term.
- The other thermophysical properties of the molten glass are based on glass composition and expressed as a function of temperature. Please note that the values of thermophysical properties are not open to the public due to confidentiality.
- Rosseland approach is valid in the molten glass that is explained in detail in Section 2.3 Heat Transfer in Glass Furnaces.
- Governing equations are time-independent (steady-state).

A three-dimensional conservation equation for continuity inside the furnace is given in Equation (3.1).

$$\frac{\partial \rho u}{\partial x} + \frac{\partial \rho v}{\partial y} + \frac{\partial \rho w}{\partial z} = 0 \tag{3.1}$$

A three-dimensional conservation equation that describes the energy and momentum transfer in both glass bath and combustion space is given in Equation (3.2).

$$\frac{\partial(\rho u\varphi)}{\partial x} + \frac{\partial(\rho v\varphi)}{\partial y} + \frac{\partial(\rho w\varphi)}{\partial z} = \frac{\partial}{\partial x}\left(\Gamma\varphi \frac{\partial \varphi}{\partial x}\right) + \frac{\partial}{\partial y}\left(\Gamma\varphi \frac{\partial \varphi}{\partial z}\right) + \frac{\partial}{\partial z}\left(\Gamma\varphi \frac{\partial \varphi}{\partial z}\right) + S_{\varphi} \tag{3.2}$$

where x, y, and z are the space coordinates; *u, v, and w* are the velocity components in x, y, z directions, respectively; φ is the dependent variable; ρ is the mixture density in the combustion atmosphere; Γ is the exchange coefficient for the variable φ; and S is the source term.

General form of the governing differential equations except for radiation are tabulated in Table 3.1 for each dependent variable (Please see "List of Abbreviations and Acronyms" for the definitions of symbols used in this table).

For the equations given in Table 3.1, instantaneous values of flow variables and molecular values of exchange coefficients are used for laminar flows while time average values of flow variables and effective values of the exchange coefficients are used for turbulent flows. Effect of turbulence included in effective transport coefficients [46]-[52].

Table 3.1: Equations solved in the model.

Equation	$\boldsymbol{\varphi}$	$\boldsymbol{\Gamma_{\varphi}}$	$\boldsymbol{S_{\varphi}}$	
Continuity	1	0	0	(3.3)
x-momentum	u	μ	$-\frac{\partial p}{\partial x}+\frac{\partial}{\partial x}\left(\mu\frac{\partial u}{\partial x}\right)+\frac{\partial}{\partial y}\left(\mu\frac{\partial v}{\partial x}\right)+\frac{\partial}{\partial z}\left(\mu\frac{\partial w}{\partial x}\right)$	(3.4)
y-momentum	v	μ	$-\frac{\partial p}{\partial y}+\frac{\partial}{\partial x}\left(\mu\frac{\partial u}{\partial y}\right)+\frac{\partial}{\partial y}\left(\mu\frac{\partial v}{\partial y}\right)+\frac{\partial}{\partial z}\left(\mu\frac{\partial w}{\partial y}\right)$	(3.5)
z-momentum	w	μ	$-\frac{\partial p}{\partial z}+\frac{\partial}{\partial x}\left(\mu\frac{\partial u}{\partial z}\right)+\frac{\partial}{\partial y}\left(\mu\frac{\partial v}{\partial z}\right)+\frac{\partial}{\partial z}\left(\mu\frac{\partial w}{\partial z}\right)$	(3.6)
Turbulent kinetic energy	k	$\mu_{eff}/\sigma_{k,\,eff}$	$G_k-\rho\varepsilon$	(3.7)
Turbulent dissipation	ε	$\mu_{eff}/\sigma_{\varepsilon}$	$(C_1G_k-C_2\rho\varepsilon)\varepsilon/k$	(3.8)
Mixture fraction	f	μ/σ_{eff}	0	(3.9)
Species fluctuation	g	μ/σ_g	$C_{g,1}\mu_t\left[\left(\frac{\partial f}{\partial x}\right)^2+\left(\frac{\partial f}{\partial y}\right)^2+\left(\frac{\partial f}{\partial z}\right)^2\right]-C_{g,2}\rho\frac{\varepsilon}{k}g$	(3.10)
Soot mass fraction	m_s	μ/σ_{ms}	$S_{s,f}-S_{s,0}$	(3.11)

Thermal radiation is the dominant heat transfer mechanism in glass furnaces due to the high-temperature profile in the furnace. The computation of thermal radiation is a complex problem since the presence of the radiation brings a set of coupled differential and integral equations. In this study, the radiation model is a finite volume method of Raithby and Chuie [67]. The Equation (3.12) defines the convection-diffusion equation that is arranged for the divergence of the radiation flow vector $\boldsymbol{q_r}$ ***(r)*** that stands for the heat produced by radiation at each point of the solution domain is given below. In the following Equations from (3.12) to (3.15), symbols that are written in *bold-italic* represents the vectored form [59].

$$\rho c\left(\frac{\partial T}{\partial t}+\boldsymbol{u}\nabla T\right)=\nabla(\lambda\nabla \mathrm{T})-\nabla \boldsymbol{q_r} \tag{3.12}$$

where T is the temperature, ρ is the density, c is the specific heat, λ is the heat conductivity (phononic), and $\boldsymbol{u}$ is the velocity field. The last term in the equation, $\boldsymbol{q_r}$ ***(r),*** is obtained in the following ways shown in Equation (3.13) and Equation (3.14).

$$\boldsymbol{\Omega}\nabla \mathrm{I}(\boldsymbol{r},\boldsymbol{\Omega},\nu)=\kappa\,(\nu,\mathrm{T})\,[\mathrm{B}\big(\mathrm{T}(\boldsymbol{r})\big)-\mathrm{I}(\boldsymbol{r},\boldsymbol{\Omega},\nu)] \tag{3.13}$$

where;

$\boldsymbol{I}(\boldsymbol{r},\boldsymbol{\Omega},\nu)$: The spectral radiation intensity in the equation of radiation transport where $\boldsymbol{r}$ indicates a point with a direction in space $\boldsymbol{\Omega}$ and frequency ν

$\mathrm{B}\big(\mathrm{T}(\boldsymbol{r})\big)$: The Plank function

$\kappa\,(\nu,\mathrm{T})$: The absorption coefficient

Thus, the radiation flow vector, $\boldsymbol{q_r}$ ***(r)***, is computed in Equation (3.14).

$$\mathbf{q_r}(\mathbf{r})=\int_0^{\infty} d\nu \int_{\Omega=4\Pi} d\Omega\ \ \boldsymbol{\Omega I}(\boldsymbol{r},\boldsymbol{\Omega},\nu) \tag{3.14}$$

Rearranging Equation (3.14), Equation (3.15) is obtained.

$$\nabla\mathbf{q_r}(\mathbf{r})=\int_0^{\infty} d\nu\,\kappa \int_{\Omega=4\Pi} d\Omega\,[\mathrm{B}\big(\mathrm{T}(\boldsymbol{r})\big)-\mathrm{I}(\boldsymbol{r},\boldsymbol{\Omega},\nu)] \tag{3.15}$$

From now on, in the following equations from (3.16) to (3.23), boundary conditions are given.

The boundary condition for refractories which govern the heat loss from walls to ambient is expressed in Equation (3.16).

$$-k_{eff}\frac{\partial T}{\partial n} = U\,(T - T_{amb}) \tag{3.16}$$

where U is the overall heat transfer coefficient including conduction resistance across the refractories, natural convection at ambient temperature, and radiation resistance to the surroundings.

Velocity boundary conditions at the bottom and the four walls are no slip and impermeable boundary conditions as seen in Equation (3.17).

$$u = v = w = 0 \tag{3.17}$$

Combustion gas-glass melt interface is described in from Equation (3.18) to Equation (3.20). Molten glass is surrounded by refractories at the bottom and four sides. The top surface is both partially covered by the batch and partially exposed to radiation from the combustion atmosphere. The velocity boundary condition at the combustion gas-glass melt interface, continuity of the normal and traverse components of velocity and shear stress are used.

The viscous stresses of the combustion gases are negligible due to the fact that the viscosity of molten glass is significantly bigger than the viscosity of combustion gases. Therefore, the equation is expressed as;

$$p = p_0 \tag{3.18}$$

$$\mu\frac{\partial u}{\partial z} = \mu\frac{\partial v}{\partial z} = 0 \tag{3.19}$$

Vertical velocity component is assumed to equal zero at the glass surface.

$$w = 0 \tag{3.20}$$

Batch-glass melt interface is described in from Equation (3.21) to (3.23).

Batch melting modeling is one of the challenging parts in the modeling of glass melting furnaces. A general application in literature assumes non-slip boundary conditions for the momentum equations of the glass melt in the horizontal direction. Also, a melting velocity in the vertical direction and a temperature distribution on the surface of the batch and glass melt interface are assumed as given in from Equation (3.21) to Equation (3.23).

$$u = v = 0 \tag{3.21}$$

$$w = w_{melting} \tag{3.22}$$

$$T = T_{batch} \tag{3.23}$$

The melting of raw materials *(batch)* is comprised of many chemical reactions that are advanced forms of physicochemical processes taking place from 1000 K to 1500 K [48]. Therefore, the melting of the batch is not to be formulated as an ordinary phase change from solid to liquid. The general energy balance for the batch is written in Equation (3.21) [70].

$$Q'_{melt \rightarrow batch} L_b + \int_0^L q''(x) W dx = \dot{m}_{pull} \Delta H_{melt} \tag{3.21}$$

where $Q'_{melt \rightarrow batch}$ is the heat transfer rate from glass melt to the batch per unit length of the batch, L_b is the batch length, W is the width of the furnace, $q''(x)$ is the heat flux from the combustion atmosphere to the molten glass surface, m_{pull} is the capacity of the furnace per day *(pull rate)*, ΔH_{melt} is the enthalpy per unit mass of molten glass to have desired glass at the melting temperature from the temperature that raw materials are introduced to the furnace.

4. PARAMETRIC STUDY

In this chapter, the study cases that are specified based on factorial design are described. The input conditions of the furnace variables and the geometry of the furnace that is subject to this study are introduced. The chapter is concluded with the gridding structure of both the combustion atmosphere and the glass bath of the furnace.

4.1. The Method of the Study

In this study, three combustion space design parameters related to a conventional container glass furnace have been investigated to obtain a statistical relationship between these parameters to increase energy efficiency. In order to do so, 27 numbers of cases with varying burner angle, port crown angle, and port base angle were examined. By doing so, it is aimed to provide a practical approach at the design stage of a container glass furnace in terms of combustion space to enhance energy efficiency.

The model and the solution procedure explained in Section 3.3 were used to analyze the cases. The investigation range of angles for each parameter was selected based on real container glass furnaces that are in operation in both Turkey and abroad. The beyond of these ranges, except burner angle, exceeds industrial limits and are not in use under today's conditions. In the case of burner angle, for container glass furnaces, the angle goes up to 13^0 in some cases. The burner angle is adjusted according to the port angles, amount of fuel required to melt the batch and capacity of the furnace. Therefore, it is not the one that sets all criteria in a glass furnace.

Table 4.1: Investigation angles for each parameter.

Independent variables	**Codes**	**Range and Levels (Coded)**		
		-1	**0**	**1**
Burner angle	x_1	5	7	9
Port crown angle	x_2	10	20	30
Port base angle	x_3	10	15	20

The 3-level full factorial experimental design; a factorial arrangement with *k* factors, which is shown as 3^k, was employed in the study. Including all possible combinations, 27 number of experiments (=3^3) was required for 3-level/3-factorial experimentation. Independent factors are burner angle, port crown angle, and port base angle. The independent factors were coded to (-1, 0, 1) interval where -1, 0, and 1 indicate the low, intermediate, and high levels, respectively. The ranges of the variables are given in Table 4.1 while the experimental cases are tabulated in Table 4.2.

Table 4.2: The experimental cases.

Run	**Codes**			x_1	x_2	x_3
1	-1	-1	-1	5	10	10
2	-1	0	-1	5	20	10
3	-1	1	-1	5	30	10
4	0	-1	-1	7	10	10
5	0	0	-1	7	20	10
6	0	1	-1	7	30	10
7	1	-1	-1	9	10	10
8	1	0	-1	9	20	10
9	1	1	-1	9	30	10
10	-1	-1	0	5	10	15
11	-1	0	0	5	20	15
12	-1	1	0	5	30	15
13	0	-1	0	7	10	15
14	0	0	0	7	20	15
15	0	1	0	7	30	15
16	1	-1	0	9	10	15
17	1	0	0	9	20	15
18	1	1	0	9	30	15
19	-1	-1	1	5	10	20
20	-1	0	1	5	20	20
21	-1	1	1	5	30	20
22	0	-1	1	7	10	20

Table 4.2: Continuation of the table.

Run	Codes			x_1	x_2	x_3
23	0	0	1	7	20	20
24	0	1	1	7	30	20
25	1	-1	1	9	10	20
26	1	0	1	9	20	20
27	1	1	1	9	30	20

The method followed in this study is to analyze 27 cases statistically provided above using Minitab statistical software [71]. For this purpose, the Glass Furnace Model described in Section 3.3 was used. It was run for each case, and the energy efficiency of the furnace was calculated according to the run results. The energy efficiency is described in Equation (4.1).

$$\eta\ (\%) = \frac{Energy\ transferred\ into\ the\ glass\ bath}{Total\ energy\ supplied\ to\ the\ furnace} x\ 100 \qquad (4.1)$$

Although the total energy supplied to the furnace is constant for all cases, energy transferred into the glass bath changes due to varied angles of port and burner in each case. The input parameters of the furnace used in the study, which is taken from an industrial container glass furnace, are tabulated in Table 4.3 and constant for 27 cases.

Table 4.3: Input parameters of the container glass furnace used in the study.

Input	Value
Capacity (tons/day)	350
Cullet (%)	20
Color	Clear
Air flow rate (m^3/s)	29.671
Fuel flow rate (m^3/s) [1]	0.5719
The temperature of air (^0C)	1200
The temperature of fuel (^0C)	27

[1] The amount of fuel (natural gas) equals 16442.05 kW power supplied into the furnace.

After having an energy efficiency of the furnace for each case, the statistical analysis was performed. The analysis is divided into two parts: (1) The investigation to obtain cubic equation model; (2) The investigation to obtain quadratic equation model, respectively to obtain a statistical relationship between three combustion space design parameters in a container glass furnace.

4.2. The Geometry of the Furnace

A regenerative end-fired container glass furnace with 9.10 m in width and 15.15 m in length was studied for three combustion space design parameters. The furnace with four burners is symmetric along the length. The capacity of the furnace is 350 metric tons per day, clear glass.

There are several combustion space design parameters in glass furnaces. The geometrical configuration of the parameters that are subjected to this study, which are burner angle, port crown angle, and port base angle, is given in Figure 4.1.

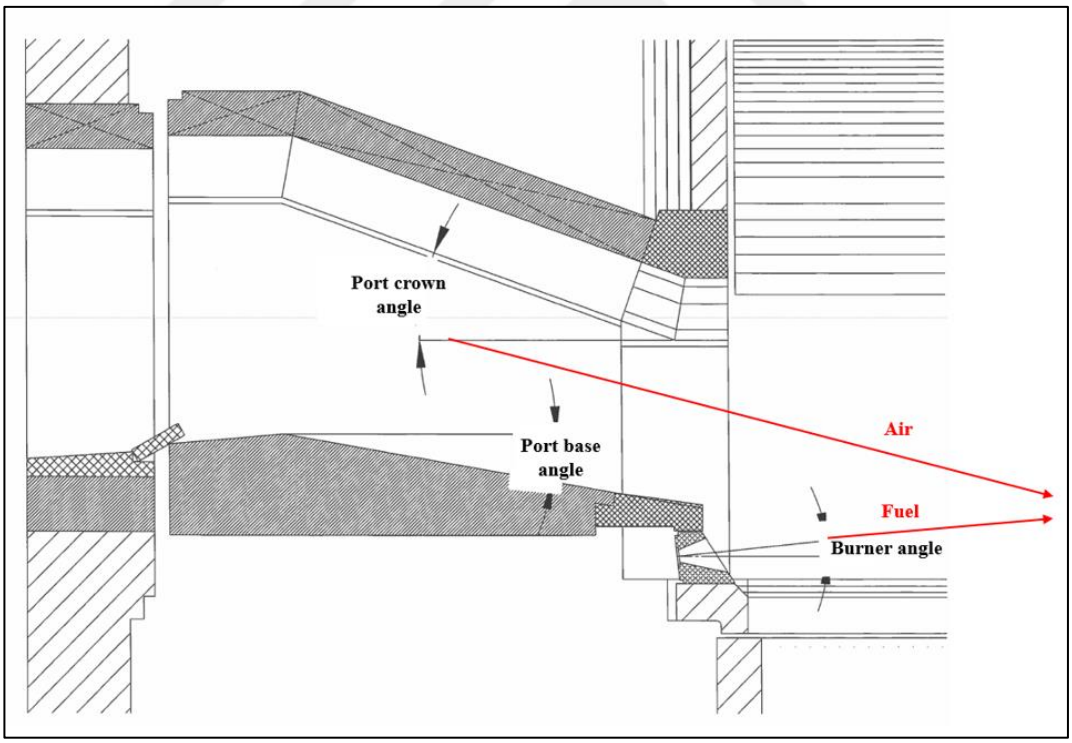

Figure 4.1: The geometrical configuration of port and burner.

In addition to that, the other parameters related to combustion space of a glass furnace are seen in Figure 4.2.a while the combustion space image taken from a real

industrial furnace is shown in Figure 4.2.b. All the parameters in combustion space shown in Figure 4.2.a, except angles of ports and burners, are constant in the entire study and tabulated in Table 4.4. Please note that the numerical values of these parameters are not open to the public due to confidentiality. Lastly, the glass bath is the same for all cases.

Table 4.4: Combustion space parameters related to ports and burners.

Number	**Parameter**
1	The distance between burner and port
2	The distance between two burners
3	The distance between burner and glass surface
4	The distance between port and glass surface
5	The radius of the port crown
6	Height of port
7	Width of port
8	The radius of the burner

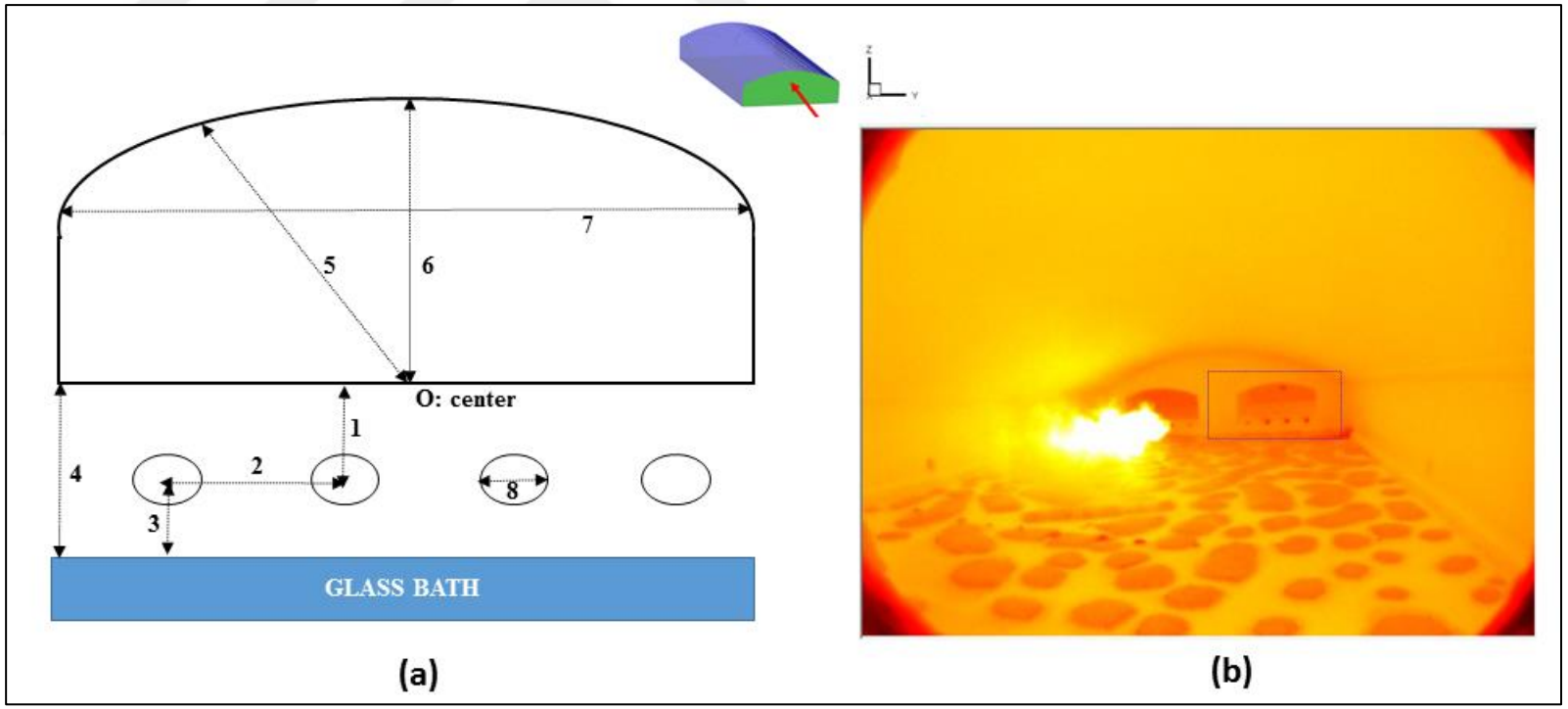

Figure 4.2: a) Representation of combustion space parameters related to ports and burners b) The combustion atmosphere of a real industrial furnace.

4.3. Gridding of the Model

The partial differential equations that define the complex physical phenomena in a glass furnace need to be discretized to solve the problem. In order to do so, the domain is divided into grids that characterize the solution (Appendix C). The geometry is divided into structured and rectangular shaped grids in Cartesian coordinates (Figure 4.3). In order to avoid excessive CPU time and memory usage while maintaining a sufficient resolution, the local grid refinements are performed in the regions having steep gradients such as burner and port (Figure 4.4). 240312 number of grids are used in combustion space while 106784 number of grids are used in glass bath. The gridding of the glass bath is coarser than the combustion space, except for the inlet-outlet of the furnace, since the main interest of this study is combustion space (Figure 4.5). The visualization of the grid structures is drawn by a CFD visualization programmed called TECPLOT [75].

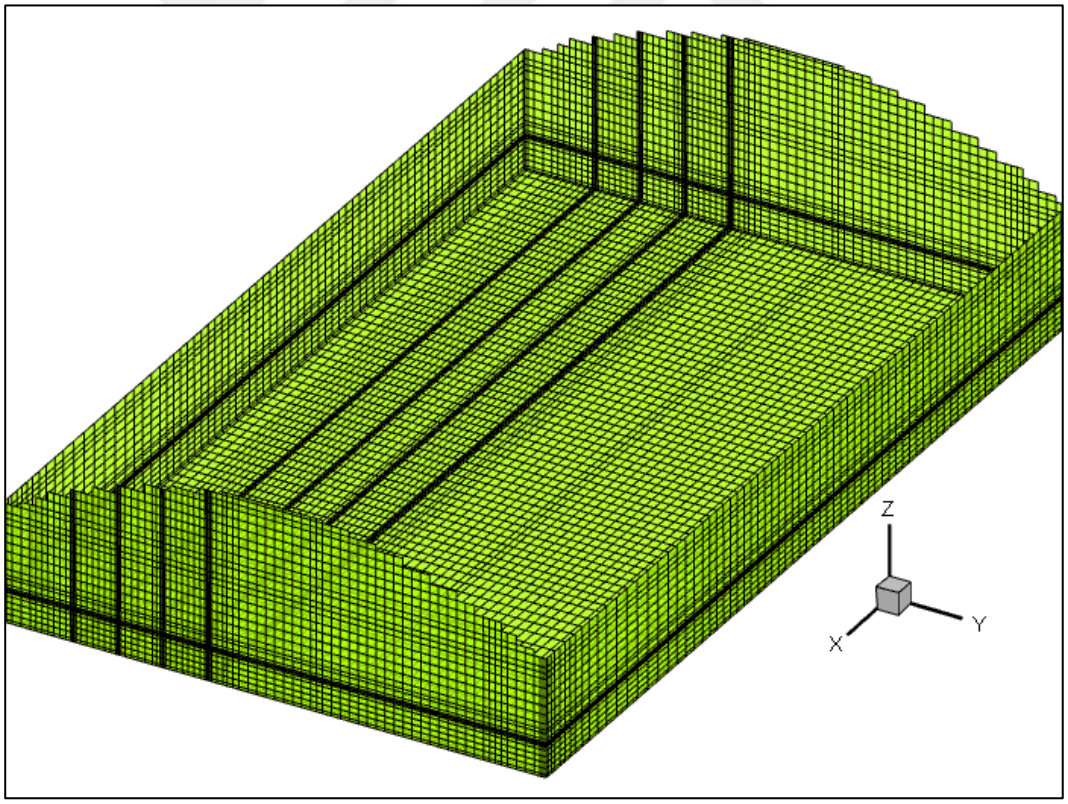

Figure 4.3: Grid structure of the combustion space solution domain.

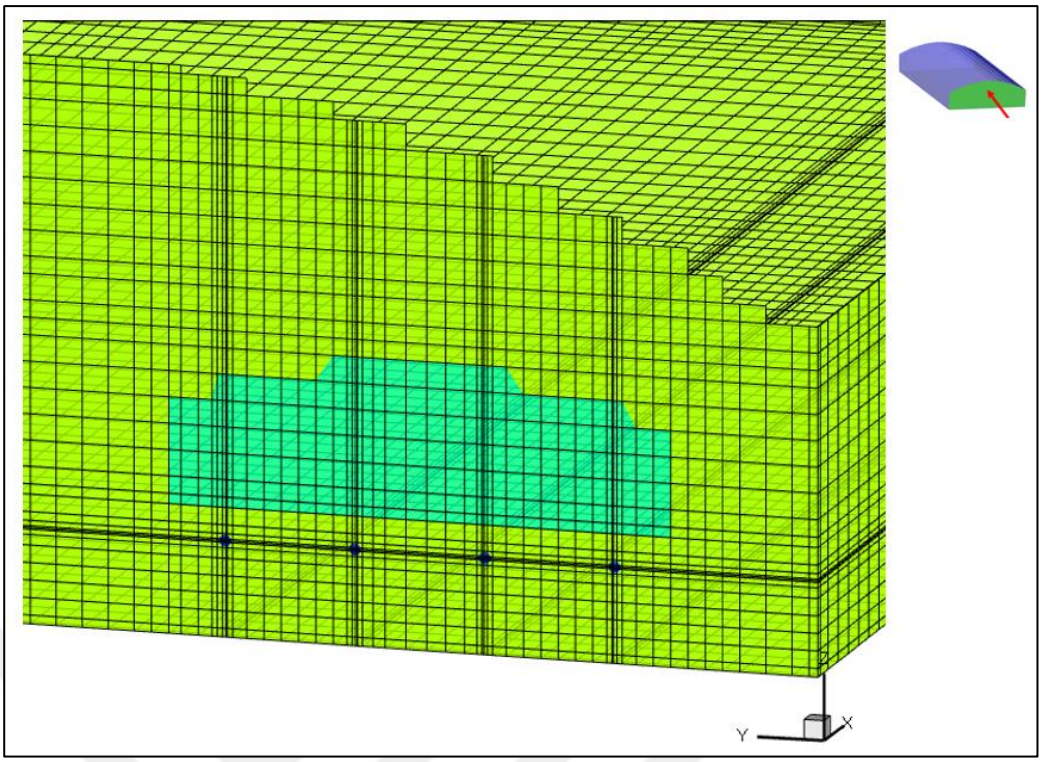

Figure 4.4: Finer grid structure around the burners and ports.

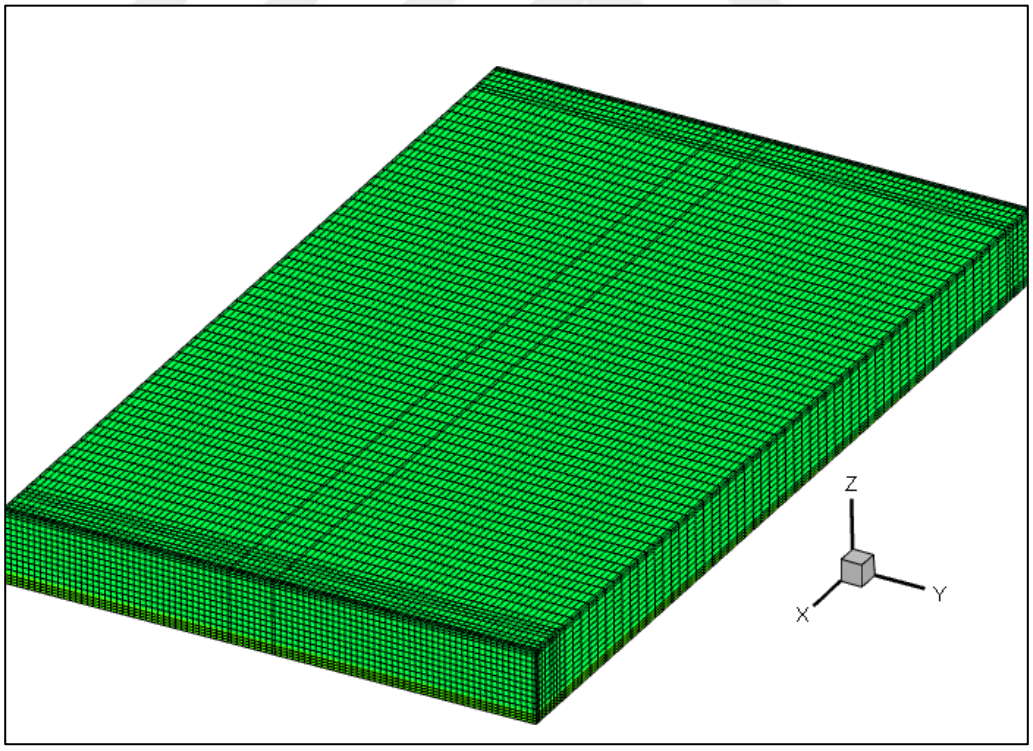

Figure 4.5: Grid structure of the glass bath solution domain.

In glass bath, the inlet and outlet of the furnace are also meshed denser as seen in Figure 4.5.

5. RESULTS AND DISCUSSIONS

In this chapter, a statistical analysis is performed to investigate the interactive effects of three combustion space design parameters that are burner angle, port crown angle, and port base angle of a container glass furnace. The aim is to decrease the required number of computational runs at the design stage of a furnace by providing a practical approach. Firstly, a total number of 27 experimental cases determined by full factorial design is set to run computationally and the results of energy efficiency data are fitted to the empirical third-order polynomial model for maximum energy efficiency. Secondly, 27 experiments are classified into three groups, each having nine cases, according to their port base angle. Results of energy efficiency data are fitted to the empirical second-order polynomial model for maximum energy efficiency for each group while burner angle and port crown angle vary. Then, optimization is carried out to find the optimal point at which the maximum furnace efficiency obtained. A new computational run is performed for the optimal point for each analysis. The energy efficiency difference between the computational simulation and statistical analysis is stated after a new run for each case. Next, the graphical representations of the combustion space results are presented. Lastly, evaluation of the results in terms of economic sense is performed at the end of the chapter.

5.1. General

In this study, the total energy supplied to the furnace is constant for all cases. However, energy transferred into the glass bath changes for each case due to varied burner angle, port crown angle, and port base angle. The results of the computational runs are presented in Table 5.1 with x_1, x_2, and x_3 state the independent variables that denote burner angle, port crown angle, and port base angle, respectively. Iterations of computational analysis, which is three dimensional and steady state, continued until residuals reach $1x10^{-6}$ for mass balance and $1x10^{-2}$ for energy balance. It took approximately 2100 minutes for each case with a different number of iterations (Appendix E).

Table 5.1: Results of computational runs.

Run	Burner angle	Port crown angle	Port base angle	Efficiency (η) (%)	Energy transferred into the glass bath (kW)
	x_1	x_2	x_3		
1	5	10	10	57.9050419	9520.7771
2	5	20	10	58.89480826	9676.5150
3	5	30	10	59.22825205	9738.3400
4	7	10	10	58.21597876	9571.9015
5	7	20	10	58.85183309	9683.4490
6	7	30	10	59.17907327	9730.2540
7	9	10	10	58.54010254	9625.1941
8	9	20	10	59.12152571	9720.7920
9	9	30	10	59.27147050	9745.4460
10	5	10	15	57.19556720	9404.1249
11	5	20	15	58.87664751	9680.5290
12	5	30	15	59.29773851	9749.7650
13	7	10	15	57.22801570	9409.4601
14	7	20	15	59.03122068	9705.9440
15	7	30	15	59.28684571	9747.9740
16	9	10	15	57.29486685	9420.4518
17	9	20	15	58.85076267	9676.2730
18	9	30	15	59.22732759	9738.1880
19	5	10	20	58.43950013	9608.6530
20	5	20	20	58.97478003	9696.6640
21	5	30	20	59.26841735	9744.9440
22	7	10	20	58.69719303	9651.0230
23	7	20	20	59.28209569	9747.1930
24	7	30	20	59.38663860	9764.3820
25	9	10	20	58.31637073	9588.4080
26	9	20	20	59.01423983	9703.1520
27	9	30	20	59.39008708	9764.9490

The Glass Furnace Model described in Section 3.3 was used to obtain energy efficiency of the furnace for each case. In the context of this study, the energy efficiency (η) is described in Equation (5.1) given below.

$$\eta\ (\%)=\frac{\text{Energy transferred into the glass bath}}{\text{Total energy supplied to the furnace}}\ \text{x}\ 100 \qquad (5.1)$$

After computational runs had completed, energy efficiency for each run calculated by employing Equation (5.1) stated above. Then, statistical analysis was carried out for energy efficiency results. Firstly, energy efficiency results were fitted to the empirical third-order polynomial model for maximum energy efficiency. Then, the same procedure was applied to the second-order polynomial model. The results of the statistical analysis are presented in following sub-chapters for both cubic equation model and the quadratic equation model, respectively.

5.2. Empirical Cubic Equation

In this section, the relationship between 3 independent variables and the response was established with applying the cubic model. The general form of the cubic equation model is given in Equation (5.2). Here, coded variables x_i's are the independent variables (burner angle, port crown angle, and port base angle) and y is the dependent response variable (energy efficiency), and β_i's are the coefficients of the equation terms.

$$\begin{aligned} y = {} & \beta_0 + \beta_1 x_1 + \beta_2 x_2 + \beta_3 x_3 + \beta_{12} x_1 x_2 + \beta_{13} x_1 x_3 + \beta_{23} x_2 x_3 + \beta_{11} {x_1}^2 \\ & + \beta_{22} {x_2}^2 + \beta_{33} {x_3}^2 + \beta_{121} {x_1}^2 x_2 \\ & + \beta_{122} x_1 {x_2}^2 + \beta_{131} {x_1}^2 x_3 \\ & + \beta_{133} x_1 {x_3}^2 + \beta_{232} {x_2}^2 x_3 + \beta_{233} x_2 {x_3}^2 + \beta_{123} x_1 x_2 x_3 \\ & + \beta_{111} {x_1}^3 + \beta_{222} {x_2}^3 + \beta_{333} {x_3}^3 \end{aligned} \qquad (5.2)$$

Adequacy of the empirical model was confirmed by analysis of variance (ANOVA). In the following sub-chapters, ANOVA analysis was performed for both the cubic equation model and the quadratic equation model, respectively. The coefficients of the general equations were obtained for each analysis. It is assumed that

the correlation coefficient (R^2) is indicative of the strength of the statistical relationship.

5.2.1. 27 Cases

Firstly, the energy efficiency results of 27 cases stated in Section 5.1 were analyzed statistically to establish a cubic equation model. Minitab was used for this purpose. The result of the analysis is a 17-coefficient regression model as given in Equation (5.3). The probability of the individual coefficients and the analysis of variance of the resulting model are given Table 5.2. In this study, the significance level was chosen as 0.05 which means above this limit is considered as rejection region in terms of the null hypothesis. In fact, as Raykov and Marcoulides say [72], there is no restriction on the particular choice of significance level between zero and one. Selection of significance level depends on the research question and the conditions under which the interpretation is to be made.

$$\begin{aligned} y = {} & 61.58 + 0.332x_1 - 0.091x_2 - 0.866x_3 + 0.00342{x_1}^3 \\ & - 0.000085{x_2}^3 + 0.001097{x_3}^3 + 0.00119{x_1}^2x_2 \\ & + 0.000094x_1{x_2}^2 - 0.00748{x_1}^2x_3 + 0.00156x_1{x_3}^2 \\ & + 0.000059{x_2}^2x_3 - 0.002192x_2{x_3}^2 \\ & + 0.001046x_1x_2x_3 - 0.0382x_1x_2 + 0.0298x_1x_3 \\ & + 0.0554x_2x_3 \end{aligned} \tag{5.3}$$

In Table 5.2, the regression coefficients (R^2 =97.15% and S=0.180533) suggest that the resulting model is an accurate estimate. Also, F-value (21.32) obtained by dividing the mean square (Adj. MS) of the model to that of error was greater than that of tabulated $F_{16,\ 10,\ 0.05}$ value (2.83) [73]. This model was adequate with a 95% significance level.

Table 5.2: ANOVA results for response parameters for 27 cases.

Source	DF	Adj. SS	Adj. MS	F-Value	P-Value
Regression	16	11.1173	0.69483	21.32	0
x_1	1	0.0063	0.00632	0.19	0.669
x_2	1	0.0089	0.0089	0.27	0.613
x_3	1	0.2213	0.22134	6.79	0.026
${x_1}^3$	1	0.0241	0.02409	0.74	0.41
${x_2}^3$	1	0.0476	0.04763	1.46	0.255
${x_3}^3$	1	0.3601	0.36005	11.05	0.008
${x_1}^2 x_2$	1	0.009	0.009	0.28	0.611
$x_1 {x_2}^2$	1	0.0014	0.00141	0.04	0.84
${x_1}^2 x_3$	1	0.0896	0.08959	2.75	0.128
$x_1 {x_3}^2$	1	0.0244	0.02439	0.75	0.407
${x_2}^2 x_3$	1	0.0034	0.00345	0.11	0.752
$x_2 {x_3}^2$	1	1.2016	1.20164	36.87	0
$x_1 x_2 x_3$	1	0.0875	0.0875	2.68	0.132
$x_1 x_2$	1	0.0334	0.03342	1.03	0.335
$x_1 x_3$	1	0.0041	0.00406	0.12	0.731
$x_2 x_3$	1	0.5249	0.52487	16.1	0.002
Error	10	0.3259	0.03259		
Total	26	11.4432			
Model Summary	S	R^2	R^2 (adj.)	R^2 (pred.)	
	0.180533	97.15%	92.59%	83.29%	

At the first glance, the larger probability of values in Table 5.2 (P-value>0.05) of individual coefficients of the terms indicated that these terms are needed to be examined since some of them may be insignificant in the empirical model equation. In Section 5.2.2, to obtain the improved model, these terms were eliminated one by one observing the probability values, S (standard error), and R^2 values until a model was obtained for all the individual coefficients being significant.

Additionally, residuals plots for response were drawn to reveal more elaborate information on data. In Figure 5.1, the plots of normal probability (i), fitted value versus residual (ii), histogram (iii), and observation order versus residual (iv) are presented with y1 being the response which is energy efficiency of the furnace. The optimal point where the maximum efficiency is obtained was found using Equation (5.3). The point is (9, 25.3, and 10) as burner angle, port crown angle, and port base angle, respectively. A new computational run was carried out with using the optimal point. The energy efficiency result of the computational simulation at this point is 59.1369% while the result of the empirical cubic equation model is 59.3584%. The difference between these results equals the residual value which is 0.3732%.

The residual value is shown in Figure 5.1 with an orange triangle. In *observation order versus residual plot* at the right-end corner of the graph, the numbers of observation order indicate the computational run order which is given in Table 5.1. It reveals that the data with number 13 and 14 are the furthest points to the zero-residual level. Although the convergence of all the runs is within the acceptance range, these points may be considered for further investigation in terms of computational fluid dynamics.

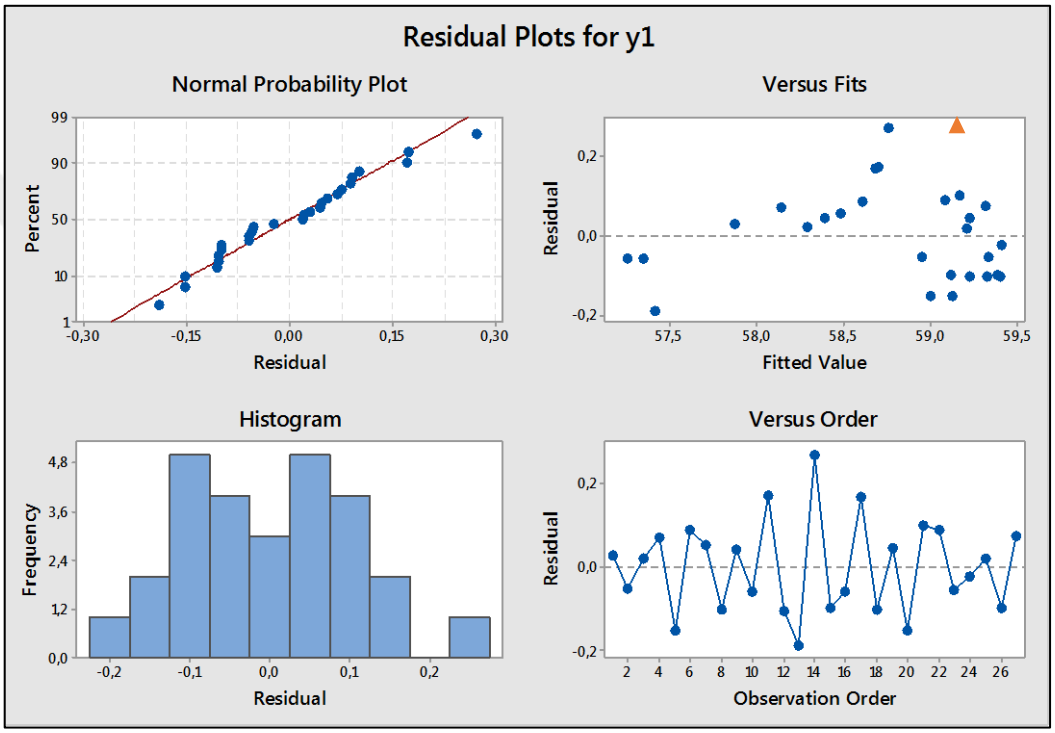

Figure 5.1: Residual plots for the cubic analysis of 27 cases.

5.2.2. 27 Cases With The Improved Model

A selection approach called *backward elimination* was applied at this stage [74]. In backward elimination, all predictors in the initial set in Equation (5.3) was included in the model at the start. Then, the analysis was carried out in the previous part has been repeated by eliminating the coefficients one by one beginning with the highest probability value (P-value>0.05) to obtain the improved empirical cubic model. The elimination procedure began with discarding the coefficient with the highest probability value in Table 5.2. The probability values, S, and R^2 values were checked at each step until all the probability values of the coefficients are smaller than 0.05.

When all the coefficients are smaller than 0.05, it is seen that the established cubic equation model does not depend on variable x_1. For that reason, it was decided to stop elimination procedure when three independent variables are present in the model with their possible lowest P-values. The results of the final elimination step are given in Table 5.3.

An improved version of Equation (5.3) has been established in (5.4). The result is an 11-coefficient cubic regression model with discarding 6 coefficients in the previous version. The regression coefficients (R^2=96.27% and S=0.163411) suggest that the resulting model is also an accurate estimate. When F-test was applied, it is seen that the F-value resulted in Table 5.3 (41.25) is greater than the tabulated F value (2.46) for $F_{10, 16, 0.05}$ which also states that the model is an adequate one.

Table 5.3: ANOVA results for response parameters after eliminating coefficients with p-value>0.05.

Source	DF	Adj. SS	Adj. MS	F-Value	P-Value
Regression	10	11.016	1.1016	41.25	0
x_1	1	0.2347	0.23468	8.79	0.009
x_2	1	0.1254	0.12538	4.7	0.046
x_3	1	1.2821	1.28212	48.01	0
${x_2}^3$	1	0.765	0.76501	28.65	0
${x_3}^3$	1	1.9473	1.94732	72.93	0
${x_1}^2 x_3$	1	0.1894	0.18939	7.09	0.017
$x_2 {x_3}^2$	1	1.2016	1.20164	45	0
$x_1 x_2 x_3$	1	0.1077	0.1077	4.03	0.062
$x_1 x_2$	1	0.1286	0.12863	4.82	0.043
$x_2 x_3$	1	0.8493	0.84933	31.81	0
Error	16	0.4272	0.02670		
Total	26	11.4432			
Model Summary	S		R^2	R^2 (adj.)	R^2 (pred.)
	0.163411		96.27%	93.93%	90.44

In empirical applications of statistical modeling, it is preferred to search for a *parsimonious model* which is based on the reduced form of the equation [72]. Equation (5.4) contains fewer predictors compared to Equation (5.3). Although R^2 values of Table 5.2 (97.15%) and Table 5.3 (96.27%) differ by 0.88%, it is advantageous to choose Equation (5.4) which has a fewer number of predictors. The cubic equation model is given in Equation (5.4).

$$y = 61.52 - 0.453x_1 - 0.1904x_2 + -0.812x_3 - 0.000060{x_2}^3 \quad (5.4)$$
$$+ 0.001340{x_3}^3 - 0.001826{x_1}^2x_3 - 0.002192x_2{x_3}^2$$
$$+ 0.000935x_1x_2x_3 + 0.01618x_1x_2 + 0.0585x_2x_3$$

Residual plots for this analysis are presented in Figure 5.2. The triangle with the orange color illustrated in the top-right of Figure 5.2 represents the residual of the maximum efficiency point, which is 0.3269%, obtained by using Equation (5.4). This point is (7.04, 30, and 13.83) as burner angle, port crown angle, and port base angle, respectively. It was run computationally for comparison with the empirical model. The efficiency results are 59.2534% for a computational run and 59.4479% for empirical cubic equation model.

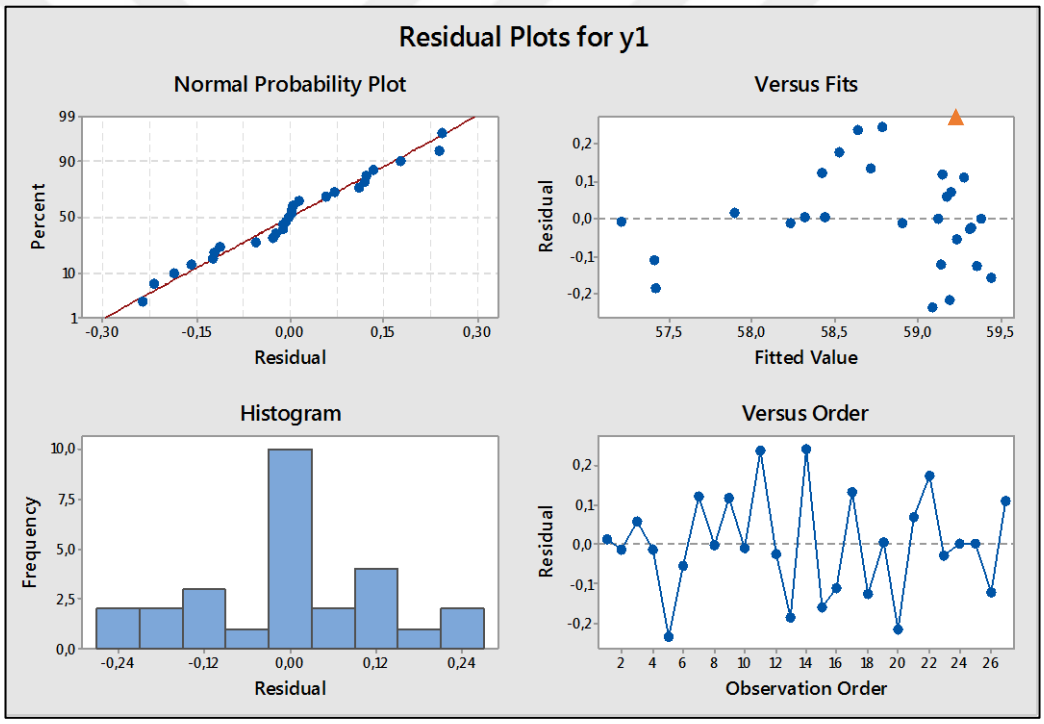

Figure 5.2: Residual plots for the cubic analysis of 27 cases with an improved model.

5.2.3. Extra 4 Cases

The cubic equation model established in previous section is an accurate model in the 0.05 significance level since R^2 values are greater than 95%. After obtaining Equation (5.3) and (5.4), the analysis was extended to cover extra 4 cases with increasing the upper limit of burner angle from 9^0 to 13^0 in order to see if the cubic model will satisfy the relationship between these parameters in the extended region. Therefore, a middle point, which is 11^0, was added to provide the transition from 9^0 to 13^0. The extra cases and the results of the computational runs are given in Table 5.4.

Table 5.4: Description and results of extra computational runs.

Run	Burner angle	Port base angle	Port crown angle	Efficiency (η) (%)	Energy transferred into the glass bath (kW)
	x_1	x_2	x_3		
28	11	20	10	59.09111588	9715.792
29	11	20	20	59.29995234	9750.129
30	13	20	10	58.8965842	9683.807
31	13	20	20	58.90375484	9684.986

The analysis was carried out including an extra four cases at this stage to obtain an empirical cubic equation model. The result is a 17-coefficient regression model that is given in Equation (5.5).

$$\begin{aligned} y = {} & 58.22 + 1.25x_1 - 0.124x_2 - 0.526x_3 - 0.00068{x_1}^3 - 0.000059{x_2}^3 \\ & + 0.001066{x_3}^3 + 0.00119{x_1}^2x_2 - 0.000020x_1{x_2}^2 \\ & + 0.00019{x_1}^2x_3 + 0.00179x_1{x_3}^2 + 0.000002{x_2}^2x_3 \\ & - 0.002192x_2{x_3}^2 + 0.001046x_1x_2x_3 - 0.0236{x_1}^2 \\ & - 0.0336x_1x_2 - 0.0816x_1x_3 + 0.0577x_2x_3 \end{aligned} \quad (5.5)$$

The probability of the individual coefficients and the analysis of variance of the resulting model are given in Table 5.5. The regression coefficients (R^2=96.10% and S=0.188668) in Table 5.5 suggest that the resulting model is an accurate estimate.

Table 5.5: ANOVA results for response parameters for 31 cases.

Source	DF	Adj. SS	Adj. MS	F-Value	P-Value
Regression	17	11.3974	0.67043	18.83	0
x_1	1	0.0471	0.04709	1.32	0.271
x_2	1	0.0172	0.01724	0.48	0.499
x_3	1	0.1243	0.12431	3.49	0.084
${x_1}^3$	1	0.0019	0.0019	0.05	0.821
${x_2}^3$	1	0.0252	0.02522	0.71	0.415
${x_3}^3$	1	0.3471	0.34708	9.75	0.008
${x_1}^2 x_2$	1	0.009	0.009	0.25	0.624
$x_1 {x_2}^2$	1	0.0001	0.00008	0	0.964
${x_1}^2 x_3$	1	0.0008	0.00081	0.02	0.882
$x_1 {x_3}^2$	1	0.0333	0.03325	0.93	0.351
${x_2}^2 x_3$	1	0	0	0	0.993
$x_2 {x_3}^2$	1	1.2016	1.20164	33.76	0
$x_1 x_2 x_3$	1	0.0875	0.0875	2.46	0.141
${x_1}^2$	1	0.0023	0.00232	0.07	0.803
$x_1 x_2$	1	0.0268	0.02684	0.75	0.401
$x_1 x_3$	1	0.0633	0.06327	1.78	0.205
$x_2 x_3$	1	0.5791	0.57906	16.27	0.001
Error	13	0.4627	0.0356		
Total	30	11.8601			
Model Summary	S	R^2	R^2 (adj.)	R^2 (pred.)	
	0.188668	96.10%	91.00%	81.75%	

In Table 5.5, F-value (18.83) obtained by dividing the mean square (Adj. MS) of the model to that of error was greater than that of tabulated $F_{17, 13, 0.05}$ value (2.50). This model was adequate within the 95% significance level.

The maximum efficiency point was found after optimization of the Equation (5.5) in Excel. The optimal point is (9, 25.36, and 10) as burner angle, port crown angle, and port base angle, respectively. It was run computationally for comparison to the empirical model. The efficiency results are 59.1104% for a computational run and 59.3166% for empiric cubic equation model. The residual plots are given in Figure 5.3 in which the orange triangle represents the difference between the efficiency results of the computational run and empiric cubic equation model.

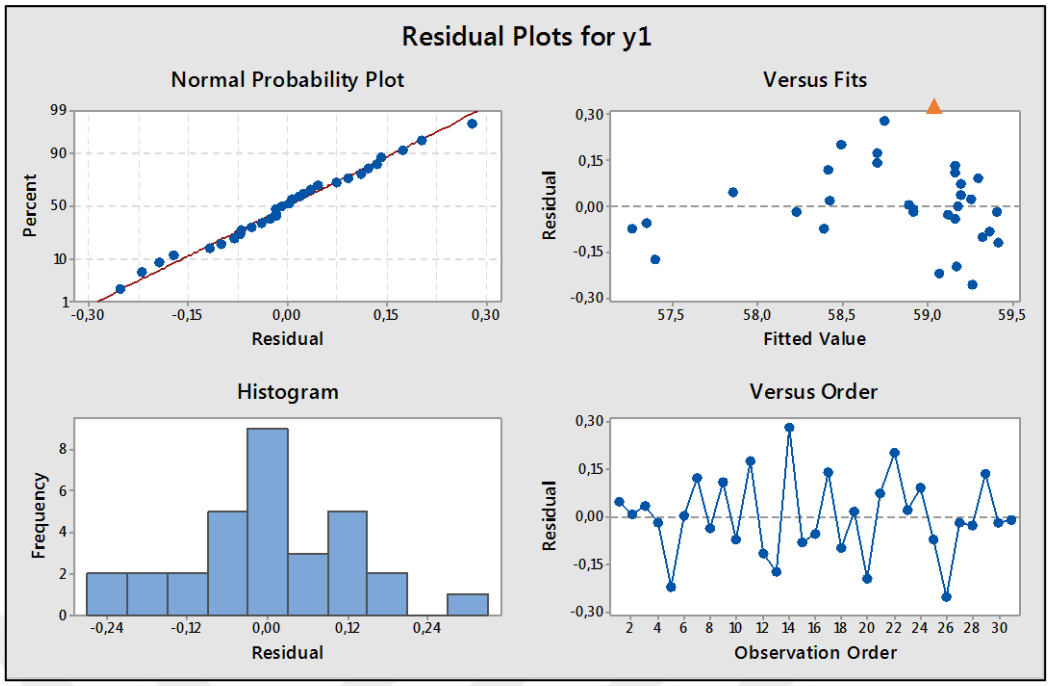

Figure 5.3: Residual plots for the cubic analysis of 31 cases.

5.2.4. Extra 4 Cases With The Improved Model

The analysis presented in the previous section was carried out again applying backward elimination at this stage. After elimination of the coefficients with the highest P-values ($x_2{}^2x_3, x_1x_2, x_1{}^2x_3, x_1{}^2, x_1{}^2x_2, x_1x_3{}^2, x_1x_2x_3$), Equation (5.6) with 12 coefficients has been obtained that is given in the following pages. The probability of the individual coefficients and the analysis of variance of the resulting model are given in Table 5.6. The regression coefficients (R^2=95.73% and S=0.163269) are slightly lower than the previous Equation (5.5). However, Equation (5.6) with fewer predictors are chosen over Equation (5.6) for the sake of simplicity to represent the 31-cases-investigation.

As seen in Table 5.6, there are still some predictors with their P-value>0.05. After the elimination of all the predictors with P-value>0.05, the R^2 value of the last equation drops to 94% with only three predictors left in the equation. Because of that, the elimination of the predictors was stopped at the sixth step. S-value of the sixth equation is the lowest one as seen in Figure 5.4.

Table 5.6: ANOVA results for response parameters after eliminating coefficients with P-value>0.05 for 31 cases.

Source	DF	Adj. SS	Adj. MS	F-Value	P-Value
Regression	11	11.3537	1.03215	38.72	0
x_1	1	0.1957	0.19572	7.34	0.014
x_2	1	0.0919	0.09193	3.45	0.079
x_3	1	0.7421	0.7421	27.84	0
${x_1}^3$	1	0.1575	0.15745	5.91	0.025
${x_2}^3$	1	0.8627	0.86266	32.36	0
${x_3}^3$	1	1.9674	1.96739	73.8	0
$x_2{x_3}^2$	1	1.2016	1.20164	45.08	0
$x_1x_2\,x_3$	1	0.0875	0.0875	3.28	0.086
x_1x_2	1	0.1054	0.10536	3.95	0.061
x_1x_3	1	0.1143	0.11429	4.29	0.052
$x_2\,x_3$	1	0.7853	0.78527	29.46	0
Error	19	0.5065	0.02666		
Total	30	11.8601			

Model Summary	S	R^2	R^2 (adj.)	R^2 (pred.)
	0.163269	95.73%	93.26%	90.53%

Elimination steps in cubic equation model with extra 4 cases are given below.

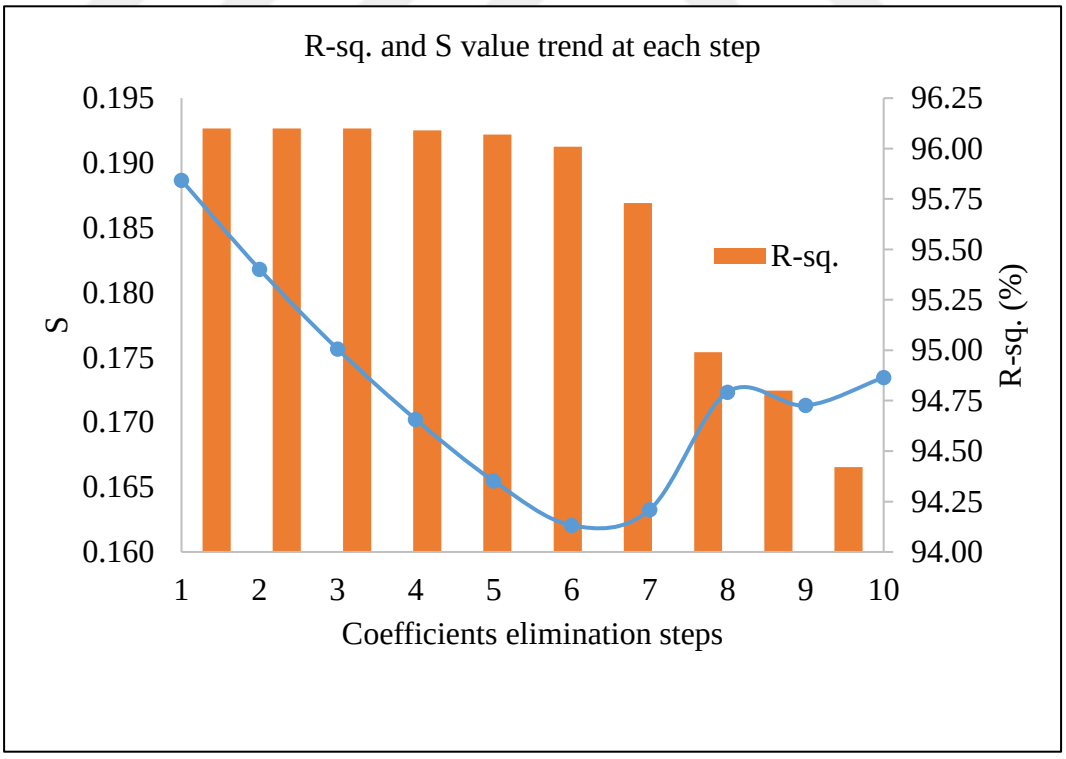

Figure 5.4: Elimination steps in cubic equation model with extra 4 cases.

The cubic equation model that was obtained after completion of elimination steps is given in Equation (5.6).

$$y = 61.26 + 0.513x_1 - 0.1760x_2 - 0.736x_3 - 0.000459{x_1}^3 - 0.000062{x_2}^3 + 0.001346{x_3}^3 - 0.002192x_2{x_3}^2 + 0.001046x_1x_2x_3 - 0.01784x_1x_2 - 0.0246x_1x_3 + 0.0577x_2x_3 \quad (5.6)$$

In Figure 5.5, the residuals of this analysis are given with y1 representing the response which is the energy efficiency in the analysis. The triangle with the orange color illustrated in the top-right of the figure represents the maximum efficiency point obtained by using Equation (5.6). This point is (8.60, 26.20 and 20) as burner angle, port crown angle, and port base angle, respectively. The point was run computationally for comparison to the empirical model. The efficiency results are 59.2365% for a computational run and 59.4270% for empiric cubic equation model.

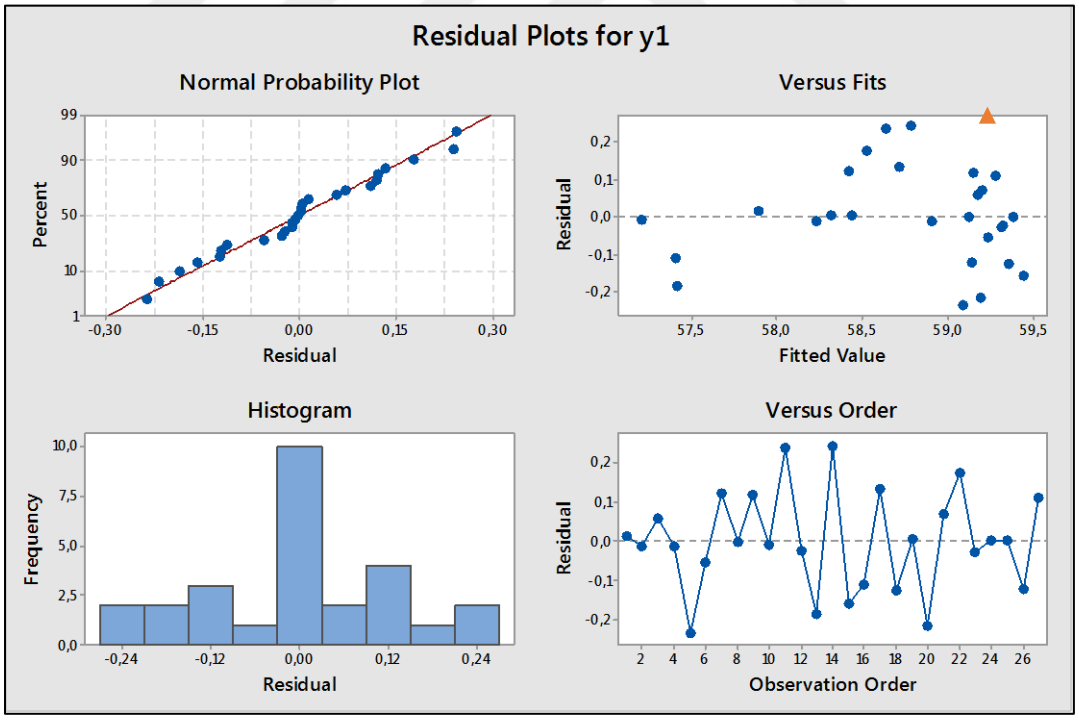

Figure 5.5: Residual plots for the cubic analysis of 31 cases with an improved model.

The analysis could have been extended to cover different ranges for each parameter within the industrial physical limits. However, the time limit and computational cost of the Glass Furnace Model restrict the study to be conducted in a broader range for the duration of this study.

5.3. Empirical Quadratic Equation

In this section, 27 cases analyzed previously were divided into three groups with respect to their port base angle. Hence, there are three investigation groups having port base angle 10^0, 15^0, and 20^0, respectively. Results of energy efficiency data are fitted to the empirical second-order polynomial model for maximum energy efficiency.
Port base angle was selected as a constant parameter because the burner angle has mobility contrary to port crown angle and port base angle. Port crown angle could have been selected as a constant parameter as well. Because of the time limit and computational cost, the only port base angle has been examined in this section.

Table 5.7 is added to remind the results of the investigation cases at the beginning of the study. In the following sub-chapters with using Table 5.7, the relationship between two independent variables (x_1: burner angle and x_2: port crown angle) and the response (y: efficiency) were investigated to obtain an empirical quadratic equation model with keeping port base angle constant for each investigation group. The general form of the quadratic equation model is given in Equation (5.7).

$$y = \beta_0 + \beta_1 x_1 + \beta_2 x_2 + \beta_{12} x_1 x_2 + \beta_{11} {x_1}^2 + \beta_{22} {x_2}^2 \qquad (5.7)$$

Table 5.7: Results of computational runs classified with respect to port base angle.

Run	Burner angle	Port crown angle	Port base angle	Efficiency (η) (%)	Energy transferred into the glass bath (kW)
	x_1	x_2	x_3		
1	5	10		57.90504190	9520.7771
2	5	20		58.89480826	9676.5150
3	5	30		59.22825205	9738.3400
4	7	10		58.21597876	9571.9015
5	7	20	10	58.85183309	9683.4490
6	7	30		59.17907327	9730.2540
7	9	10		58.54010254	9625.1941
8	9	20		59.12152571	9720.7920
9	9	30		59.27147050	9745.4460
10	5	10		57.19556720	9404.1249
11	5	20		58.87664751	9680.5290
12	5	30		59.29773851	9749.7650
13	7	10		57.22801570	9409.4601
14	7	20	15	59.03122068	9705.9440
15	7	30		59.28684571	9747.9740
16	9	10		57.29486685	9420.4518
17	9	20		58.85076267	9676.2730
18	9	30		59.22732759	9738.1880
19	5	10		58.43950013	9608.6530
20	5	20		58.97478003	9696.6640
21	5	30		59.26841735	9744.9440
22	7	10		58.69719303	9651.0230
23	7	20	20	59.28209569	9747.1930
24	7	30		59.3866386	9764.3820
25	9	10		58.31637073	9588.4080
26	9	20		59.01423983	9703.1520
27	9	30		59.39008708	9764.9490

In the following sections, analysis with constant port base angles for 10^0, 15^0 and 20^0 are given respectively.

5.3.1. Base 10^0

The analysis was performed with constant base angle 10^0 for this section. 10^0 for the port base angle of container glass is the most common and conventional choice in the industry. The result is a 6-coefficient regression model that is given in Equation (5.8). The probability of the individual coefficients and the analysis of variance of the resulting model are given in Table 5.8. The regression coefficients (R^2=99.37% and S=0.0625503) suggest that the resulting model is a quite precise estimate.

Table 5.8: ANOVA results for response parameters for constant base angle 10^0.

Source	DF	Adj. SS	Adj. MS	F-Value	P-Value
Regression	5	1.86227	0.372453	95.19	0.002
x_1	1	0.00038	0.000379	0.1	0.776
x_2	1	0.33924	0.339235	86.7	0.003
${x_1}^2$	1	0.01214	0.012138	3.1	0.176
${x_2}^2$	1	0.10833	0.108332	27.69	0.013
x_1x_2	1	0.08757	0.087569	22.38	0.018
Error	3	0.01174	0.003913		
Total	8	1.87401			

Model Summary	S	R^2	R^2 (adj.)	R^2 (pred.)
	0.0625503	99.37%	98.33%	93.92%

The quadratic equation model for constant base angle 10^0 is given in Equation (5.8).

$$y = 56.358 - 0.049x_1 + 0.1952x_2 + 0.0195{x_1}^2 - 0.002327{x_2}^2 - 0.00740x_1x_2 \quad (5.8)$$

Equation (5.8) was optimized to find the optimal point where the maximum efficiency was obtained. It was found that 5^0 for burner angle and 30^0 for port crown angle provide the maximum efficiency, 59.2522 %, within the investigation range. The combined effect of burner angle and port crown angle on the furnace efficiency for constant port base angle 10^0 is seen in Figure 5.6.

It is seen in Figure 5.7; 9^0 burner angle for 10^0 port base angle case is the most energy efficient one throughout the investigation range. It indicates that the amount of heat transferred from combustion space into the glass bath is the maximum when the burner angle is 9^0.

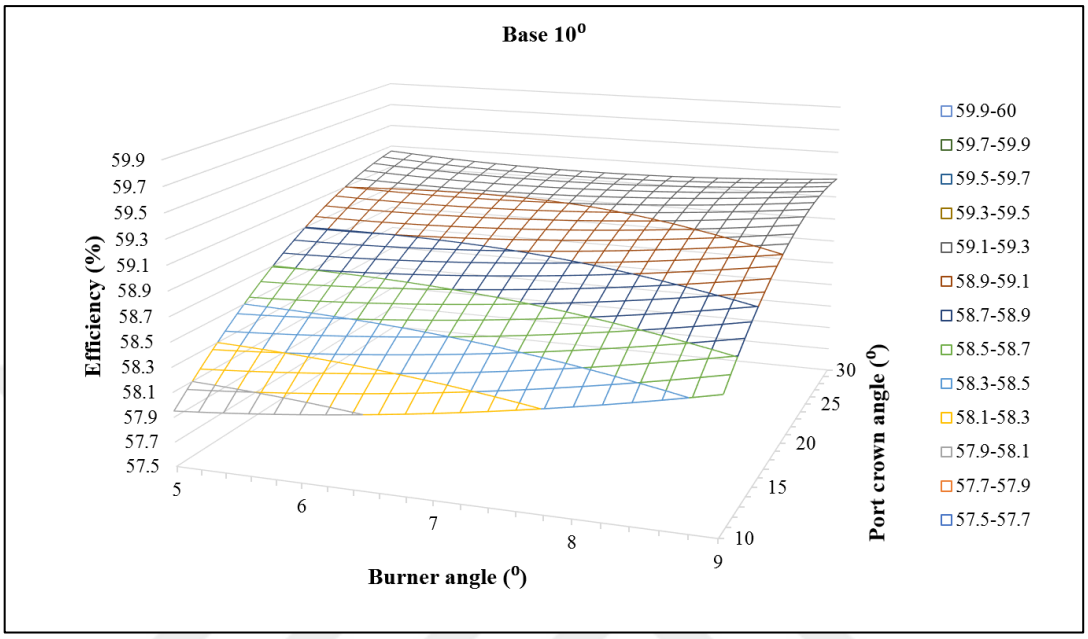

Figure 5.6: Energy efficiency diagram as a function of burner angle and port crown angle for constant port base angle, $x_3=10^0$.

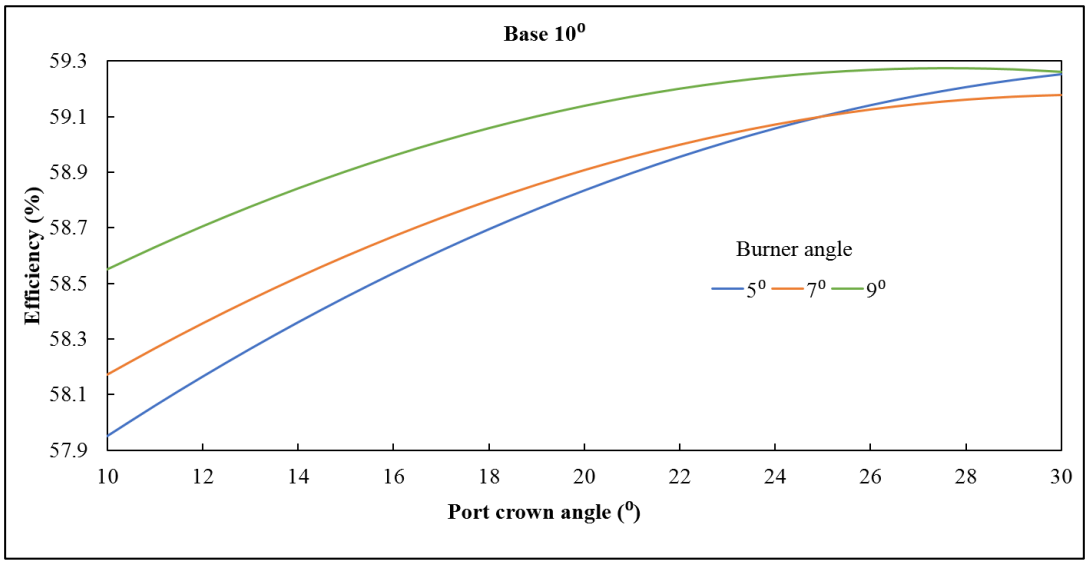

Figure 5.7: Effects of port crown angle and burner angle on the energy efficiency of the furnace for constant port base angle, $x_3=10^0$.

In Figure 5.7, 7^0 for burner angle is the dominant one for energy efficiency until the port base angle becomes 26^0. After this point, the equation shifts towards 5^0 for burner angle. The graph proves that the value of the energy efficiency of the furnace is specific to a pair of port and burners.

The residual plots for this analysis are given in Figure 5.8. The triangle with the orange color illustrated in the top-right of the figure represents the maximum efficiency point obtained by using Equation (5.8). This point is (5, 30, and 10) as burner angle, port crown angle, and port base angle, respectively.

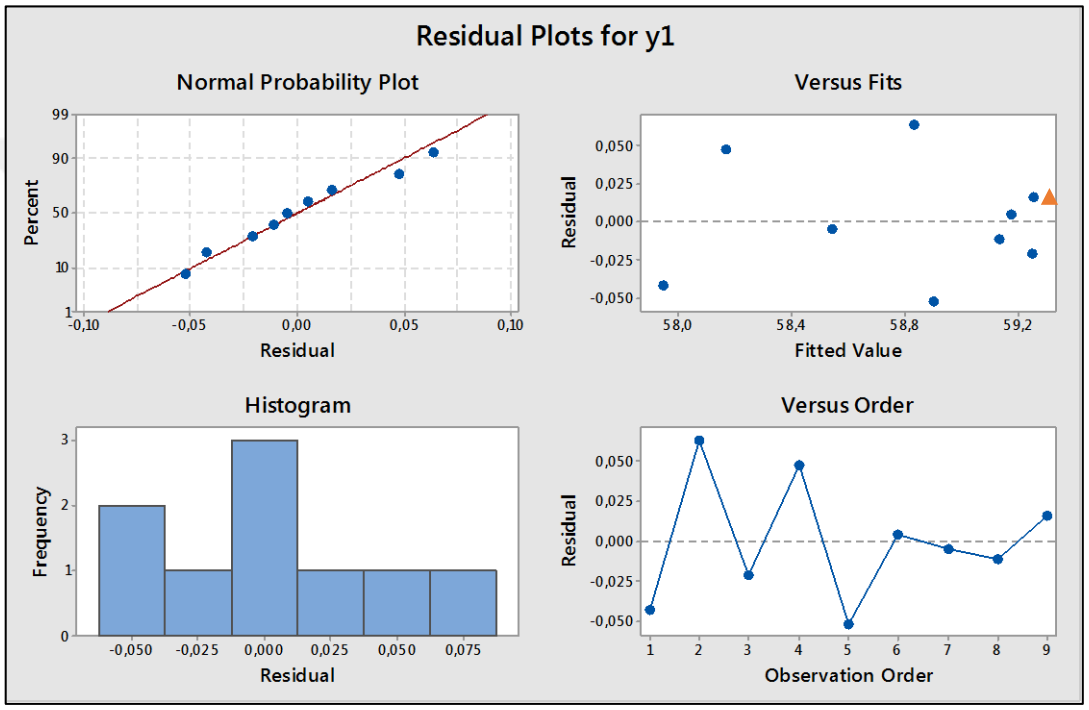

Figure 5.8: Residual plots for quadratic analysis for constant base angle 10^0.

The optimal point for the maximum energy efficiency was run computationally to compare to the result of the empirical model. The efficiency results are 59.2441% for the computational run and 59.2522% for the empiric quadratic equation model.

5.3.2. Base 15^0

The analysis was performed with constant base angle 15^0 for this section. The result is a 5-coefficient regression model that is given in Equation (5.9). The probability of the individual coefficients and the analysis of variance of the resulting model are given in Table 5.9. The regression coefficients (R^2=99.82% and S=0.065991) suggest that the resulting model is a quite precise estimate.

Table 5.9: ANOVA results for response parameters for constant base angle 15^0.

Source	DF	Adj. SS	Adj. MS	F-Value	P-Value
Regression	5	7.08543	1.41709	325.4	0
x_1	1	0.00946	0.00946	2.17	0.237
x_2	1	1.30087	1.30087	298.72	0
${x_1}^2$	1	0.00678	0.00678	1.56	0.301
${x_2}^2$	1	0.88308	0.88308	202.78	0.001
x_1x_2	1	0.0072	0.0072	1.65	0.289
Error	3	0.01306	0.00435		
Total	8	7.0985			
Model Summary	S	R^2	R^2 (adj.)	R^2 (pred.)	
	0.065991	99.82%	99.51%	98.56%	

The quadratic equation model is given with calculated coefficients in Equation (5.9). According to the equation, 8.4 degree (8° 24′) for burner angle and 28^0 for port crown angle provides maximum furnace efficiency that is 59.78898% within the investigation range.

$$y = 53.257 + 0.246x_1 + 0.3822x_2 - 0.0146{x_1}^2 - 0.006645{x_2}^2 \quad (5.9)$$

The combined effect of the burner angle and port crown angle on the furnace efficiency for constant port base angle 15^0 is seen in Figure 5.9 and Figure 5.10.

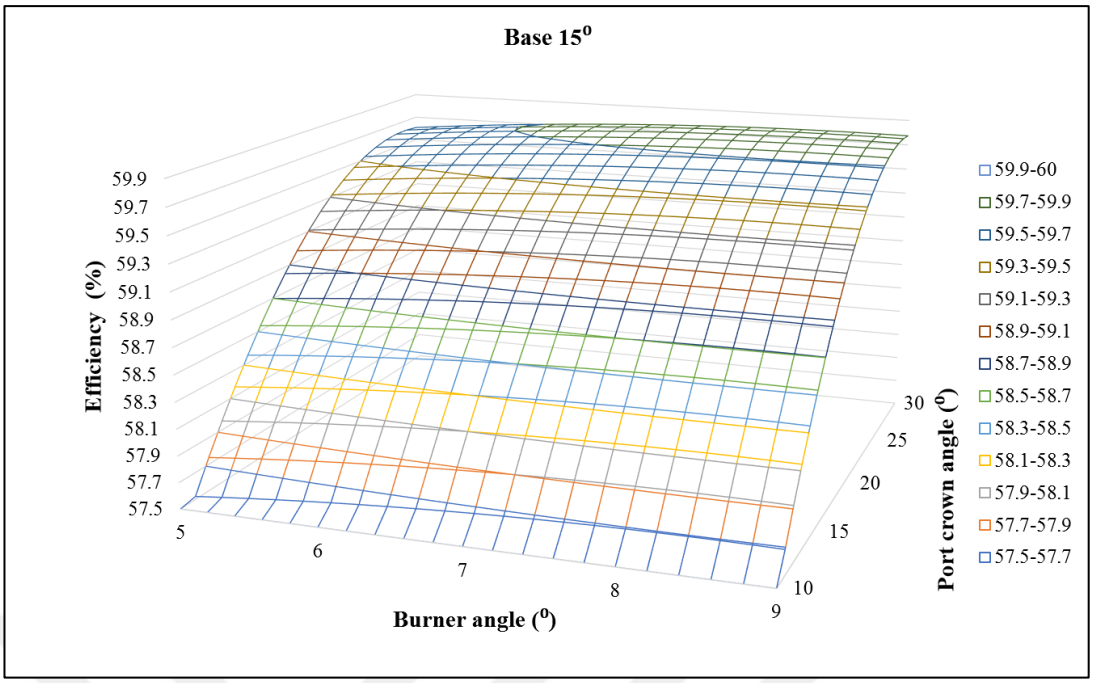

Figure 5.9: Energy efficiency diagram as a function of burner angle and port crown angle for constant port base angle, $x_3=15^0$.

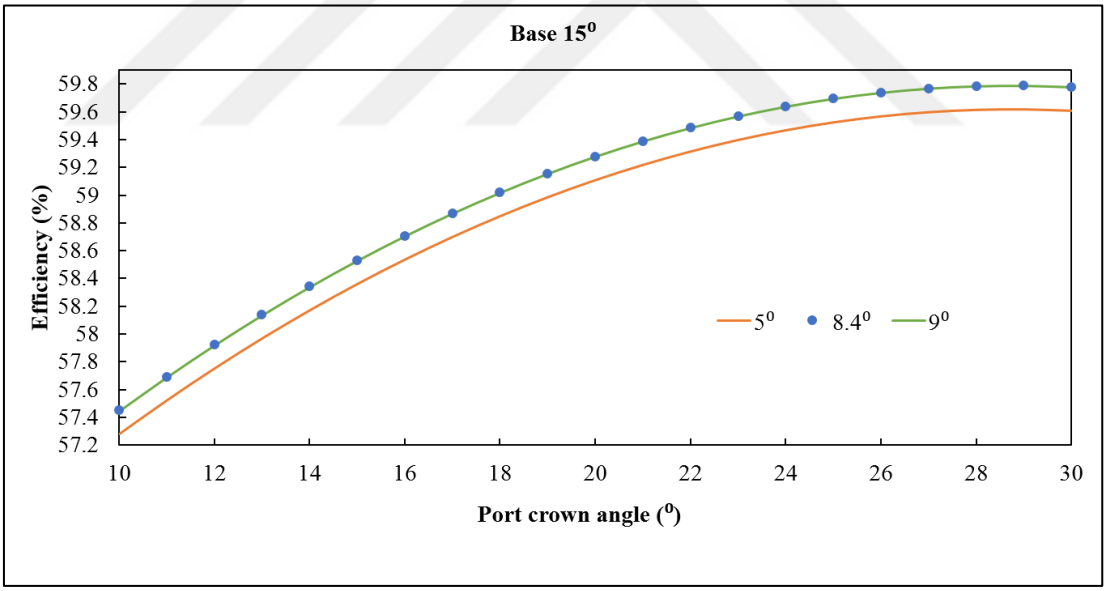

Figure 5.10: Effects of port crown angle and burner angle on the energy efficiency of the furnace for constant port base angle, $x_3=15^0$.

In Figure 5.10, the calculated burner angle for maximum furnace efficiency, 8.4 degree (8° 24′), is the leading value all through the study range of 10^0 to 30^0 for the port crown angle. It coincides with the results of 9^0 angle for the burner. It can be deduced that approximately 9^0 for burner angle provides maximum furnace efficiency for both the cases of constant port base angle 10^0 and 15^0.

In Figure 5.11, the residual plots for the constant base angle 15^0 are presented. The point where the maximum efficiency is obtained, which is 8.4 degree (8° 24′) for burner angle and 28^0 for port crown angle, run computationally to compare to the result of the quadratic equation model. The efficiency results are 59.5644% for a computational run and 59.7890% for empiric cubic equation model. The residual is 0.3770%. Since it is larger than the data range drawn in Figure 5.11, it could not be shown on the graph.

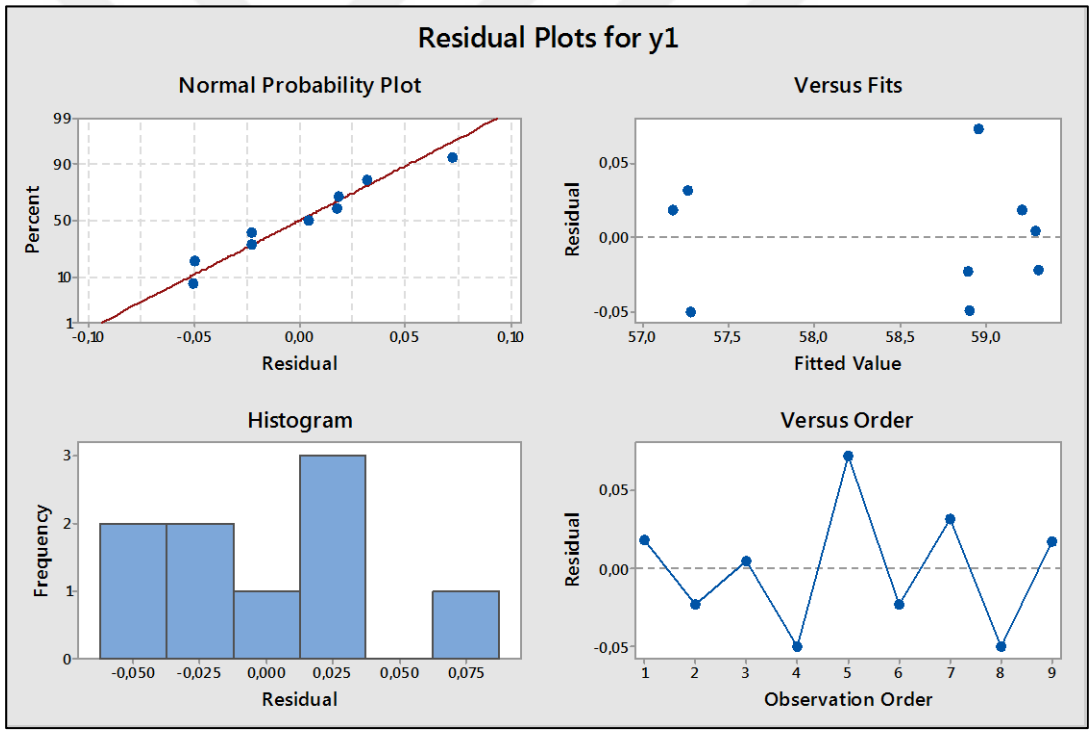

Figure 5.11: Residual plots for quadratic analysis for constant base angle 15^0.

5.3.3. Base 20^0

The analysis was performed with constant base angle 20^0 for this section. The result is a 6-coefficient regression model that is given in Equation (5.10). The probability of the individual coefficients and the analysis of variance of the resulting model are given in Table 5.10. The regression coefficients (R^2=97.90% and S=0.0962228) suggest that the resulting model is a quite precise estimate.

Table 5.10: ANOVA results for response parameters for constant base angle 20^0.

Source	DF	Adj. SS	Adj. MS	F-Value	P-Value
Regression	5	1.29363	0.258727	27.94	0.01
x_1	1	0.0801	0.080096	8.65	0.06
x_2	1	0.07437	0.074368	8.03	0.066
${x_1}^2$	1	0.09804	0.098045	10.59	0.047
${x_2}^2$	1	0.06055	0.060555	6.54	0.083
x_1x_2	1	0.01498	0.014982	1.62	0.293
Error	3	0.02778	0.009259		
Total	8	1.32141			
Model Summary	S	R^2	R^2 (adj.)	R^2 (pred.)	
	0.0962228	97.90%	94.39%	75.95%	

The quadratic equation model for this case is given in Equation (5.10). By solving the equation for the point of maximum furnace efficiency, it is found that 7.3 degree (8° 18′) and 30^0 for burner angle and port crown angle, respectively give the maximum energy efficiency, 59.50%. In Figure 5.12 and Figure 5.13, the combined effect of the burner angle and port crown angle on efficiency for constant port base angle 20^0 is presented.

$$y = 55.372 + 0.717x_1 + 0.0914x_2 - 0.0554{x_1}^2 - 0.00174{x_2}^2 + 0.00306x_1x_2 \quad (5.10)$$

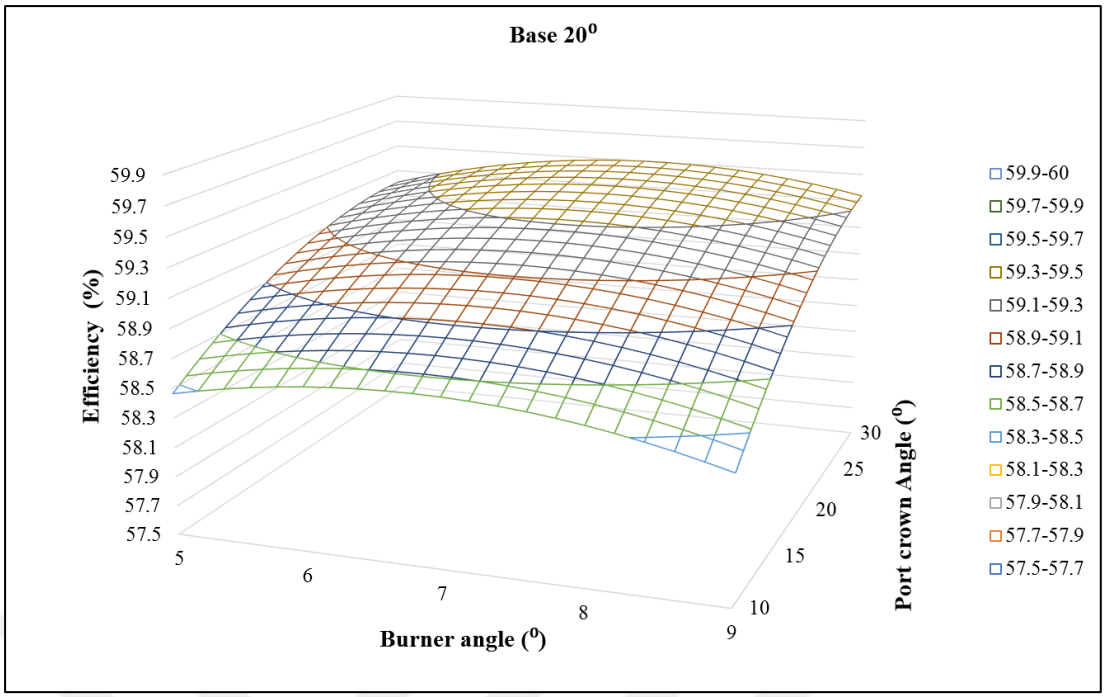

Figure 5.12: Energy efficiency diagram as a function of burner angle and port crown angle for constant port base angle, $x_3=20^0$.

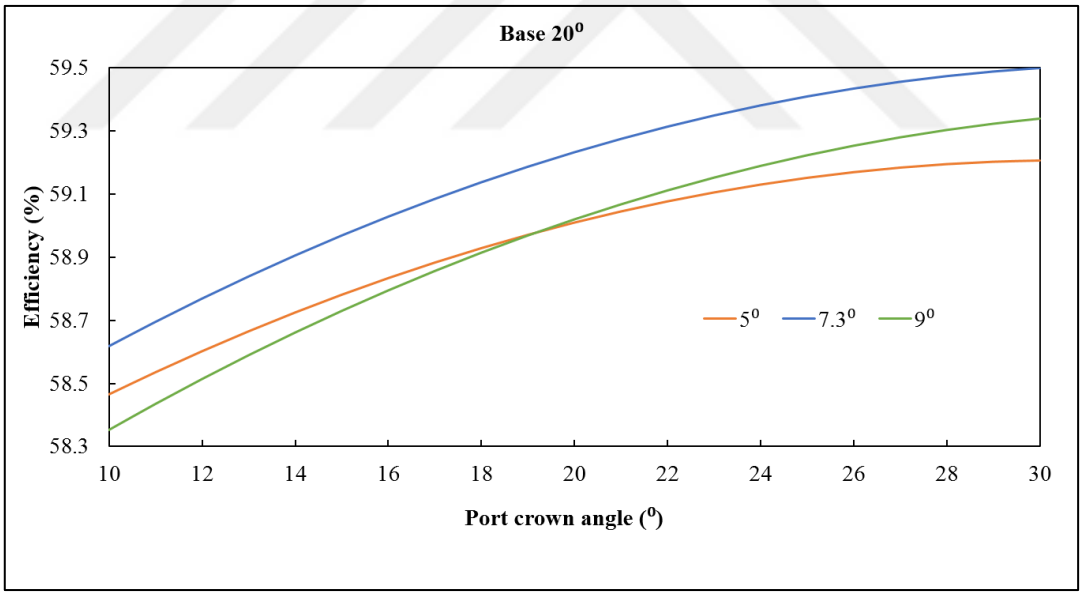

Figure 5.13: Effects of port crown angle and burner angle on the energy efficiency of the furnace for constant port base angle, $x_3=20^0$.

In Figure 5.14, the residual plots of the analysis for constant base angle 20^0 are given. The residual for the maximum efficiency point is 0.3076 as a result of 59.3175% efficiency from computational run whereas 59.5000% efficiency from the quadratic equation model. Since the residual is larger than the data range drawn in Figure 5.14, it could not be shown on the graph.

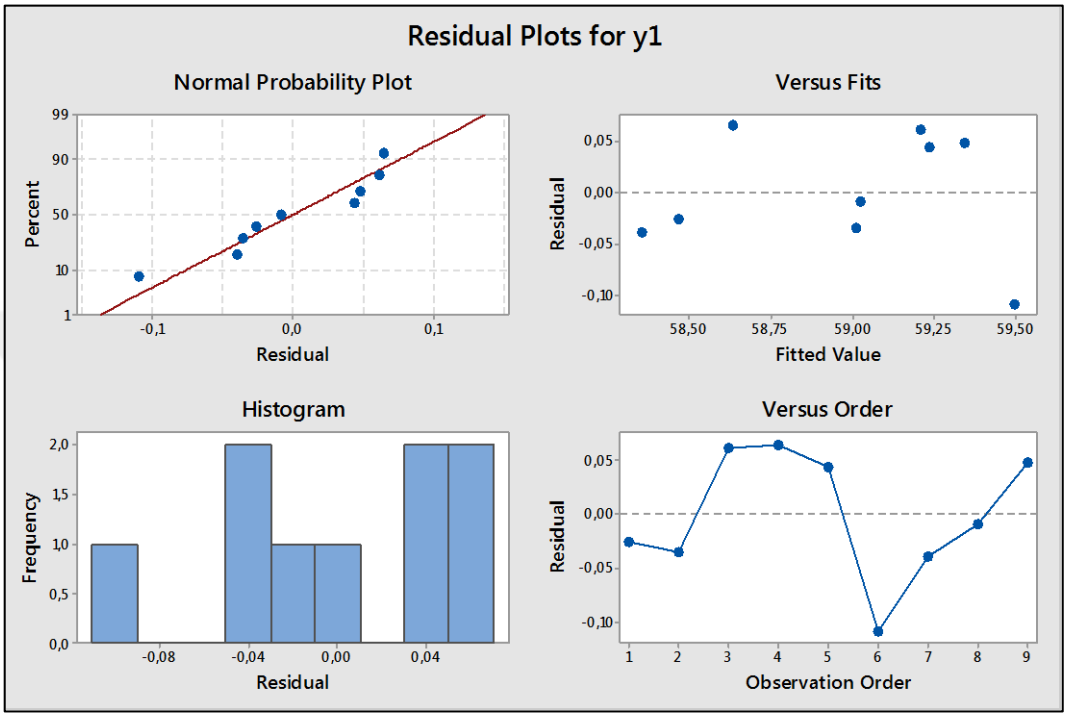

Figure 5.14: Residual plots for quadratic analysis for constant base angle 20^0.

5.4. Comparison of the Efficiency Results of the Statistical Model and Computational Runs

In Section 5.2 and 5.3, the statistical analysis was carried out for 27 investigation cases. Equations (5.3) to (5.10) were obtained as a result of the analysis. Next, the angles for the maximum energy efficiency for each analysis within the investigation range were found after optimization with Excel add-in solver using the equations mentioned above. Then, these points for each experiment were run computationally to compare the efficiency results to the empirical equation model. The results are tabulated in Table 5.11 in which η_s, η_c, and $\Delta_{\eta_s-\eta_c}$ correspond to the efficiency of the statistical equation model, the efficiency of the computational run, and the difference between these two in terms of percentage, respectively.

Table 5.11: Comparison of Efficiency Results of the Statistical Model and Computational Runs.

	Burner angle	**Port crown angle**	**Port base angle**	η_s **(%)**	η_c **(%)**	$\Delta_{\eta_s-\eta_c}$ **(%)**
	x_1	x_2	x_3			
27 cases	9	25.30	10	59.3584	59.1369	0.3732
27 cases with improved model	7.04	30	13.8	59.4479	59.2534	0.3269
27+4 extra cases	9	25.3	10	59.3166	59.1104	0.3476
27+4 extra cases with improved model	8.6	26.2	20	59.4270	59.2365	0.3206
Base 10^0	5	30	10	59.2522	59.2441	0.0136
Base 15^0	8.4	28.75	15	59.7890	59.5644	0.3770
Base 20^0	7.3	30	20	59.5000	59.3175	0.3076

The difference between the statistical model and computational runs are smaller than 0.5% for all the cases given in Table 5.11. This shows that all the listed results are within the 5% significance level which indicates that the statistical model is in good correlation with the computational runs.

5.5. Results in Terms of Combustion Space Evaluation

Energy efficient glass furnace cannot be designed without examination of flame shape and length throughout the furnace which is a result of the mixing of air and fuel, hence flame formation. In the following pages, combustion spaces of the study cases in terms of two and three-dimensional figures were depicted to analyze the results. The figures were drawn by a CFD visualization and analysis programmed called TECPLOT [75].

5.5.1. Burner Angle

Flame formation with three different burner angles, which are 5^0, 7^0, and 9^0, was investigated. Burner angle affects the length, height, and position of flame at constant gas velocity for each burner for all study cases. An example of burner angle effect with a velocity of 120 m/s for the inner pipe and 40 m/s the for outer pipe for the case of crown angle 20^0 and base angle 10^0 with varying burner angles are shown in Figure 5.15, which was selected to represent the general trend. The other study cases show the same trend with the one given in Figure 5.15. Please note that the temperature units in all the figures in this chapter in Celsius (^{0}C).

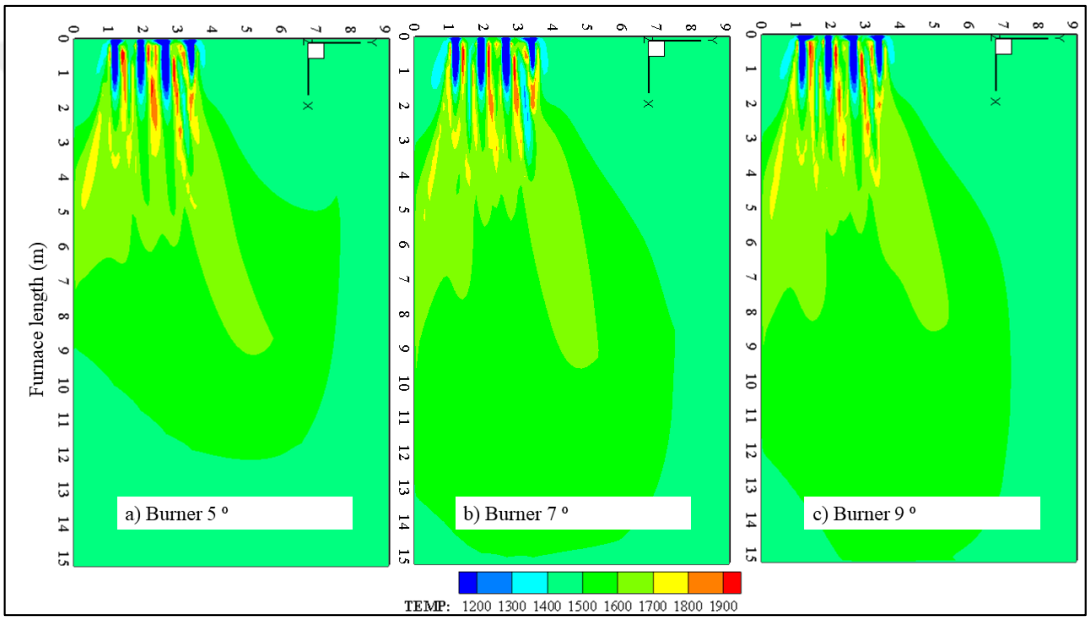

Figure 5.15: Top view of combustion space at burner axis for the angle of 5^0, 7^0, and 9^0.

It is noticeable in Figure 5.15 that higher burner angles result in higher temperature regions in flame along the length of the furnace. In literature, Eltutar *et al.* [41] also explain such a relationship between burner angle and flame temperatures. The mixing point of fuel and air with respect to varying burner angle is shown in Figure 5.16.

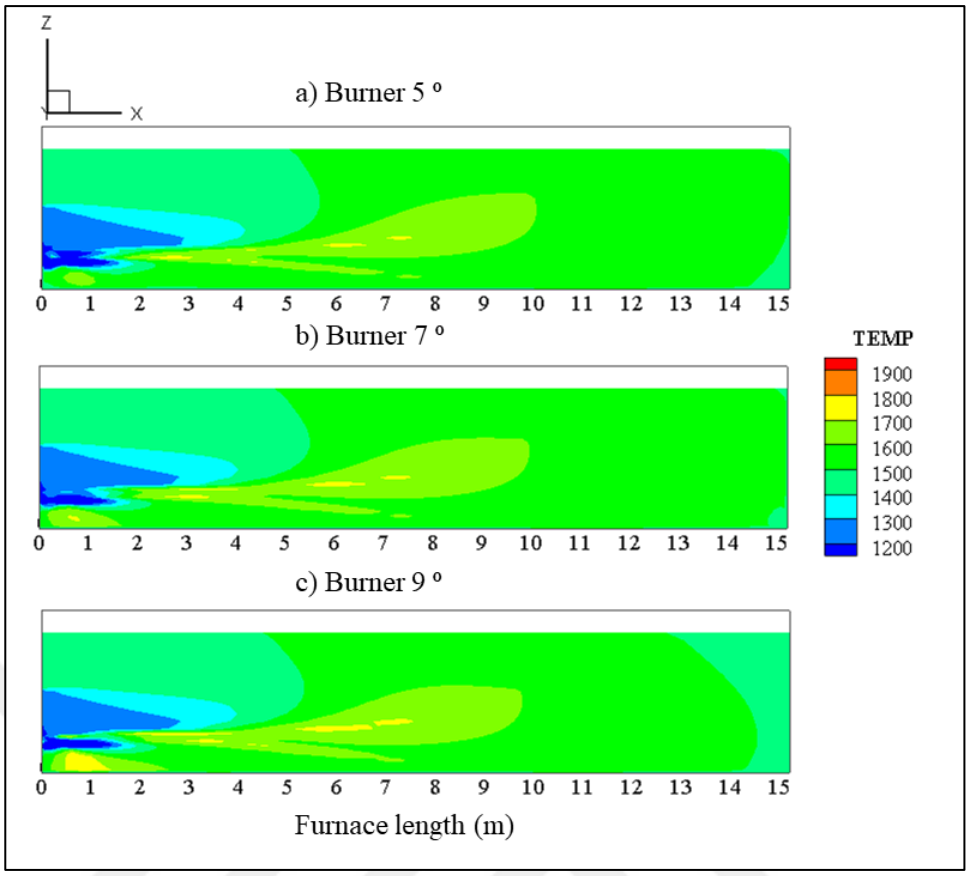

Figure 5.16: Side view of combustion space at burner axis for the burner angle of 5^0, 7^0, and 9^0.

In Figure 5.16, the air and fuel meet at an earlier point along the furnace with increasing burner angle as seen with the distinct yellow region under the burner with 9^0 case. It results in a shorter length of flames. Previously formed flame provides more amount of heat transferred from combustion space into the glass bath. As seen in Table 5.1, the amount of energy transferred from combustion space to the glass bath for the case of burner angle 5^0, 7^0, and 9^0 are 9676 kW, 9683 kW, and 9720 kW, respectively.

The temperature profile of the roof section of the combustion space is an indicative during glass production. Thermocouples are placed at the roof of the furnace to measure the temperature. The smoother and concave curves are favored for the roof temperature of a furnace. In Figure 5.17, for the first half of the furnace, the roof temperatures are higher for the higher burner angle. It shows that the flame formation is quicker, and more amount of heat is transferred into the glass. Therefore, the glass surface is covered fewer batch compared to the lower angle case due to the melting of the batch. Hence, batch-free-glass-surface results in more radiation to the furnace roof which increases roof temperatures.

As seen in Figure 5.17, the maximum temperature point in the combustion atmosphere moves forward with decreasing burner angle along the furnace length. It is another indicative point to check the furnace operation to sustain heat flux throughout the furnace. Lower temperatures at the end of the furnace may result in lower glass temperatures and it has a negative effect on glass quality. Since the molten glass exiting the furnace is sent to annealing and then secondary processes, exiting molten glass should be at the definite temperatures specific to each process. If it is too hot, it needs to be cooled down with air. If it is too cold, it needs to be extra heated up with auxiliary burners. Both applications are energy inefficient. For that reason, the temperatures at the end of the furnace should be also checked. The temperatures seen in Figure 5.17 is within the limits of furnace operation in terms of industrial sense. In practice as well as in literature illustrated by Auchet [19] and Boerstoel [20], the roof temperatures should not exceed 1600^0C not to damage furnace building material which is silica refractory.

In parallel to roof temperatures, the glass temperatures are also controlled during operation. In Figure 5.18, solid lines indicate glass surface temperatures while dashed lines indicate glass bottom temperatures. It is seen that the glass surface temperatures increase with decreasing burner angle. It is a consequence of closer and parallel flame to the glass surface followed by a longer flame length with decreasing burner angle. On the other hand, glass bottom temperatures do not change significantly with the decreasing burner angle. It may be due to free convection currents in the glass bath as a result of a temperature gradient along the depth of the furnace [76]. It may be deduced that the temperature gradient between the cases might decrease along the glass depth and nearly diminish at the bottom of the glass. In order to understand the nearly identical temperature profile at the bottom of the glass, glass velocities also should be examined which is out of the context of the thesis.

The requirement for the glass temperature profile is specific to each color and type of glass. For that reason, the burner angle could be adjusted to each glass color to meet the temperature criteria for exit temperature of that molten glass. In this thesis, clear glass is subjected to study. The obtained glass temperature trends for clear glass in Figure 5.18 for both surface and bottom are in good correlation with industrial data.

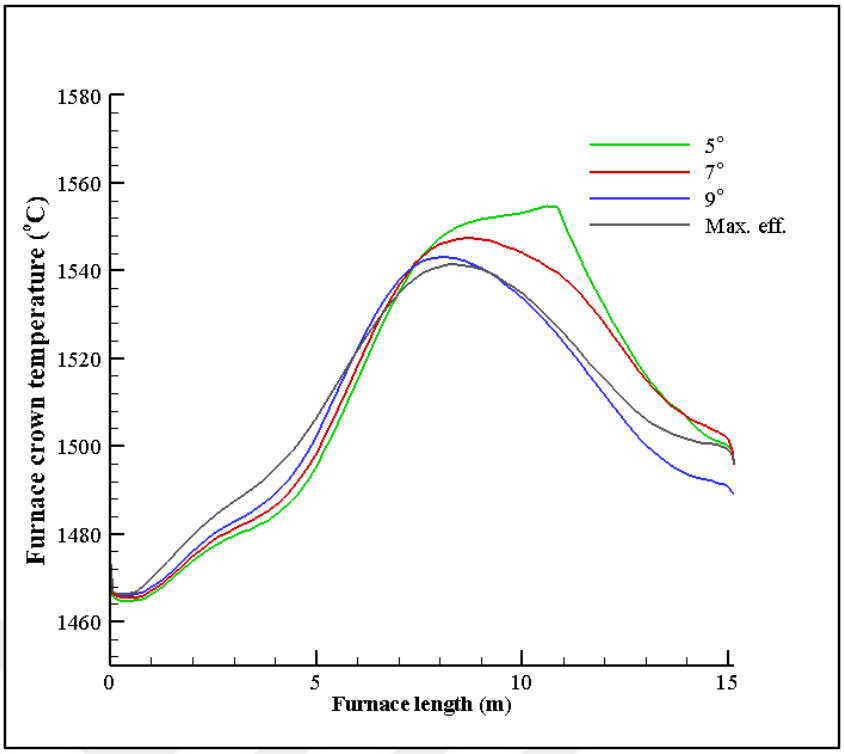

Figure 5.17: Combustion space temperatures at the roof of the furnace along the length for the burner angle of 5^0, 7^0, and 9^0.

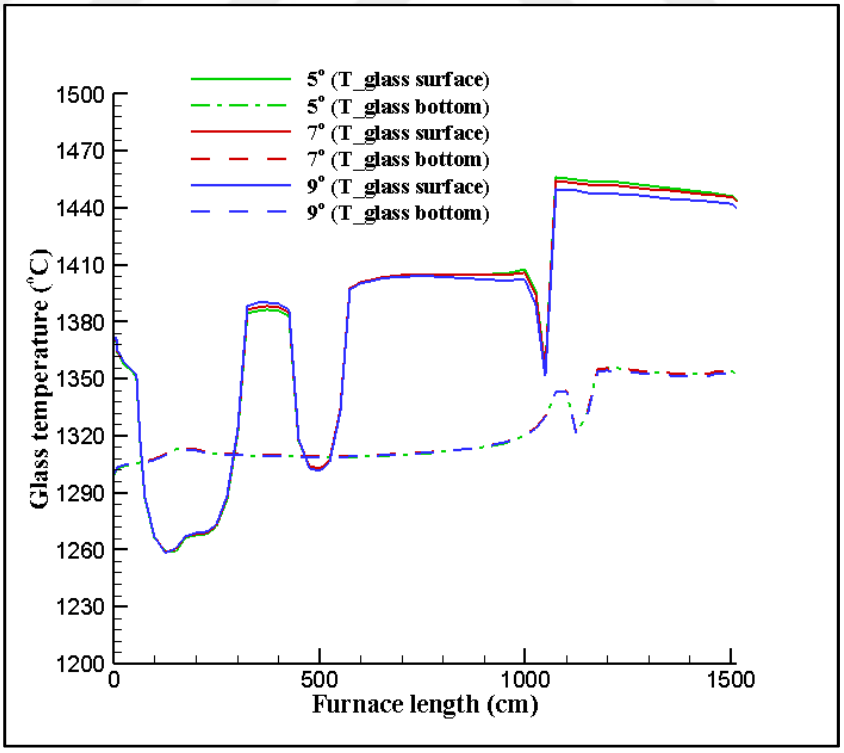

Figure 5.18: Surface and bottom temperatures of glass for the burner angle of 5^0, 7^0, and 9^0.

5.5.2. Port Crown Angle

Port crown angle also affects the flame formation including length, height, and position of flame. Three different port crown angles, which are 10^0, 20^0, and 30^0, were investigated in the thesis. An example of the case of burner angle 7^0 and port base angle 10^0 with varying port crown angles are shown in Figure 5.19. Since the other study cases show the same trend with the one given in Figure 5.19, it was selected to represent the general trend.

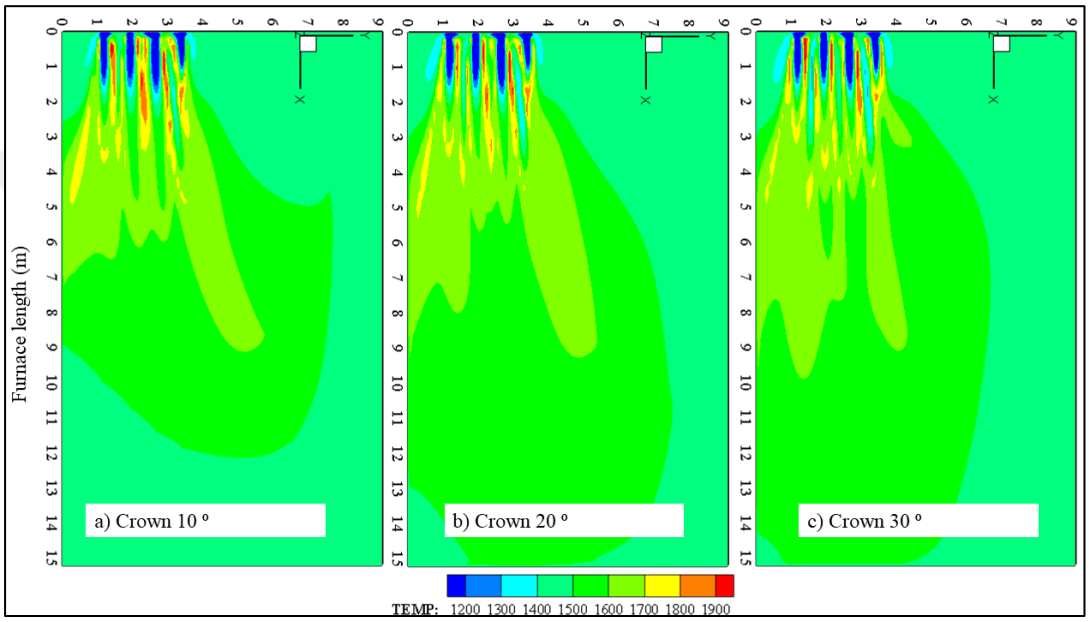

Figure 5.19: Top view of combustion space at burner axis for the port crown angle of 10^0, 20^0, and 30^0.

In Figure 5.19, higher crown angle leads to longer flame length and higher temperature regions in the second half of the furnace. In addition to this, the flame coverage extends along the furnace width with the increasing crown angle. As seen in Table 5.1, the amount of energy transferred from combustion space to the glass bath for the case of port crown angle 10^0, 20^0, and 30^0 are 9571 kW, 9683 kW, and 9730 kW, respectively. However, Uçar *et al.* [42] explain that the energy efficiency of the furnace and NOx emissions are affected in opposite direction by port crown angle. Therefore, the optimum port crown angle should be selected at the design stage of a furnace after considering energy efficiency and NO_x at the same time. This selection varies from country to country since NO_x emissions levels are specific to each country.

In Figure 5.20, the meeting point of air and fuel for each case is shown. The mixing of fuel and air takes place at an earlier point along the length of the furnace with the increasing crown angle. The air coming from the port is suppressed with the increased port crown angle towards the glass surface, hence, glass surface temperatures increases as seen in Figure 5.22. The rate of mixing between fuel, oxidant, and the products depends on the level of turbulence. As a result of this, the flame temperature is determined by turbulence as well [55].

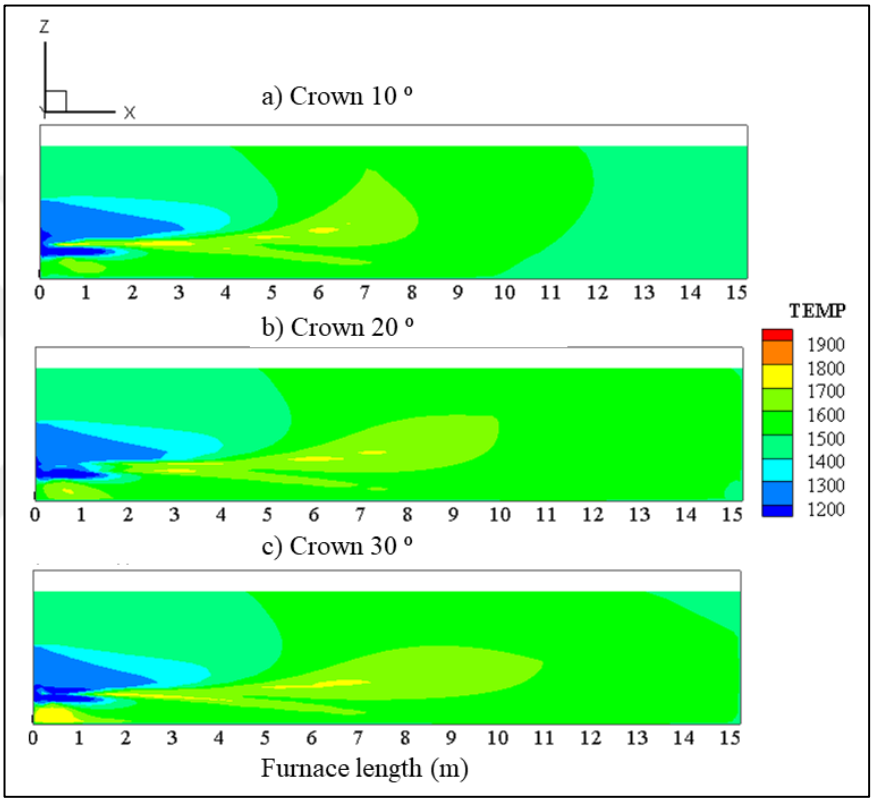

Figure 5.20: Side view of combustion space at burner axis for the port crown angle of 10^0, 20^0, and 30^0.

In Figure 5.21, combustion space temperatures at the roof of the furnace along the length for the crown angle of 10^0, 20^0, and 30^0 are given. The temperature profile for the crown angle of 10^0 is very steeper compared to the 20^0 and 30^0. The smoother curves rather than the-upside-down-V-shape temperature profile are desired along the furnace. In addition to that, the temperature profile for the case of 10^0 port crown is closer to limits of temperature endurance of silica refractory. Steep increase and decrease in the temperature profile across the furnace are not preferred.

For that reason, 10^0 is not chosen as crown angle according to these results even though the energy efficiency is found to be high for specific cases.

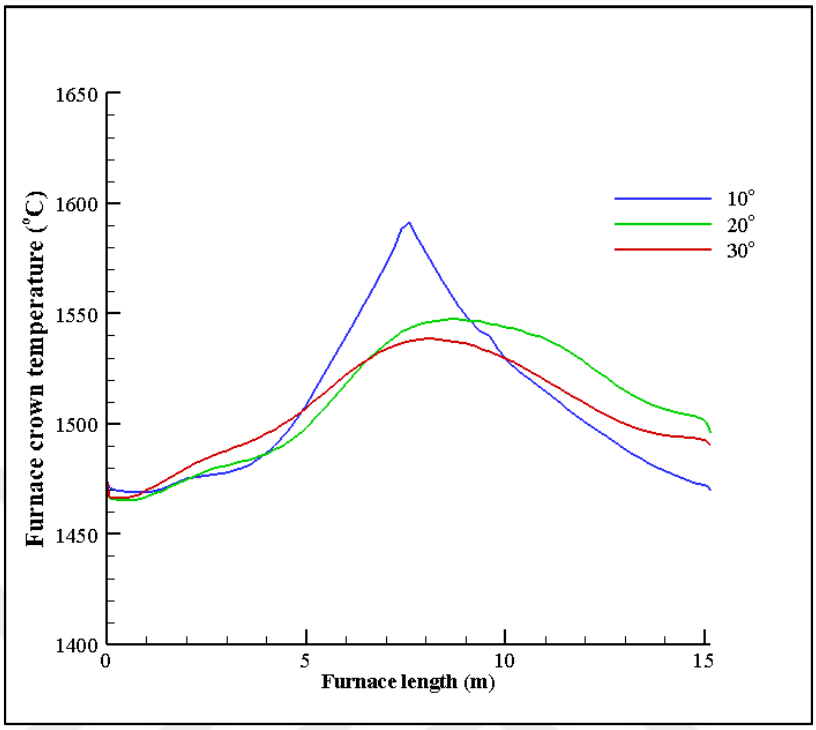

Figure 5.21: Combustion space temperatures at the roof of the furnace along the length for the crown angle of 10^0, 20^0, and 30^0.

In Figure 5.22, Surface and bottom temperatures of glass for the crown angle of 10^0, 20^0, and 30^0 is presented. It is seen that the port crown angle has more impact on glass temperatures compared to burner angle which can be seen in Figure 5.18. These graphs are in good correlation with the found equations of statistical analysis conducted in Section 5.3. In Equation (5.8) and Equation (5.9), the calculated coefficients of the port crown angle are significantly bigger than the coefficients of burner angle. In Equation (5.8), the calculated coefficient of the port crown angle is 0.1952 while the coefficient of the burner angle is 0.049. In Equation (5.9), the coefficients are 0.246 and 0.3822 for burner angle (x_1) and port crown angle (x_2), respectively.

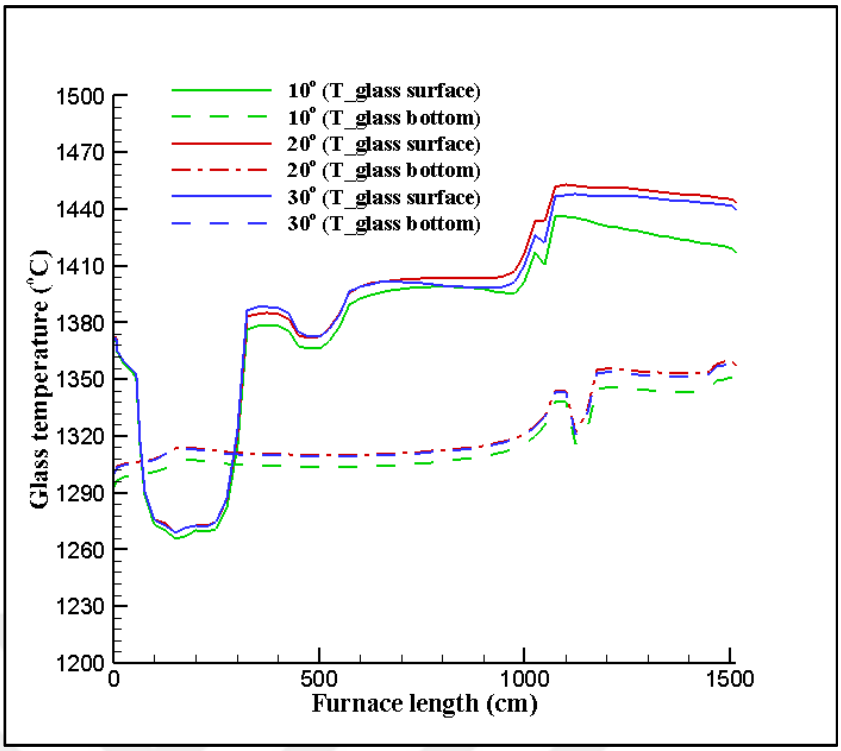

Figure 5.22: Surface and bottom temperatures of glass for the crown angle of 10^0, 20^0, and 30^0.

Figure 5.22, both the surface and bottom glass temperatures are decreasing with decreasing crown angle. However, the temperatures are closer to each other for the case of 20^0 and 30^0. It indicates that after some point, the glass temperatures do not vary with varying crown angle. Once again, the glass temperatures are within the limits of clear glass production based on production practice.

5.5.3. Port Base Angle

The last parameter investigated for the flame formation is the port base angle which includes 10^0, 15^0, and 20^0. An example representing the general trend for the case of 5^0 for burner angle and 20^0 for a port crown angle with varying port base angles are shown in Figure 5.23

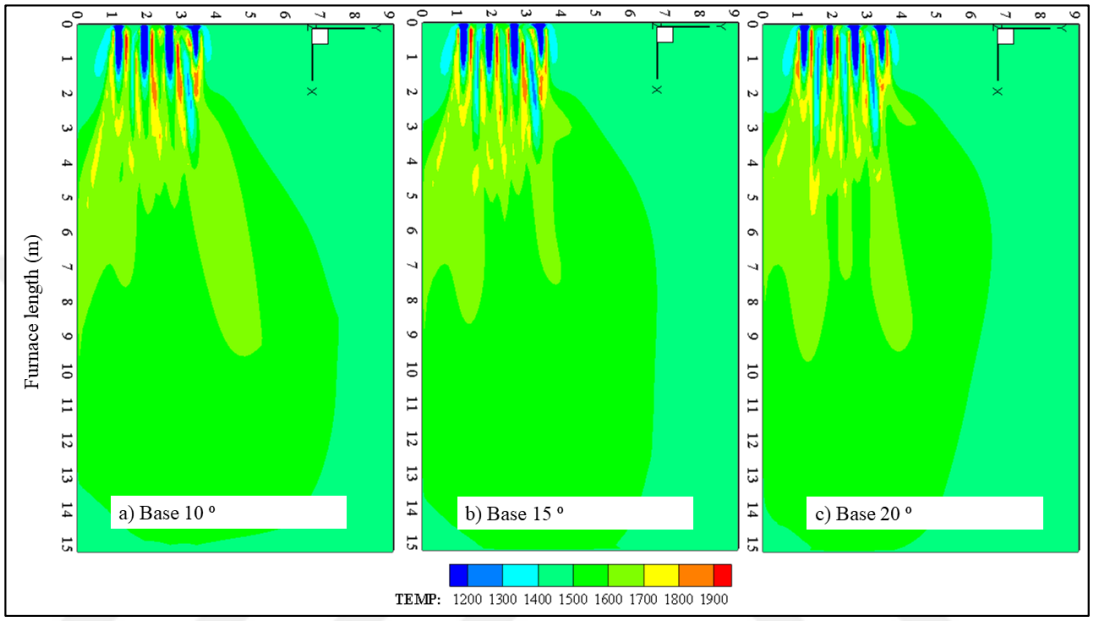

Figure 5.23: Top view of combustion space at burner axis for the port base angle of 10^0, 15^0, and 20^0.

The heat transferred from combustion space into the glass bath for the case of 10^0, 15^0, and 20^0 are 9676 kW, 9680 kW, 9696 kW, respectively. Although the case with the port base angle 20^0 has the longest flame length and it may suggest that the maximum heat transferred is achieved with this case, there is not an obvious distinction between the top view profiles in Figure 5.23 For that reason, Section 5.3 gives more information on energy efficiency for varying port base angles to illustrate the differences between the cases. However, on the side view profiles given in Figure 5.24, flame formation is earlier for the case of 20^0 port crown angle as seen with the distinct yellow region within the first meters. It also suggests that more amount of heat is transferred from combustion space to the glass bath with the earlier flame formation.

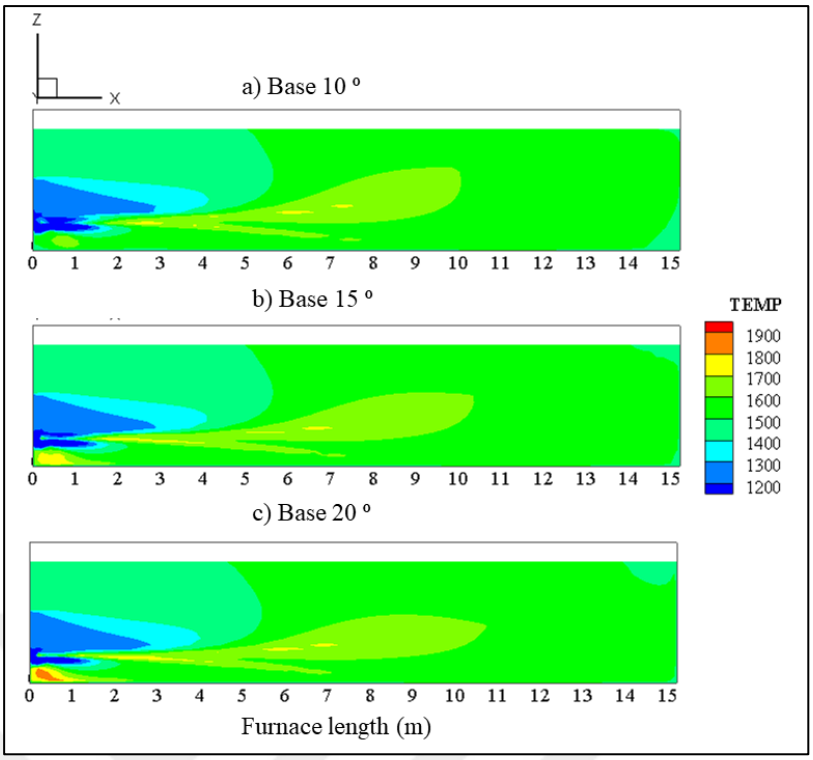

Figure 5.24: Side view of combustion space at burner axis for the port base angle of 10^0, 15^0, and 20^0.

In Figure 5.25, the roof temperatures of the furnace are significantly higher for the case of 10^0 after the sixth meter. This trend shows that there is a delayed mixing of air and fuel with decreasing the port base angle. As a result of that, the flame reaches till the end of the furnace that means increased local heat transfer at the end of the furnace, hence glass surface temperatures are higher for the lower base angles as seen in Figure 5.26. For the glass bottom temperatures, there is a slight difference between the cases.

In open literature, the port base angle has been investigated up to now in the context of NO_x formation. Therefore, there are not any available results describing the relationship between energy efficiency and port base angle in the open literature. It is stated by both Beerkens [57] and Uçar *et al.* [42] that lower base angle promotes lower NOx levels. Hence, energy efficiency and NOx are affected in inversed directions by port base angle.

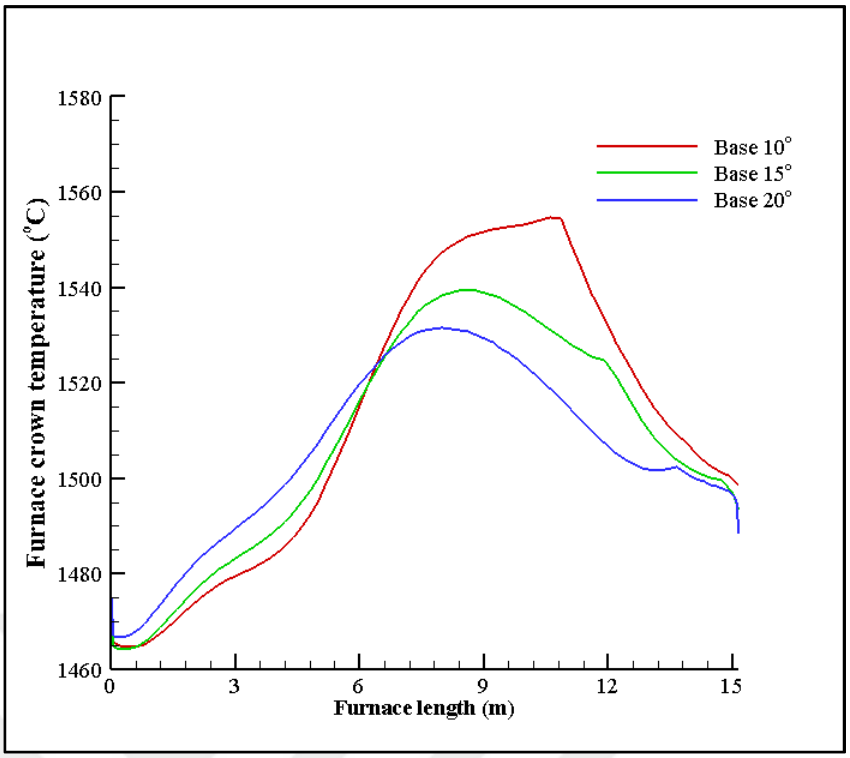

Figure 5.25: Combustion space temperatures at the roof of the furnace along the length for the port base angle of 10^0, 15^0, and 20^0.

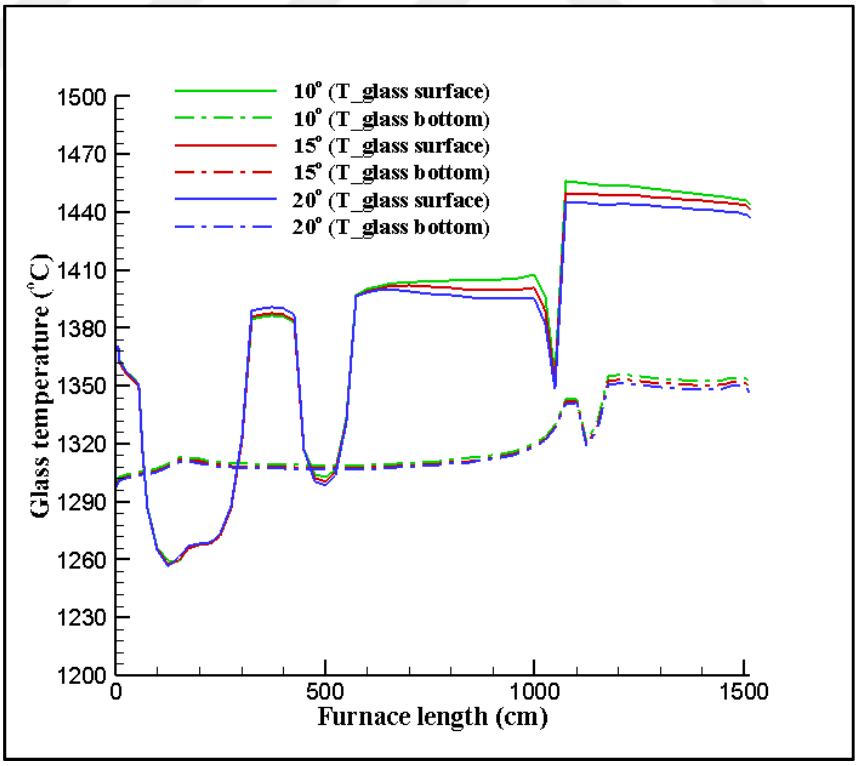

Figure 5.26: Surface and bottom temperatures of glass for the base angle of 10^0, 15^0, and 20^0.

5.5.4. Comparison of Minimum and Maximum Energy Efficiency Cases

In Section 5.2.1, a number of 27 cases were statistically analyzed. Based on Equation (5.3), which obtained as a result of the analysis, the maximum energy efficiency case is the one with angles of the burner, port crown, and port base are (9^0, 25.30^0, and 10^0) respectively whereas the minimum efficiency case is the one with angles of the burner, port crown, and port base are (5^0, 10^0, and 15^0), respectively. The computed energy efficiencies are 57.1956% and 59.1369% as minimum and maximum, respectively. In Figure 5.27, the roof temperatures for both cases are given.

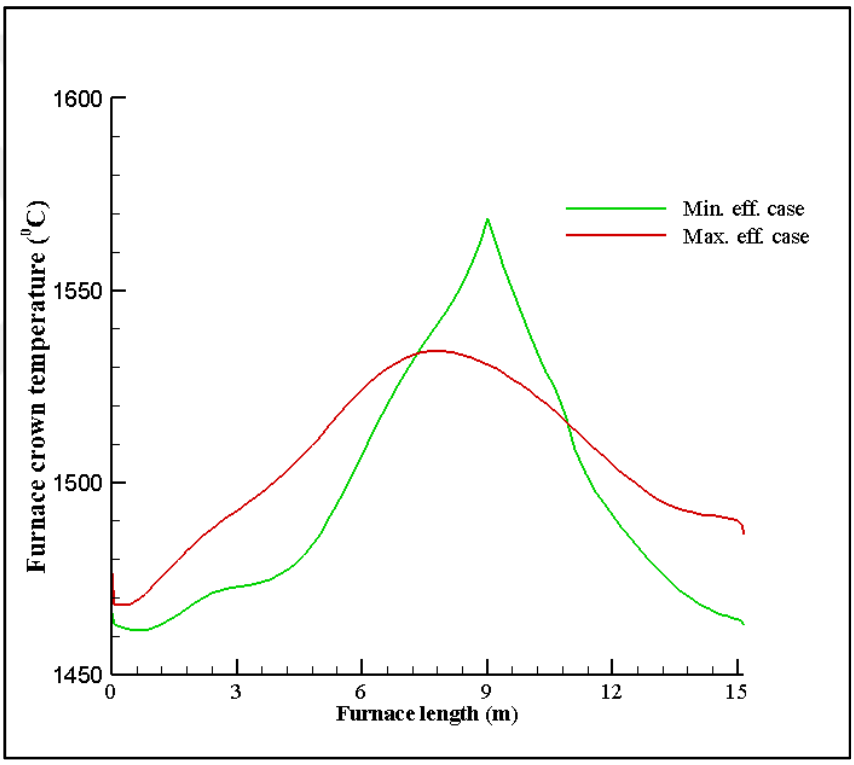

Figure 5.27: Combustion space temperatures at the roof of the furnace along the length for the minimum and maximum efficient cases^0.

In Figure 5.27, it is seen that there is a significant temperature difference between the two cases. Firstly, the temperature profile for the minimum efficiency case is not a smoother concave one, hence, it is not desirable during operation. Secondly, the difference between the profiles indicates that there is an efficient heat transfer in the maximum efficiency case with the same amount of energy supplied to the furnace. Figure 5.27 clearly shows that there is a reduction potential in the consumption of

energy by changing the angles of both burner and port in the combustion space of a glass furnace.

The energy reduction potential is supported by the temperature profiles given in Figure 5.28 for the surface and bottom of the glass for both the minimum and maximum energy efficiency cases. It is seen that approximately 15^0C temperature difference near the exit of the furnace (15 m). Since both curves are within the operational temperature limits for the clear glass production, the amount of energy given to the red-line-case could be reduced to obtain the same temperature profile with the green-line-case as far as the glass quality restrictions permit.

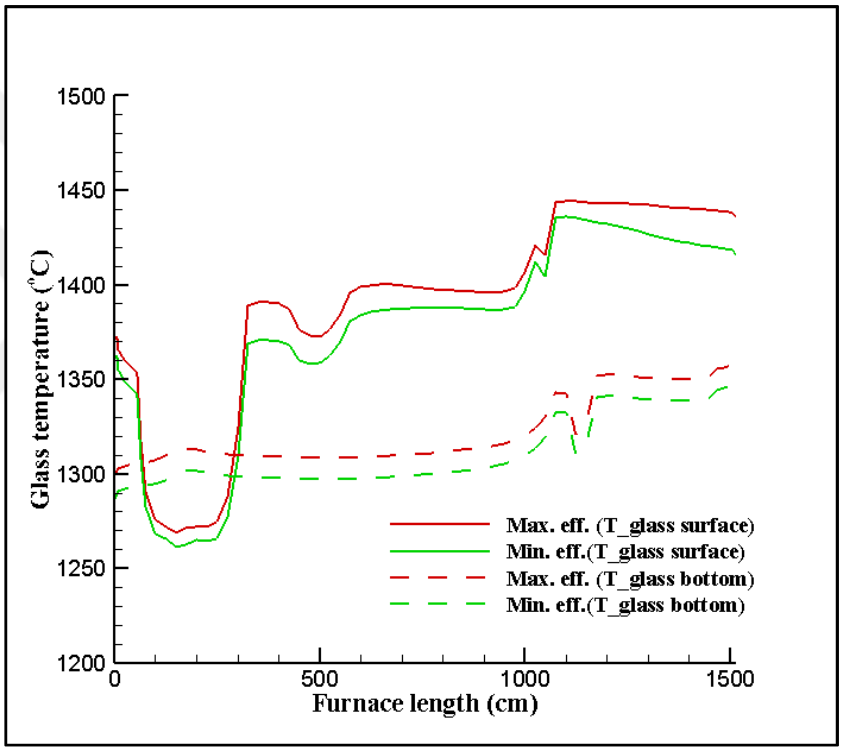

Figure 5.28: Surface and bottom temperatures of glass for the minimum and maximum efficient cases.

To give an elaborate insight, another temperature profile along the glass depth for both cases is given in Figure 5.29. There is a significant difference in the glass bottom temperatures.

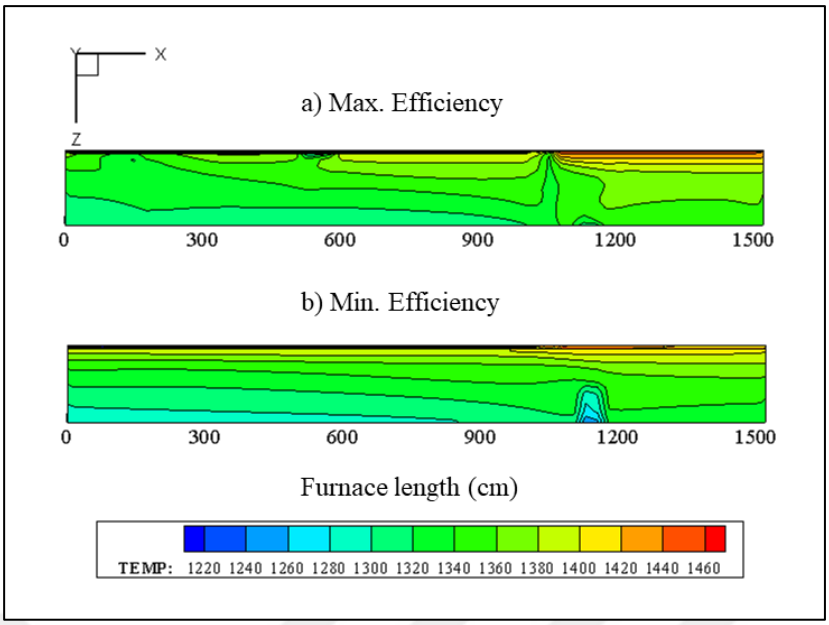

Figure 5.29: The temperatures along the depth of the glass for the minimum and the maximum energy efficient cases.

5.6. Evaluation of Results in Terms of Economic Sense

The glass furnace design has reached its limits, and the efficiency of a typical end-fired container glass furnace has squeezed between 55% and 60% in today's world. In a report published by European Commission Joint Research Centre [30] , it is stated that there is a total potential of 5% reduction in specific energy consumption in glass furnaces with improvements in both design and operation criteria. In this study, the largest difference found between the efficiencies of investigation cases is 2.2%. Although it seems a small difference at first glance, after considering the aforementioned potential of 5%, it appears to be significant.

In the previous chapters, the furnace efficiency is described as the ratio of the amount of energy transferred into the glass bath to the energy supplied to the furnace. Nearly half of the heat is lost in the furnace in the following ways: Heat loss from flue gas, heat regenerator wall losses, furnace wall losses, heat loss from furnace opening, and heat loss from the steel superstructure, batch gas losses, heat for endothermic reactions taking place in the furnace, and heat loss in moisture, etc. These losses increase with increasing amount of fuel as well as decreasing with decreasing amount of fuel. It could be said that when fuel supplied to the furnace increases, the temperature inside the furnace and the heat loss to the surroundings also increase. In

practice, there is not a linear relationship between the amount of fuel consumed and the losses stated above. However, there could be a simplistic approximation made based on the furnace efficiency results in Table 5.1.

An example of a simplistic approximation was performed using the result 2.2% which is the largest difference found between the efficiencies of investigation cases with number 13 and 27 in Table 5.1. Since all the temperature profiles are in accordance with the working temperature limits of clear glass production, the excessive temperature levels obtained in the maximum efficiency case could be lowered by decreasing the amount of fuel fed to the furnace. Hence, there could be a 2.2% reduction on a daily basis in energy consumption. In this study, the amount of fuel supplied to the furnace is 0.5719 m^3/s as given in Table 4.3. As of 2019 March, the price of natural gas per standard meter cube in Turkish glass industry is 1.4 Turkish Lira (TL). In Equation (5.11), the calculation of the annual expense of natural gas for a subjected furnace is carried out. The furnace is in continuous operation in 24 hours and 365 days in a whole year.

$$\begin{aligned} 0.5719\frac{m^3}{s}\,1440\frac{min}{day}\,3600\frac{s}{min} &= 2\,964\,729\frac{m^3}{day} \\ 2964729\frac{m^3}{day}\,365\,\frac{day}{year} &= 1\,082\,126\,304\,\frac{m^3}{year} \\ 1\,082\,126\,304\,\frac{m^3}{year}\,1.4\frac{TL}{m^3} &= 1\,514\,976\,826\,TL \end{aligned} \tag{5.11}$$

With the 2.2% reduction in energy consumption, the new annual expense of the natural gas calculated in Equation (5.12).

$$(1\,514\,976\,826\,TL)\,(\,97.8\,\%) = \,1\,481\,647\,335\,TL \tag{5.12}$$

So that the amount of savings per annum as a result of furnace efficiency improvement equals;

$$33\,329\,491\,Turkish\,Lira$$

Please note that the amount of savings stated above is for the most ideal case. It depends heavily on the furnace operation as well as furnace design. Furnace operation

includes not only control and automation of the process but also a human factor as well. For that reason, the amount of savings could be lower than the calculated amount.

6. CONCLUSIONS

- The aim of this thesis is to investigate the interactive effects of the three combustion space design parameters of a container glass furnace statistically in order to increase the energy efficiency of the furnace. These parameters are burner angle, port crown angle, and port base angle which affect the mixing of fuel and air, hence combustion and flame formation in the furnace. An end-port furnace having a capacity of 350 metric tons per day for clear container glass production was used in this study while the total energy supplied to the furnace is constant.
- A parametric study was carried out computationally to obtain energy efficiency results by employing an in-house developed 3D mathematical model to investigate 27 experiments which are determined by full factorial design. The energy efficiency data were fitted to the empirical third-order and second order polynomial model for maximum energy efficiency. The statistical analysis in this study was within a 95% significance level.
- For the cubic polynomial model; burner angle of 9^0, port crown angle 25.30^0 and port base angle 10^0 were found to be optimal for the maximum furnace efficiency. Analysis of variance of the cubic model showed that the model was highly significant (R^2=0.9715). Then, the analysis was extended to cover an extra 4 cases which are outside the specified investigation range to see if the analysis is still consistent with extra data. In order to improve the equations obtained, predictors with probability values higher than 0.05 were eliminated in backward starting with the highest probability value.
- For quadratic polynomial model; study cases were classified into three groups each having nine cases according to their port base angle. Results of energy efficiency data were fitted to the empirical second-order polynomial model for maximum energy efficiency for each group while burner angle and port crown angle vary.
- Then, the point at which the maximum furnace energy efficiency obtained for each analysis was calculated by using the optimization solver in Excel add-in. Then a new computational run was conducted for each analysis with using this point to compare the efficiency results with the empirical equation model.

- After statistical analysis, combustion space temperature profiles of the study cases were drawn to evaluate the results since temperature is an important variable with respect to furnace efficiency, glass melting process, and glass quality.
- In glass furnace analysis; quality of glass melt, and the quality of the ultimate product is the most important aspects considering the outcomes of the study. It is known that higher the quality of the glass, higher the energy consumption of the furnace. Therefore, energy efficiency is not the only criteria in glass manufacturing. There could be a case in which a furnace could be energy efficient but could not meet the customer demand related the glass quality. For that reason, a furnace analysis is a complex one where all the factors which have an impact on the glass furnace performance should be considered as a whole.
- Lastly, the difference between the efficiency results of the cases was evaluated in terms of economic sense by applying a simplistic approximation. It is found that 33 329 491 Turkish Lira could be saved per annum with 2.2% reduction in energy supplied to the furnace.
- As a result of the work done in this thesis, a case study was provided to utilize a statistical approach to increase the energy efficiency of a container glass furnace. It was performed at the design stage of the furnace in terms of investigation of three combustion space parameters by decreasing the required number of computational runs. In conclusion, a practical approach for glass furnace design to be used by furnace design engineers was presented in this study.
- This approach is helpful for understanding the relations between the parameters and eliminating some cases in mathematical modelling investigations required for the determination of design criteria of a new furnace or optimization of the operating parameters of an existing furnace. As stated above, results of this statistical approach and also mathematical modelling studies are specific for the investigated furnace.

6.1. Recommendations for Future Work

A set of ideas that could be further carried out for this study are suggested in this section. The recommendations for future work include:

- This study outlines a generalized statistical analysis on the relationship of three combustion space design parameters to increase the energy efficiency of a container glass furnace. A further study can be carried out to investigate the wider range of combustion space design parameters (port dimensions, furnace crown height, the distance of burner tip-glass surface, etc.) with a varied number of burner configurations (distance between burners, a different number of burners, etc.).
- Simulation of a glass furnace requires complex physical and chemical mechanisms, hence high computational time. In order to investigate all combustion space parameters mentioned above in a reasonable amount of time, the simulation code could be developed to reduce computational cost and completion time.
- More data collection is encouraged for the statistical analysis. This would enhance the outcome of the analysis of variance (ANOVA) tests. However, high CPU time is required for the simulations of the cases due to the complexity of the furnace code.
- This study is specific to a definite clear container glass furnace. More numbers of computational runs could be performed in order to generalize the statistical results of this study. Furthermore, this study could be applied to a production of a different color of glass such as green with low-iron content. Thus, the change in bottom temperatures of the glass bath between the investigation cases with varying burner angle could be more significant because radiative heat transfer is reduced due to the high iron content in the glass.
- A major extension for this study could be about an investigation of NO_x levels with varying burner angle and port angles. Because of the strict regulations have begun to be implemented by the governments around the world, minimizing the NO_x level has been of vital importance at the design stage of a glass furnace.

REFERENCES

[1] IEA, (2017), "2017 Key World Energy Statistics", International Energy Agency.

[2] U.S. EIA (2017), "International Energy Outlook 2017", United States of America Energy Information Administration.

[3] European Environment Agency, (2018), "European Energy Consumption by Sector and Fuel".

[4] UNIDO, (2010), "Global Industrial Energy Efficiency Benchmarking: An Energy Policy Tool", United Nations Industrial Development Organization.

[5] International Energy Agency, (2007), "Tracking Industrial Energy Efficiency and CO2 Emissions", Energy Policy, 30, 849–63.

[6] Levine E., Greenman M., Jamison K., (2003), "The Development of a Next Generation Melting System for Glass Production: Opportunities and Progress", ACEEE Summer Study on Energy Efficiency in Industry, Washington, D.C., USA, 29 July-1 August.

[7] World Energy Council, (2008), "Energy Efficiency Policies around the World: Review and Evaluation", London, United Kingdom.

[8] Web 1, (2019), http://ietd.iipnetwork.org/content/glass#technology-resources (Date of access: 20/03/2019).

[9] Mullinger P., Jenkins B., (2008), "Industrial and Process Furnaces", 1st Edition, Oxford, Butterworth-Heinemann.

[10] Trier W., (1987), "Glass Furnaces: Design, Construction and Operation", 1st Edition, United Kingdom, Society of Glass Technology.

[11] Web 2, (2015), https://www.lehigh.edu/imi/teched/GlassProcess/Lectures/Lecture01_Hubert_Comm_glasses_and%20Raw_Matls.pdf (Date of access: 20/03/2019).

[12] McLellan G. W., Shand E. B., (1984), "Glass Engineering Handbook", New York, McGraw-Hill, Inc.

[13] Zanotto E. D., Mauro J., (2017), "The glassy state of matter: Its definition and ultimate fate", Journal of Non-Crystalline Solids, 471, 490-495.

[14] Web 3, (2011), https://www.technologyreview.com/s/422345/glass-thats-stronger-than-steel/ (Date of access: 20/03/2019).

[15] Morse D. L., Evenson J. W., (2016), "Welcome to the Glass Age", International Journal of Applied Glass Science, 7 (4), 409-412.

[16] Web 3, (2015), https://feve.org/environmental-social-economic-contribution-container-glass-sector-europe/ (Date of access 20/03/2019).

[17] Türkiye Şişe ve Cam Fabrikaları A. Ş., (2018), "Şişecam Enerji Raporu", Türkiye.

[18] Web 4, (2013), https://www.eia.gov/todayinenergy/detail.php?id=12631&src=email (Date of access: 20/03/2019).

[19] Auchet O., Riedinger P., Malasse O., Iung C., (2008), "First-principles simplified modelling of glass furnaces combustion chambers", Control Engineering Practice, 16, 1443–56.

[20] Boerstoel P., (1997), "Modelling of Gas-Fired Furnaces", Doctoral Thesis, Delft University of Technology, the Netherlands.

[21] Choudhary M. K., Venuturumilli R., Hyre M. R., (2010), "Mathematical Modeling of Flow and Heat Transfer Phenomena in Glass Melting, Delivery, and Forming Processes", International Journal of Applied Glass Science, 1, 188–214.

[22] Tan Y. M., (2013), "Electromagnetic Inspection Techniques for Glass Production", Doctoral Thesis, The University of Manchester, the UK.

[23] Doremus R. H., (1994), "Glass Science", 2nd Edition, Wiley-Interscience.

[24] Web 5, (2019), https://www.believersinglass.com/GlassMaking.php (Date of access: 20/03/2019).

[25] Web 6, (2019), https://www.bdfindustriesgroup.com/products/melting-furnaces-burners/ (Date of access: 20/03/2019).

[26] Web 7, (2019), http://www.cham.co.uk/phoenics/d_polis/d_lecs/general/combust.htm (Date of access: 20/03/2019).

[27] U.S. Department of Energy Office of Industrial Technologies, (2000), "Energy and Environmental Profile of the U.S. Chemical Industry", Washington, DC.

[28] Beerkens R. G. C., Limpt J. van, (2001), "Energy Efficiency Benchmarking of Glass Furnaces", 62nd Conference on Glass Problems, University of Illinois at Urbana-Champaign, USA, 16-17 October.

[29] Galitsky C., Worrell E., Masanet E., Graus W., (2008), "Energy Efficiency Improvement and Cost Saving Opportunities for the Glass Industry. An Energy Star Guide for Energy and Plant Managers", USA.

[30] European Commission Joint Research Center, (2013), "Best Available Techniques (BAT) Reference Document for the Manufacture of Glass", Seville, Spain.

[31] Glass Technology Services, (2004), “A Study of The Balance Between Furnace Operating Parameters and Recycling Glass in Melting Furnaces”, Sheffield, United Kingdom.

[32] Beerkens R. G. C, (2008), “Energy Saving Options for Glass Furnaces and Recovery of Heat from Their Flue Gases and Experiences with Batch and Cullet Pre-Heaters Applied in the Glass Industry”, 69th Conference on Glass Problems, The Ohio State University, Columbus, Ohio, USA, 4-5 November.

[33] Beerkens R. G. C, (2006), “Energy Balances of Glass Furnaces: Parameters Determining Energy Consumption of Glass Melt Processes”, 67th Conference on Glass Problems, The Ohio State University, Columbus, Ohio, USA, 31 October-1 November.

[34] Lankhorst A., Thielen A., van der Dennen J., del Arroya M. H. A., (2014), “Application of an energy balance model for improving the energy efficiency of glass melting furnaces”, 74th Conference on Glass Problems, Greater Columbus Convention Center, Columbus, Ohio, USA, 14-17 October.

[35] Dorn C., Behrend R., Uhlig V., Trimis D., Krause H., (2017), “A technology comparison concerning scale dependencies of industrial furnaces. A case study of glass production”. Energy Procedia, 120, 388–94.

[36] Leicher J., Giese A., (2014), “Investigations into the Numerical Modelling of Oxy-Fuel Combustion in Glass Melting Furnaces”, Journal of International Flame Research Foundation.

[37] Dolianitis I., Giannakopoulos D., Hatzilau C. S., Karellas. S, Kakaras E., Nikolova E., Skarpetis G., Christodoulou N., Giannoulas N., Zitounis T., (2016), “Waste heat recovery at the glass industry with the intervention of batch and cullet preheating”, Thermal Science, 20(4), 1245–58.

[38] Basso D., Cravero C., Reverberi A., Fabiano B., (2015), “CFD Analysis of Regenerative Chambers for Energy Efficiency Improvement in Glass Production Plants”, Energies, 8, 8945–61.

[39] Danon B., Cho E. S., de Jong W., Roekaerts D. J. E. M., (2011), "Numerical investigation of burner positioning effects in a multi-burner flameless combustion furnace", Applied Thermal Engineering, 31(17–18), 3885–3896.

[40] Helder G., (1988), “Modelling of Flow and Combustion in a Glass Melting Furnace”, Doctoral Thesis, Delft University of Technology, the Netherlands.

[41] Eltutar Z., Önsel L., Uçar S., (2009), “Simulation and Evaluation of NOx in Glass Furnaces”, 10th International Seminar on Furnace Design, Operation and Process Simulation, Velké Karlovice, Czech Republic, 16-19 June.

[42] Uçar S., Eltutar Z., Önsel L., (2011), “An Analysis of the Effect of Combustion Space Design on Glass Furnace Performance and NOx Emissions with Mathematical Modeling”, 11th International Seminar on Furnace Design, Operation and Process Simulation, Velké Karlovice, Czech Republic, 21-23 June.

[43] Cable M., (2005), “A Century of Developments in Glassmelting Research”, Journal of the American Ceramic Society, 81(5), 1083–1094.

[44] Mase H., Oda K., (1980), “Mathematical model of glass tank furnace with batch melting process”, Journal of Non-Crystalline Solids, 38–39, 807–812.

[45] Hrma P., (1982), “Thermodynamics of batch melting”, Glastechnische Berichte, 55, 138–50.

[46] Xiqi W., Viskanta R., (1986), “Modeling of heat transfer in the melting of a glass batch”, Journal of Non-Crystalline Solids, 80(1–3), 613–622.

[47] Ungan A., Viskanta R., (1987), “Identification of the Structure of the Three Dimensional Thermal Flow in an Idling Container Glass Melter”, Glass Technology, 28(6), 252-260.

[48] Ungan A., Viskanta R., (1986), "Melting behavior of continuously charged loose batch blankets in glass melting furnaces", Glastechnische Berichte, 59(10), 279–291.

[49] Ungan A., Viskanta R., (1986), “Three-Dimensional Numerical Simulation of Circulation and Heat Transfer in an Electrically Boosted Glass Melting Tank”, IEEE Transactions on Industry Applications, IA-22(5), 922 – 933.

[50] Ungan A., Viskanta R., (1986), "Effect of Air Bubbling on Circulation and Heat Transfer in a Glass-Melting Tank", Journal of the American Ceramic Society, 69, 382–91.

[51] Ungan A., Viskanta R., (1987), “Three-dimensional Numerical Simulation of Circulation and Heat Transfer in an Electrically Boosted Glass Melting Tank. Part 2: Sample Simulations”, Glastechnische Berichte, 60(4), 115–124.

[52] Ungan A., (1985), “Three-Dimensional Numerical Modelling of Glass Melting Process”, Doctoral Thesis, Purdue University, West Lafayette, Indiana, USA.

[53] Shill P., (1983), "Mathematisches modell des abschmelzens der gemengeschicht in vollelektrischen öfen", Glastechnische Berichte, 56K, 179–84.

[54] Carvalho M. G., Speranskaia N., Wang J., Nogueira M., (1997), “Modeling of glass melting furnaces: applications to control, design, and operation optimization”, Advances in Fusion and Processing of Glass, II. vol. 82, (Clare, Jones (Ed)), 109-135, Ceramic Transactions.

[55] Carvalho M. G., Nogueira M., (1997), “Improvement of energy efficiency in glass-melting furnaces, cement kilns and baking ovens”, Applied Thermal Engineering, 17, 921–33.

[56] Beerkens R. G. C, (2008), “Analysis of elementary process steps in industrial glass melting tanks - Some ideas on innovations in industrial glass melting”, Ceramics – Silikáty, 52(4), 206-217.

[57] Beerkens R. G. C, van Limpt H., (2007), “Low NOx Combustion in Regenerative Glass Furnaces”, 68th Conference on Glass Problems, The Ohio State University, Columbus, Ohio, USA, 16-17 October.

[58] Schill P., Chmelar J., (2004), “Use of computer flow dynamics in glass technology”, Journal of Non-Crystalline Solids, 345–346, 771–776.

[59] Loch H., Krause D., (2002), “Mathematical Simulation in Glass Technology”, Berlin, Springer Berlin Heidelberg.

[60] Ungan A., Payli R. U., Balkanli B., (1994), “Numerical Model of Polydispersed Silica Grain Dissolution in Glass Melting Furnaces”, Journal of the American Ceramic Society, 77, 1921–7.

[61] Ungan A., (1996), "Numerical Simulation of Glass Melting Furnaces: A Review", International Symposium on Glass Problems, Istanbul, Turkey.

[62] Oruç O., Önsel L., Eltutar Z., Özturan C., (2002), "Parallel Computing of Combustion Space Model for Glass Furnaces", AcerS Glass & Optical Materials Division.

[63] Domazet E., (2014), “Parallelization of a Furnace Simulation Code for Multi-Core Machines”, Master Thesis, Boğaziçi Üniversitesi, Turkey.

[64] Patankar S. V., (1980), ”Numerical Heat Transfer and Fluid Flow”, Hemisphere Publishing Corporation, New York.

[65] Harlow F. H., Nakayama P. I., (1968), "Transport of Turbulence Energy Decay Rate", U.S. Atomic Energy Commission, Los Alamos Scientific Laboratory, New Mexico, USA.

[66] Launder B. E., Spalding D. B., (1974), "The numerical computation of turbulent flows", Computer Methods in Applied Mechanics and Engineering, 3, 269-289.

[67] Raithby G. D., Chui E. H., (1990), “A Finite-Volume Method for Predicting a Radiant Heat Transfer in Enclosures With Participating Media”, Journal of Heat Transfer, 112(2), 415.

[68] Thomas L.H., (1949), “Elliptic Problems in Linear Difference Equations over a Network”, Watson Sc. Comp. Lab. Rep., Columbia University, New York.

[69] Meijerink J. A., van der Vorst H. A., (1977), “An Iterative Solution Method for Linear Systems of Which the Coefficient Matrix is a Symmetric M-Matrix”, Mathematics of Computation, 31(137), 148.

[70] Pilon L., Zhao G., Viskanta, R., (2002), "Three-Dimensional Flow and Thermal Structures in Glass Melting Furnaces. Part I. Effects of the Heat Flux Distribution", Glass Science and Technology, 75(2), 55-68.

[71] Minitab 17 Statistical Software, State College, PA: Minitab, Inc.

[72] Raykov T., Marcoulides, G. A., (2013), "Basic Statistics: An Introduction With R", Plymouth, UK, Rowman & Littlefield Publishers, Inc.

[73] Web 8, (2019), https://web.ma.utexas.edu/users/davis/375/popecol/tables/f005.html (Date of access: 20/03/2019).

[74] Web 9, (2019), http://www.biostat.jhsph.edu/~iruczins/teaching/jf/ch10.pdf (Date of access: 20/03/2019).

[75] TECPLOT 360 Software, Bellevue, WA, Tecplot, Inc.

[76] Sevast’yanov R. I., (2004), “The Role of Convection in Glass-Melting Furnaces”, Glass and Ceramics, 61(5/6), 139–141.

BIOGRAPHY

Penbe Merve Durubal received her Bachelor of Science degree in Chemical Engineering from Middle East Technical University, Ankara, Turkey in 2013. She started her graduate studies in Mechanical Engineering at Gebze Technical University, Kocaeli, Turkey in 2016.

Since 2014, she has been working as a full-time researcher at Glass Furnace Modelling and Simulation Group at Sisecam Glass Science and Technology Center in Kocaeli, Turkey. Her research interests are glass industry, modeling of glass melting furnaces, and optimization of glass melting process.

APPENDICES

APPENDIX A: Publications within the Scope of this Thesis

Durubal P. M., Gul B., Konukman A. Ş., (2017), "Investigation of Port and Burner Angle Design in Glass Furnaces for High Energy Efficiency", 21. Ulusal Isı Bilimi ve Tekniği Kongresi, Çorum Hitit University, Çorum, Turkey, 13-16 September 2017.

Durubal P. M., Konukman A. Ş., (2017), "Investigation of Two Parameters Affecting Thermal Performance of Glass Furnaces", Gebze Teknik Üniversitesi Fen Bilimleri Enstitüsü, Lisansüstü Araştırmalar Sempozyumu & Tanıtım Günleri, Kocaeli, Turkey, 17-18 May 2017.

APPENDIX B: Screen Views from the Furnace Simulation Program

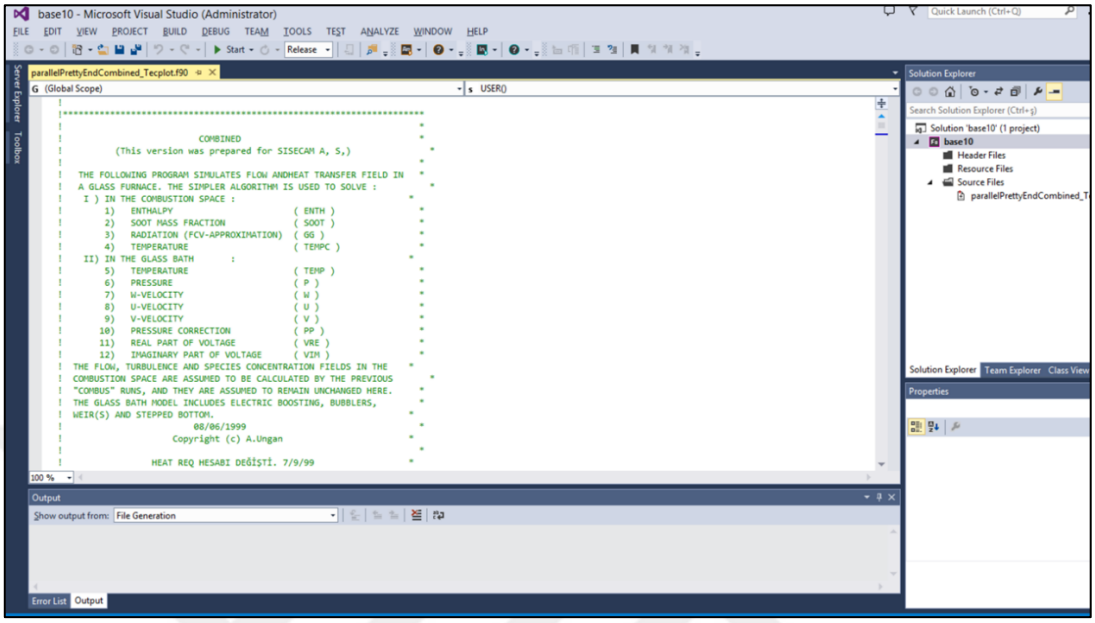

Figure B1.1: Screen view (1) from the Furnace Simulation Program.

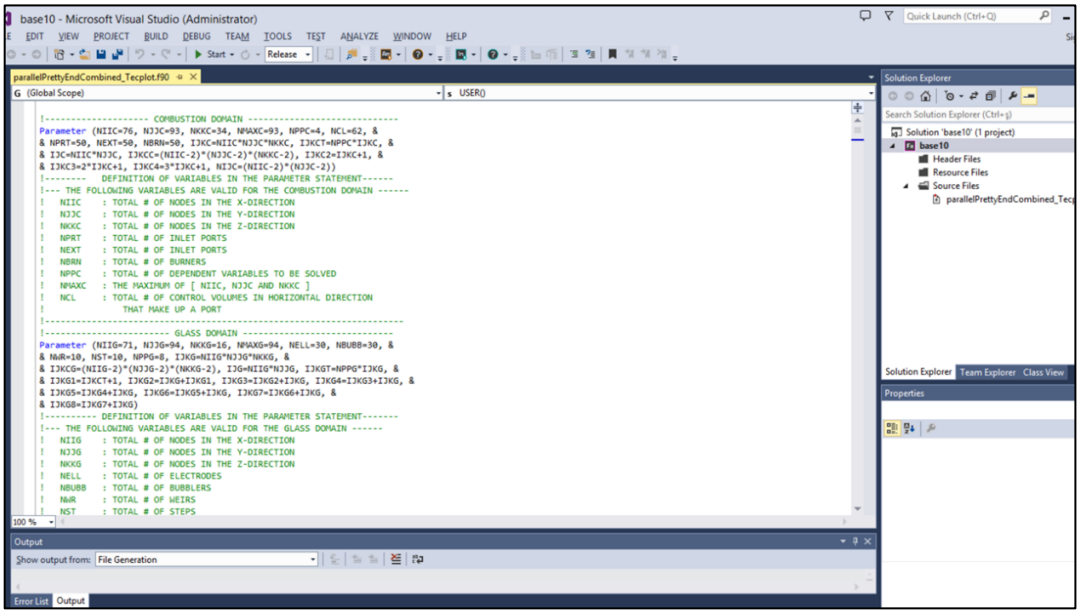

Figure B1.2: Screen view (2) from the Furnace Simulation Program.

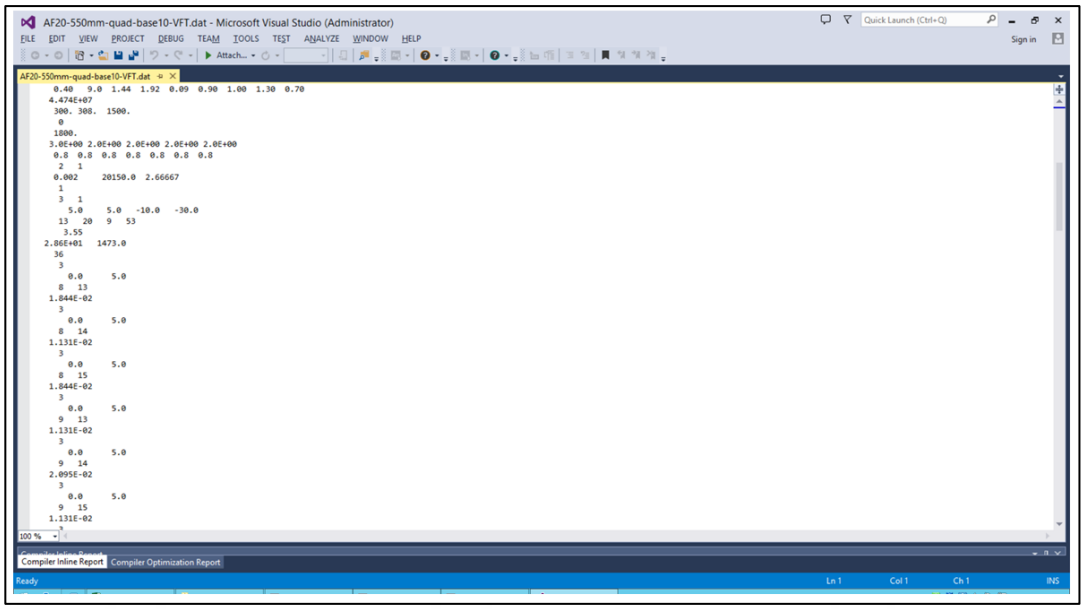

Figure B1.3: Screen view from the input of the Furnace Simulation Program.

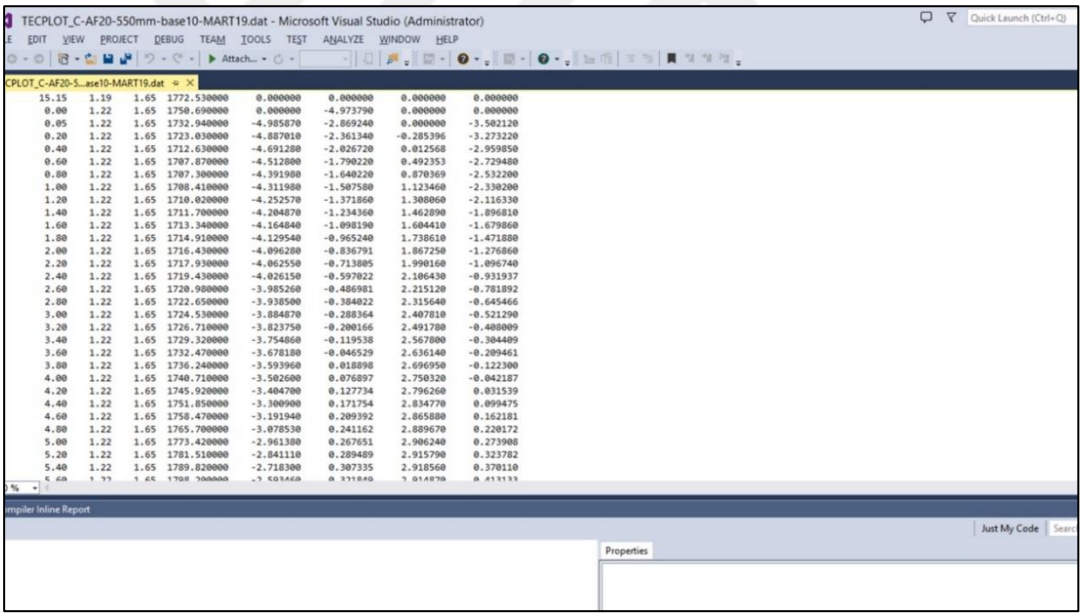

Figure B1.4: Screen view from the nodes; temperature, velocity, etc. output of the Furnace Simulation Program.

APPENDIX C: Grid Representation

Grid representation of the solution domain is shown in Figure C1.1 [63]. In the figure, solid and dashed lines constitute a staggered grid. The spacing of grid points could be non-uniform. Nodes are described as follows;

- The intersection of solid lines forms a basic node → scalar variables are stored in it.
- The intersection of a solid line and dashed line form a velocity node → velocity components are stored in it.
- The intersection of two dashed lines forms pseudo-nodes.

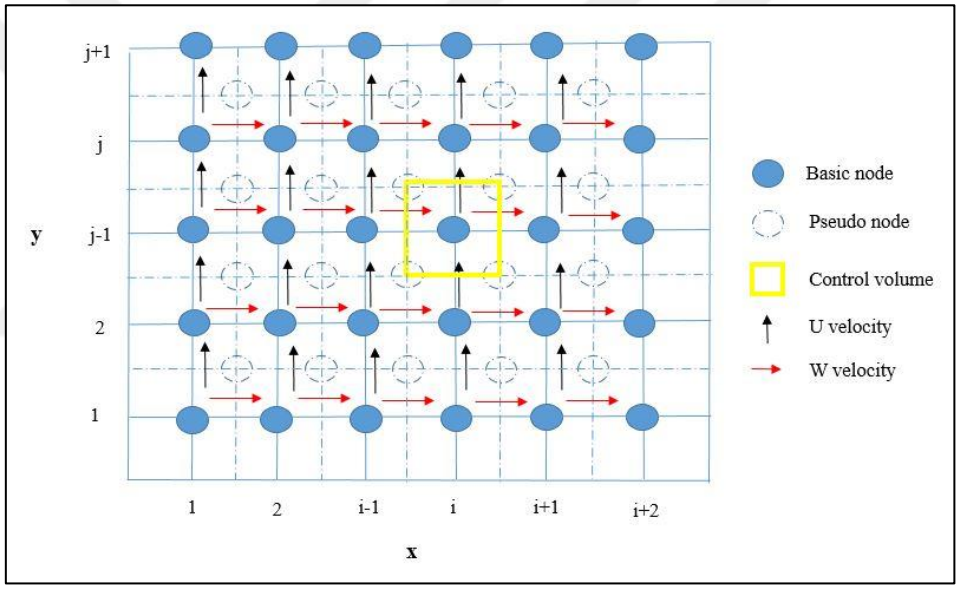

Figure C1.1: Grid representation of the solution domain.

APPENDIX D: An Example of Energy Efficiency Calculation

- The energy efficiency of the 22nd run from Table 5.1 is calculated as an example below in Table D.1.
- The amount of fuel equals 1.644205E+07 watts power supplied into the furnace.

Table D1.1: An example of furnace efficiency calculation.

Radiative energy out from combustion space (watts)	9.54E+06	Results of Computational Run
Conductive & convective energy out from combustion space (watts)	1.07E+05	
Total energy into the glass bath (watts)	(9.54E+06) + (1.07E+05) = 9.6510E+06	
Efficiency of the furnace (%)	(9.6510E+06) / (1.644205E+07) = 58.69719303	